REPORT DOCUMENTATION PAGE

Form Approved OMB NO. 0704-0188

1. REPORT DATE (DD-MM-YYYY)	2. REPORT TYPE	3. DATES COVERED (From - To)
31-07-2017	Final Report	1-May-2013 - 30-Apr-2017

4. TITLE AND SUBTITLE
Final Report: Antennas for Body-Centric Wireless Communications

5a. CONTRACT NUMBER
W911NF-13-1-0112

5b. GRANT NUMBER

5c. PROGRAM ELEMENT NUMBER
206022

6. AUTHORS
Rafael A. Rodriguez-Solis

5d. PROJECT NUMBER

5e. TASK NUMBER

5f. WORK UNIT NUMBER

7. PERFORMING ORGANIZATION NAMES AND ADDRESSES
University of Puerto Rico at Mayaguez
University of Puerto Rico Mayaguez
Call Box 9000
Mayaguez, PR 00681 -9000

8. PERFORMING ORGANIZATION REPORT NUMBER

9. SPONSORING/MONITORING AGENCY NAME(S) AND ADDRESS (ES)
U.S. Army Research Office
P.O. Box 12211
Research Triangle Park, NC 27709-2211

10. SPONSOR/MONITOR'S ACRONYM(S)
ARO

11. SPONSOR/MONITOR'S REPORT NUMBER(S)
62882-EL-REP.19

12. DISTRIBUTION AVAILIBILITY STATEMENT
Approved for public release; distribution is unlimited.

13. SUPPLEMENTARY NOTES
The views, opinions and/or findings contained in this report are those of the author(s) and should not contrued as an official Department of the Army position, policy or decision, unless so designated by other documentation.

14. ABSTRACT

15. SUBJECT TERMS
antennas, microwaves, millimeter-waves, body-centric communications

16. SECURITY CLASSIFICATION OF:			17. LIMITATION OF ABSTRACT	15. NUMBER OF PAGES	19a. NAME OF RESPONSIBLE PERSON
a. REPORT	b. ABSTRACT	c. THIS PAGE			Rafael Rodriguez-Solis
UU	UU	UU	UU		19b. TELEPHONE NUMBER 787-832-2825

RPPR Final Report
as of 01-Nov-2017

Agency Code:

Proposal Number: 62882ELREP **Agreement Number: W911NF-13-1-0112**
INVESTIGATOR(S):

Name: Rafael A. Rodriguez-Solis
Email: rafael.rodriguez19@upr.edu
Phone Number: 7878322825
Principal: Y

Organization: **University of Puerto Rico at Mayaguez**
Address: University of Puerto Rico Mayaguez, Mayaguez, PR 006819000
Country: USA
DUNS Number: 175303262 EIN: 660433761
Report Date: 31-Jul-2017 Date Received: 31-Jul-2017
Final Report for Period Beginning 01-May-2013 and Ending 30-Apr-2017
Title: Antennas for Body-Centric Wireless Communications
Begin Performance Period: 01-May-2013 **End Performance Period:** 30-Apr-2017
Report Term: 0-Other
Submitted By: Rafael Rodriguez-Solis Email: rafael.rodriguez19@upr.edu
Phone: (787) 832-2825
Distribution Statement: 1-Approved for public release; distribution is unlimited.

STEM Degrees: 4 **STEM Participants:** 4

Major Goals: The main objective of this work is to provide antenna alternatives for BAN at various frequency bands, based on the effects the body has on the input impedance and radiation pattern. In particular, work will be performed at the 2.4 GHz ISM band, the 3.1-10.6 UWB band, 35 GHz, and 60 GHz. The 2.4 GHz band is currently used for BANs in healthcare applications, and novel designs in this frequency band could have a more immediate impact in current applications. The UWB band is being suggested as an alternative for BAN, and although the design of small, very wideband antennas could be difficult, the potential pay-off is large, both for BAN and other applications. The 60 GHz band has also been suggested as an alternative for BAN because of the high spectrum usage at the 2.4 ISM band, the rapid attenuation with distance of the signals at 60 GHz can help in reducing interference to and from other BANs, and to offer another layer of security into the network. With the increased interest in Personal Area Networks at 60 GHz, the proposed work could also find applications in this area. The 35 GHz band will be used as a stepping stone to the 60 GHz work, since the Radiation Laboratory near-field antenna measurement system can operate up to 40 GHz. Scaled versions of the 60 GHz antennas at 35 GHz could be used to validate simulations, before fabricating the V-band antennas. In addition, Ka-band could be another alternative for BANs due to its low spectrum usage, and the results could be used in communications and sensing applications at this frequency. With the acquisition of the Agilent PNA vector network analyzer, the input impedance of all the antenna prototypes at the proposed frequencies could be measured in-house, and the radiation pattern of all but the 60 GHz prototypes can be measured in-house; these would be sent elsewhere to measure the radiation patterns.

At the lower frequency bands, the focus of the work will be in reducing the size. The UWB represents a challenge because of the large bandwidth requirements and the interest in maintaining a small size. At the higher frequencies, the challenge is not the size, since the wavelength at these frequencies is already in the order of millimeters, but more the effects of the human body interactions in the input impedance and radiation pattern. For all frequency bands, the possibility of integrating the antenna to existing sensor technology will be considered as part of the design process.

Accomplishments: See Arrachment Below

Training Opportunities: The four graduate students that participated on the project spent one summer each at the University of Colorado at Boulder, to work on their project in Dr. Dejan Filipovic's group. Through this exchange, they had the opportunity of working on a different environment, with access to many more PhD students and pos-doctoral researchers. This provided them with much better focus at their return to UPRM.

RPPR Final Report
as of 01-Nov-2017

Results Dissemination: Nothing to Report

Honors and Awards: Dr. Rodríguez-Solís was named 2012-2013 Outstanding Electrical Engineering Professor by the Faculty of Engineering.

Protocol Activity Status:

Technology Transfer: Nothing to Report

PARTICIPANTS:

Participant Type: Other Professional
Participant: Maribel Feliciano
Person Months Worked: 7.00 **Funding Support:**
Project Contribution:
International Collaboration:
International Travel:
National Academy Member: N
Other Collaborators:

Participant Type: Graduate Student (research assistant)
Participant: Emmanuel Valentin
Person Months Worked: 14.00 **Funding Support:**
Project Contribution:
International Collaboration:
International Travel:
National Academy Member: N
Other Collaborators:

Participant Type: Graduate Student (research assistant)
Participant: Jayson Maldonado
Person Months Worked: 14.00 **Funding Support:**
Project Contribution:
International Collaboration:
International Travel:
National Academy Member: N
Other Collaborators:

Participant Type: Graduate Student (research assistant)
Participant: Carlos Mulero
Person Months Worked: 14.00 **Funding Support:**
Project Contribution:
International Collaboration:
International Travel:
National Academy Member: N
Other Collaborators:

Participant Type: Graduate Student (research assistant)
Participant: Ruben Delgado
Person Months Worked: 14.00 **Funding Support:**
Project Contribution:
International Collaboration:
International Travel:
National Academy Member: N

Other Collaborators:

Participant Type: PD/PI
Participant: Rafael Antonio Rodriguez Solis
Person Months Worked: 3.00 **Funding Support:**
Project Contribution:
International Collaboration:
International Travel:
National Academy Member: N
Other Collaborators:

CONFERENCE PAPERS:

Publication Type: Conference Paper or Presentation **Publication Status:** 1-Published
Conference Name: 2014 IEEE International Symposium on Antennas and Propagation
Date Received: 12-Aug-2016 Conference Date: 06-Jul-2014 Date Published:
Conference Location: Memphis, TN
Paper Title: Characterization of a Cavity-backed Capacitively-fed Folded Slot Antenna Using DOE Techniques
Authors: Emmanuel Valentín, Rafael A. Rodríguez Solís
Acknowledged Federal Support: **Y**

Publication Type: Conference Paper or Presentation **Publication Status:** 1-Published
Conference Name: 2014 IEEE International Symposium on Antennas and Propagation
Date Received: 12-Aug-2016 Conference Date: 06-Jul-2014 Date Published:
Conference Location: Memphis, TN
Paper Title: Analysis of a Cavity Backed Annular Slot Ring Antenna Using Design of Experiments Techniques
Authors: Jayson Maldonado Vargas, Rafael A. Rodriguez Solis
Acknowledged Federal Support: **Y**

Publication Type: Conference Paper or Presentation **Publication Status:** 1-Published
Conference Name: 2015 IEEE International Simposium on Antennas and Propagation
Date Received: 12-Aug-2016 Conference Date: 22-Jul-2015 Date Published:
Conference Location: Vancouver, BC, Canada
Paper Title: Design of a Small Rectangular Patch for Body Area Network Applications
Authors: Emmanuel Valentín, Rafael A. Rodríguez Solís
Acknowledged Federal Support: **Y**

Publication Type: Conference Paper or Presentation **Publication Status:** 1-Published
Conference Name: 2015 IEEE International Symposium on Antennas and Propagation
Date Received: 12-Aug-2016 Conference Date: 21-Jul-2015 Date Published:
Conference Location: Vancouver, BC, Canada
Paper Title: Capacitively-Fed Modified Folded Slot Antenna for Body Area Network Applications
Authors: Emmanuel Valentín, Rafael A. Rodríguez Solís
Acknowledged Federal Support: **Y**

RPPR Final Report
as of 01-Nov-2017

Publication Type: Conference Paper or Presentation **Publication Status:** 1-Published
Conference Name: 2015 IEEE International Symposium on Antennas and Propagation
Date Received: 12-Aug-2016 Conference Date: 20-Jul-2015 Date Published:
Conference Location: Vancouver, BC, Canada
Paper Title: A UWB Cavity-Backed Compound Power-Archimedean Slot Spiral for Body Centric Wireless Communications Applications
Authors: Jayson Maldonado-Vargas; Rafael A. Rodríguez-Solís; Mohamed A. Elmansouri; Dejan S. Filipovic
Acknowledged Federal Support: **Y**

Publication Type: Conference Paper or Presentation **Publication Status:** 1-Published
Conference Name: 2014 IEEE/MTT-S International Microwave Symposium - MTT 2014
Date Received: 12-Aug-2016 Conference Date: 01-Jun-2014 Date Published:
Conference Location: Tampa, FL, USA
Paper Title: Microwave research at the University of Puerto Rico at Mayagüez
Authors: Rodríguez-Solís, R.A.; Colom-Ustáriz, J.G.; Cruz-Pol, S.; León-Colón, L.
Acknowledged Federal Support: **Y**

Publication Type: Conference Paper or Presentation **Publication Status:** 1-Published
Conference Name: 2016 IEEE International Symposium on Antennas and Propagation
Date Received: 19-Jul-2017 Conference Date: 28-Jun-2016 Date Published: 02-Jul-2016
Conference Location: Fajardo, Puerto Rico
Paper Title: Design of V-Band Substrate Integrated Waveguide Fed Aperture Coupled Microstrip Patch Array with Beam-Switching Capabilities
Authors: Carlos A. Mulero Hernandez, Rafael A. Rodríguez Solís
Acknowledged Federal Support: **Y**

Publication Type: Conference Paper or Presentation **Publication Status:** 1-Published
Conference Name: 2016 IEEE International Symposium on Antennas and Propagation
Date Received: 19-Jul-2017 Conference Date: 27-Jun-2016 Date Published: 02-Jul-2016
Conference Location: Fajardo, Puerto Rico
Paper Title: Design of V-Band SIW Fed Cavity Backed Aperture Coupled Microstrip Patch Array Element for Applications in Body Area Networks
Authors: Carlos A. Mulero Hernandez, Rafael A. Rodríguez Solís
Acknowledged Federal Support: **Y**

Publication Type: Conference Paper or Presentation **Publication Status:** 1-Published
Conference Name: 2016 IEEE International Symposium on Antennas and Propagation
Date Received: 19-Jul-2017 Conference Date: 27-Jun-2016 Date Published: 02-Jul-2016
Conference Location: Fajardo, Puerto Rico
Paper Title: Applying Design of Experiments to the Design of 60 GHz Antennas for Off-Body Communications
Authors: Rubén Delgado, Carlos A. Mulero Hernández, and Rafael Rodríguez Solís
Acknowledged Federal Support: **Y**

Publication Type: Conference Paper or Presentation **Publication Status:** 1-Published
Conference Name: 2016 IEEE International Symposium on Antennas and Propagation
Date Received: 19-Jul-2017 Conference Date: 27-Jun-2016 Date Published: 02-Jul-2016
Conference Location: Fajardo, Puerto Rico
Paper Title: Design of Vertical T-Junction Using H-Slot Aperture Coupling for Applications in 60 GHz Arrays
Authors: Carlos A. Mulero Hernandez, Rafael A. Rodríguez Solís
Acknowledged Federal Support: **Y**

Publication Type: Conference Paper or Presentation **Publication Status:** 1-Published
Conference Name: 2014 IEEE International Symposium on Antennas and Propagation & USNC/URSI National Radio Science Meeting
Date Received: 19-Jul-2017 Conference Date: 06-Jul-2014 Date Published: 07-Jul-2016
Conference Location: Memphis, TN, USA
Paper Title: Analysis of a cavity backed annular slot ring antenna using design of experiment techniques
Authors: Jayson Maldonado-Vargas, Rafael A. Rodríguez-Solís
Acknowledged Federal Support: **Y**

Publication Type: Conference Paper or Presentation **Publication Status:** 2-Awaiting Publicat
Conference Name: 2017 IEEE International Symposium on Antennas and Propagation
Date Received: 19-Jul-2017 Conference Date: 10-Jul-2017 Date Published: 11-Jul-2017
Conference Location: San Diego, CA, USA
Paper Title: Design of a V-Band Wideband Circularly Polarized Microstrip Patch Array Element for Applications in Body Area Networks
Authors: Rubén F.M. Delgado-Castillo, Rafael A. Rodríguez-Solís
Acknowledged Federal Support: **Y**

Publication Type: Conference Paper or Presentation **Publication Status:** 0-Other
Conference Name: 2017 IEEE International Symposium on Antennas and Propagation
Date Received: 19-Jul-2017 Conference Date: 10-Jul-2017 Date Published: 11-Jul-2017
Conference Location: San Diego, CA, USA
Paper Title: Linearly and Circularly Polarized Elements on Sequentially Rotated 2x2 Arrays for 60 GHz BANs
Authors: Rubén F.M. Delgado-Castillo, Rafael A. Rodríguez-Solís
Acknowledged Federal Support: **Y**

DISSERTATIONS:

Publication Type: Thesis or Dissertation
Institution: University of Puerto Rico, Mayaguez
Date Received: 12-Aug-2016 Completion Date: 5/30/15 5:40PM
Title: DESIGN AND ANALYSIS OF CAPACITIVELY-FED FOLDED SLOT AND RECTANGULAR PATCH ANTENNA FOR BODY CENTRIC WIRELESS COMUNICATIONS
Authors: Emmanuel Valentin
Acknowledged Federal Support: **Y**

Publication Type: Thesis or Dissertation
Institution: University of Puerto Rico, Mayaguez
Date Received: 31-Jul-2017 Completion Date: 7/19/17 8:00AM
Title: Design and Characterization of Cavity-Backed Asymmetric Annular Ring Slot Antenna and UWB Cavity-Backed Two-Arm Modified Compound Power-Archimedean Slot Spiral Antenna for Body Centric Wireless Communications Application
Authors: Jayson, Maldonado
Acknowledged Federal Support: **Y**

RPPR Final Report
as of 01-Nov-2017

Publication Type: Thesis or Dissertation
Institution: University of Puerto Rico, Mayaguez
Date Received: 29-Aug-2016 Completion Date: 7/15/16 9:40PM
Title: DESIGN OF V-BAND BEAM-SWITCHING SUBSTRATE INTEGRATED WAVEGUIDE FED APERTURE COUPLED MICROSTRIP PATCH ARRAYS WITH BEAM-SWITCHING CAPABILITIES FOR OFF-BODY COMMUNICATIONS IN BODY CENTRIC WIRELESS NETWORKS
Authors: Carlos Mulero
Acknowledged Federal Support: **Y**

Publication Type: Thesis or Dissertation
Institution: University of Puerto Rico, Mayaguez
Date Received: 19-Jul-2017 Completion Date: 7/19/17 4:00AM
Title: DESIGN OF V-BAND SUBSTRATE INTEGRATED WAVEGUIDE FED APERTURE COUPLED MICROSTRIP PATCH ARRAYS WITH CIRCULAR POLARIZATION AND PARASITIC PATCH FOR OFF-BODY COMMUNICATIONS IN BODY CENTRIC WIRELESS NETWORKS
Authors: Delgado, Ruben
Acknowledged Federal Support: **Y**

ANTENNAS FOR BODY-CENTRIC WIRELESS COMMUNNICATIONS

Final Report for Proposal Number 62882ELREP

Dr. Rafael A. Rodríguez Solís
rafael.rodriguez19@upr.edu

TABLE OF CONTENTS

Antennas for Body-Centric Wireless Communications

1 EXECUTIVE SUMMARY

Four master students, Jayson Maldonado, Emmanuel Valentín, Rubén Delgado, and Carlos Mulero worked on the project through its duration. All four students completed their MS degrees. Emmanuel defended his thesis in May 2015, Jayson in June 2015, Carlos in July 2016, and Ruben in May 2017. All of them spent a summer at the University of Colorado at Boulder, with Dr. Dejan Filipovic as their mentor. Dr. Filipovic was part of the graduate committees of Jayson, Emmanuel, and Carlos. The PI met weekly with the students via Skype during the summers they spent in Boulder.

Emmanuel worked on antennas for the 2.4 GHz band, specifically a modified folded-slot, and a compact microstrip patch. The modified folded-slot provided a 20 MHz bandwidth, similar to other works in the literature, with a gain of 4.2 dB, while placed on the body. The patch antenna covered the complete 2.4 GHz ISM band with a return loss better than 10 dB, with a gain of 5.2 dB. Both antennas had a ground plane of 40 mm x 40 mm. Jayson worked on antennas for the UWB band, specifically a compound spiral antenna, in collaboration with Dr. Dejan Filipovic and Dr. Mohamed Elmansouri from University of Colorado. Jayson's spiral covers the entire UWB band with a return loss better than 10 dB, and a stable pattern and gain. Carlos worked on a small microstrip array in substrate integrated waveguide (SIW) at 60 GHz, with 1-D scanning capability. His work included the design of the element, array, vertical feeding network, and initial work on a Rotman lens to provide the scanning. The 4x4 array provided a 15.6 dB gain at the center frequency, with a 14.29% bandwidth (56.16-64.8 GHz). Rubén designed a circularly polarized patch antenna at 60 GHz 11.6% impedance bandwidth (57-64 GHz) and 9.2% axial ratio bandwidth (58.1-63.7 GHz), with a gain of 8.5 dBic at 60 GHz. He also designed a 2x2 circularly polarized array with 12.7 dBic gain at 60 GHz, covering the entire 57-64 GHz band (11.6% bandwidth) in terms of impedance and axial ratio. The results of their work resulted in 12 conference papers. We also began the design of a dual-linear polarized microstrip patch array for operation at 24 GHz. The 2x2 array provided 11.6 dB gain, better than 16 dB of isolation between polarizations, and better than 16.8 dB cross-polarization level at 24 GHz. The impedance bandwidth started at 22.9 GHz, with better than 10 dB return loss above 28 GHz.

2 PROBLEM STATEMENT

Our goal was to provide design alternatives for body-centric antennas for off-body communications, taking into account the effects of the body on the antenna performance. We analyzed electromagnetic models for the body for the frequency bands of interest (2.4 GHz, UWB, 60 GHz) to use in the antenna design process. The work at 2.4 GHz and UWB was focused on reducing the antenna size, while providing sufficient bandwidth, while at 60 GHz, the main goal was to focus on the fabrication techniques to reduce the energy coupled to the body, and to provide a good communication link with the intended receiver, through 1-D scanning capabilities, and circular polarization.

3 SUMMARY OF RESULTS

3.1 DESIGNS FOR 2.4 GHZ

We looked into several designs to verify the gain and impedance bandwidth characteristics. We focused on single-solid-layered alternatives, as opposed to multi-layer or air-substrate designed generally used to increase the bandwidth. The use of a single, solid layer provides ease of fabrication, low-cost, and ruggedness. In addition, we limited the size of the ground plane to 40 mm x 40 mm, after verifying the effect of the ground size on the radiation pattern. This size provided good isolation with the body, while keeping the antenna compactness. A cavity-backed, slot-loaded, capacitively-fed, folded-slot antenna, and an inset-fed, slot-loaded quarter-wavelength patch with a parasitic slot-loaded quarter-wavelength patch were studied.

3.1.1 Cavity-backed, slot-loaded, capacitively-fed, folded-slot antenna

The geometry for this antenna is shown in Fig. 1. The antenna was implemented on Rogers RO 3003, on a 40 mm x 40 mm ground plane, with a folded-slot length of 18 mm. The reflection coefficient for the antenna in free-space is found in Fig. 2. There is a slight shift, about 25 MHz, in the resonance frequency between the simulation and measurement. The radiation pattern in free space is shown in Fig. 3, showing a maximum gain of 4.2 dB. Fig. 4 shows the behavior of the reflection coefficient in free-space and on the body, showing a very slight reduction in bandwidth, but no change in the resonant frequency. Fig. 5 shows the radiation pattern in free-space and on the forearm model. There is a reduction in gain due to the energy absorption on the body. Fig. 6 shows the near electric field distribution in and around the forearm. Note that the field strength is reduced by 28 dB at 120 degrees from broadside, and by 56 dB at 180 degrees.

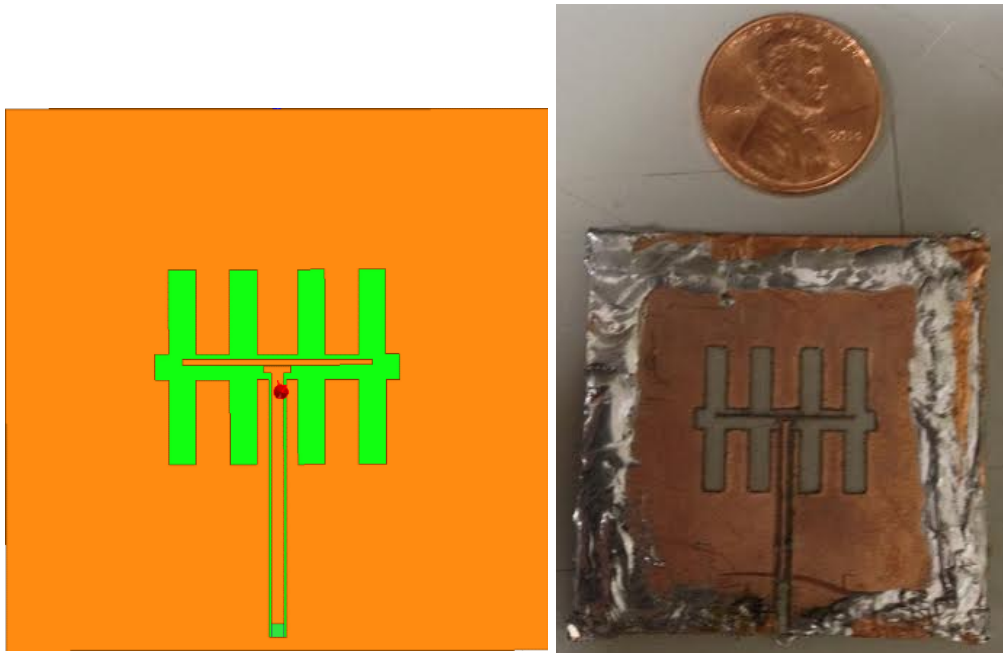

Figure 1. Cavity-backed, slot-loaded, capacitively-fed, folded-slot antenna geometry. HFSS model (left) and photograph of the prototype (right).

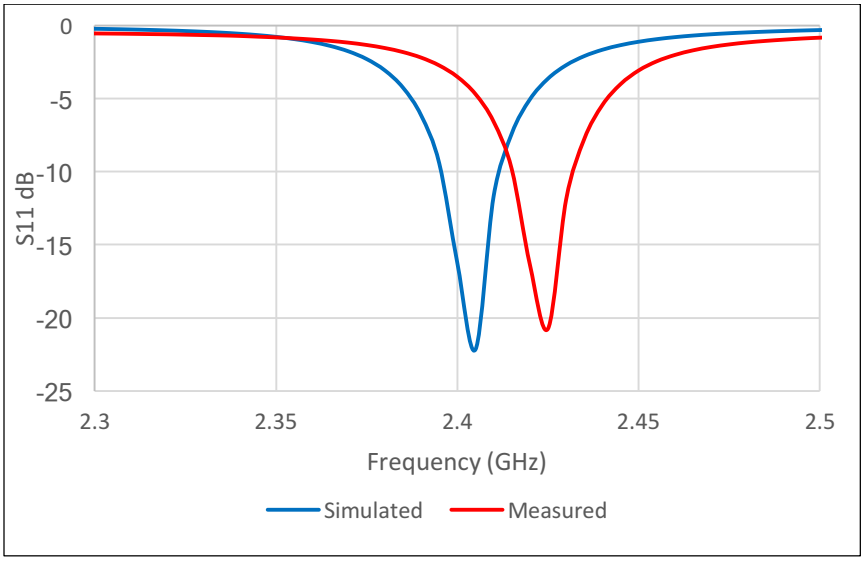

Figure 2. Reflection coefficient for the modified folded-slot in free-space, measured (red) and simulated (blue)

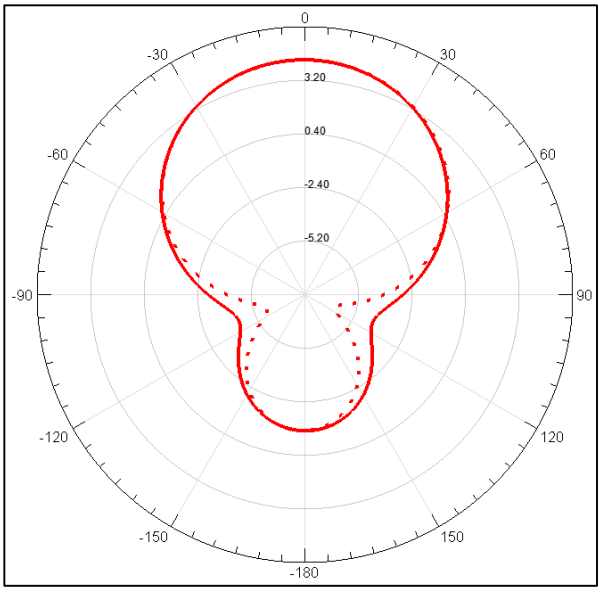

Figure 3. Radiation pattern for the modified folded-slot in free space, E-plane (dotted) and H-plane (solid). The maximum gain is 4.2 dB.

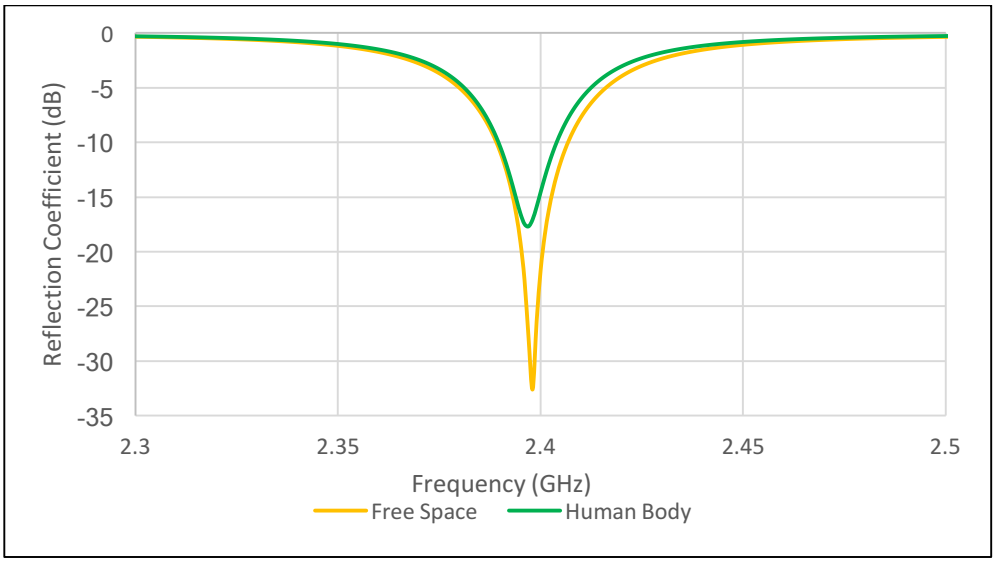

Figure 4. Reflection coefficient for the modified folded-slot in free-space (yellow) and on the forearm model (green)

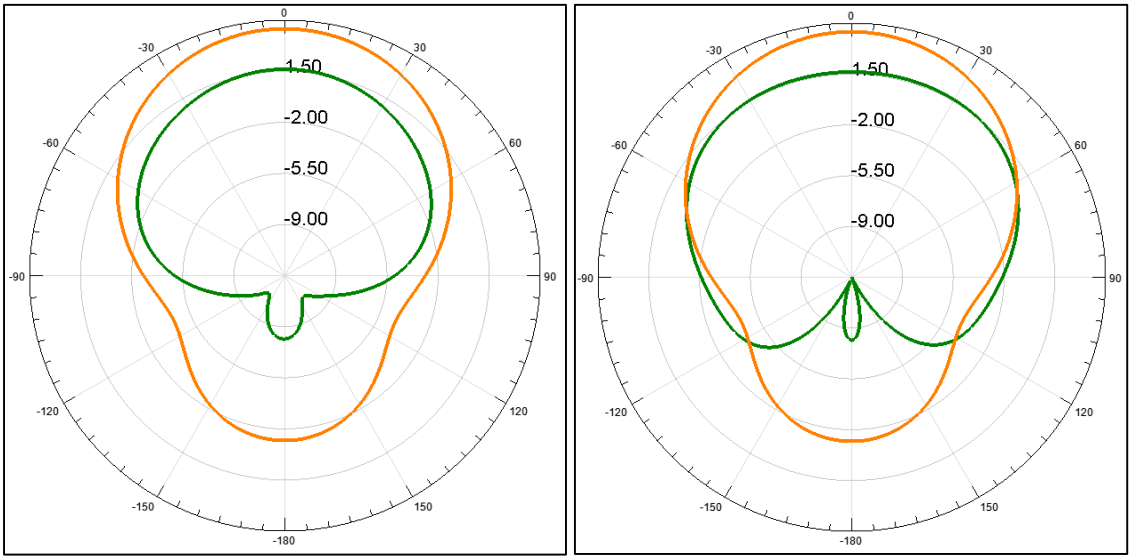

Figure 5. Radiation pattern of the modified folded-slot in free-space (yellow) and on the forearm model (green). Left plot shows the H-plane pattern and the right plot the E-plane pattern.

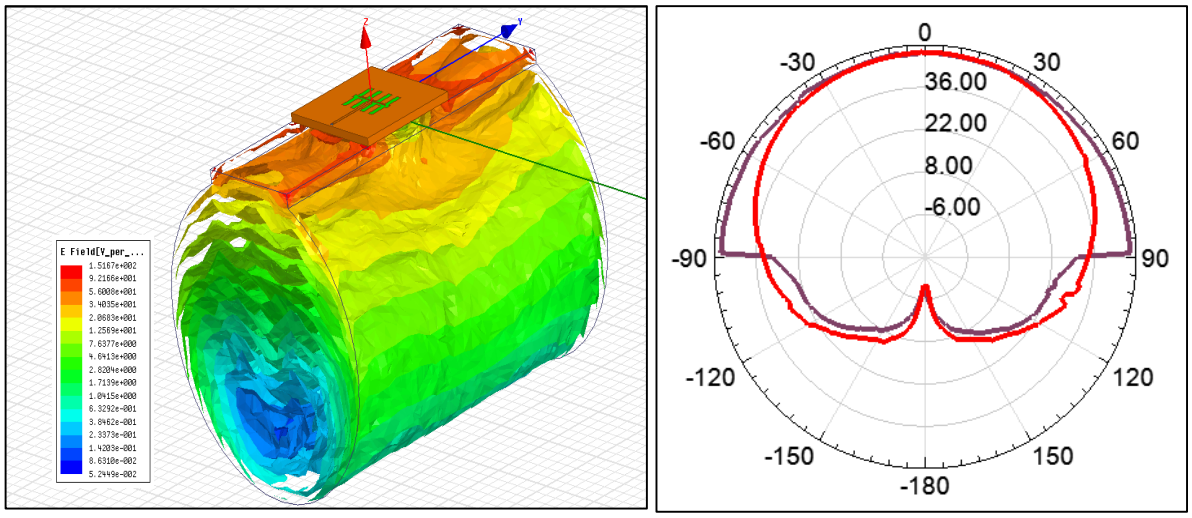

Figure 6. Electric field distribution in the forearm.

3.1.2 Inset-fed, slot-loaded quarter-wavelength patch with a parasitic slot-loaded quarter-wavelength patch

The parasitic patch configuration was designed on a Rogers RT/Duroid 5880 with a thickness of 3.175 mm and dielectric constant of 2.2. With this substrate a bandwidth of 90 MHz was obtained, 5 MHz more than desired bandwidth. The geometry is shown in Fig. 7.

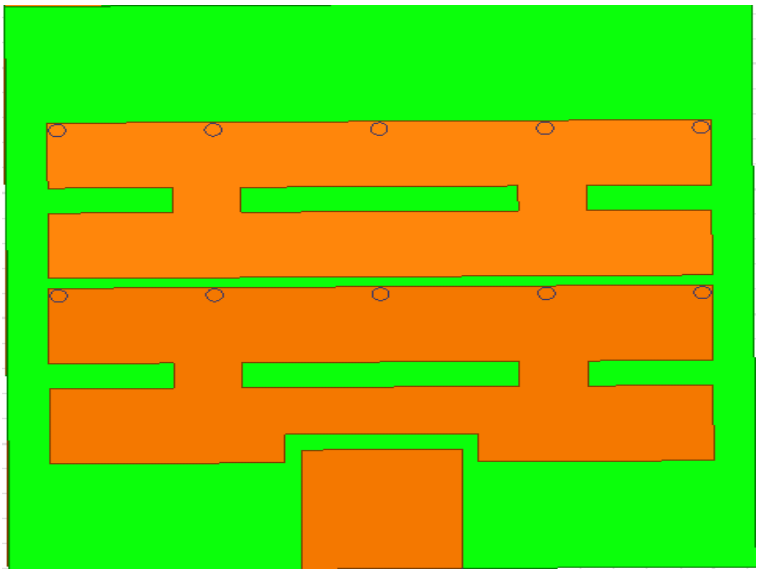

Figure 7. Slot-loaded, parasitic patch loaded quarter-wavelength patch.

The antenna was fabricated and measured, and the comparison between simulated and measured reflection coefficient is shown in Fig. 8. Fig. 9 shows the simulated radiation pattern. When the configuration was placed on the forearm model, the reflection coefficient was greatly affected, as shown in Fig. 10. The antenna was redesigned to make it less dependent on the body placement, and the reflection coefficient is shown in Fig 11. Note that the antenna exceeds the bandwidth required for

the 2.45 ISM band. Fig. 12 shows the simulated radiation pattern comparison between the modified parasitic patch in free-space and on the forearm model. Note that the body has the effect to tilt the E-plane pattern by 40 degrees due to the parasitic element.

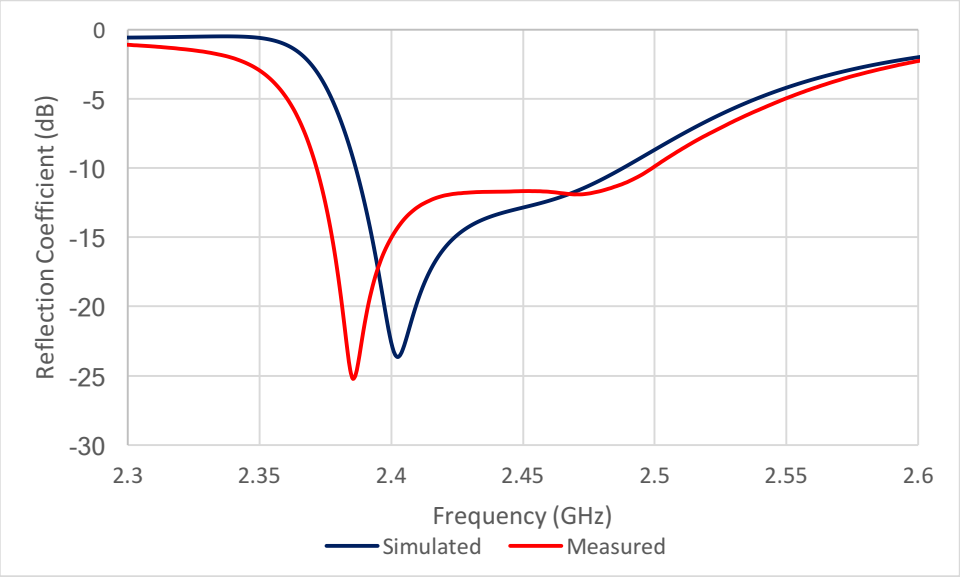

Figure 8. Reflection coefficient in dB, for the parasitic patch antenna; measured (red) and simulated (blue)

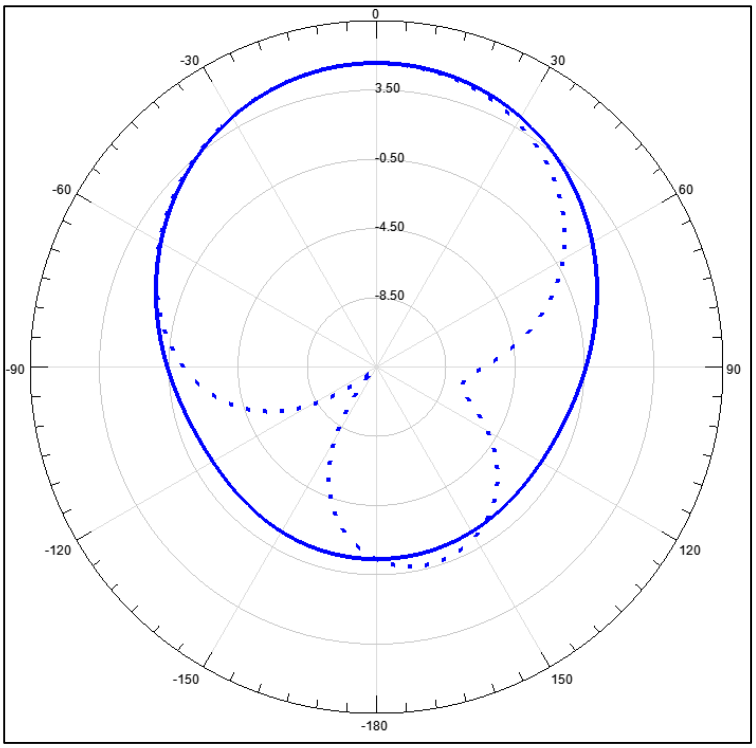

Figure 9. Simulated radiation pattern for the parasitic patch antenna; E-plane (dotted), H-plane (solid).

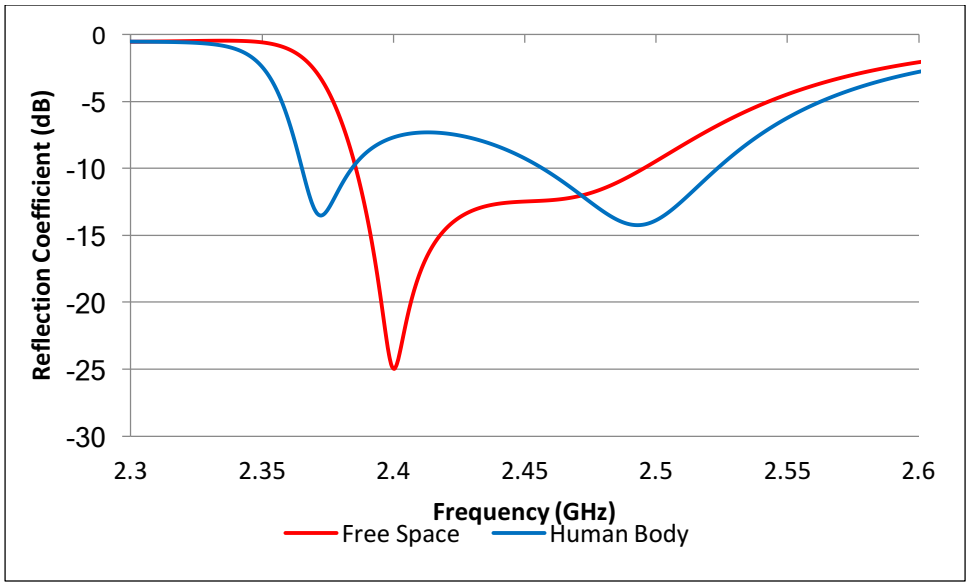

Figure 10. Simulated reflection coefficient for the parasitic patch in free-space (red) and on the forearm model (blue).

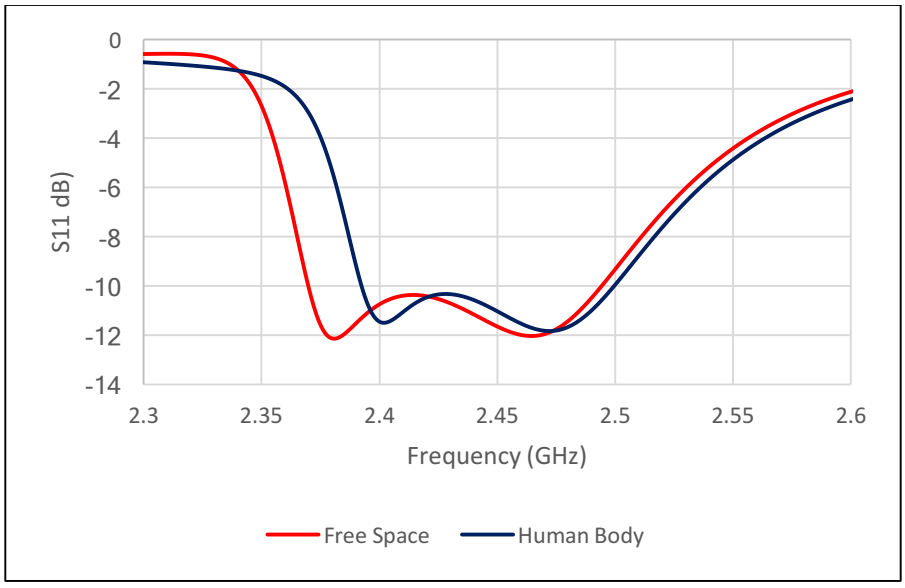

Figure 11. Simulated reflection coefficient for the modified parasitic patch in free-space (red) and on the forearm model (blue).

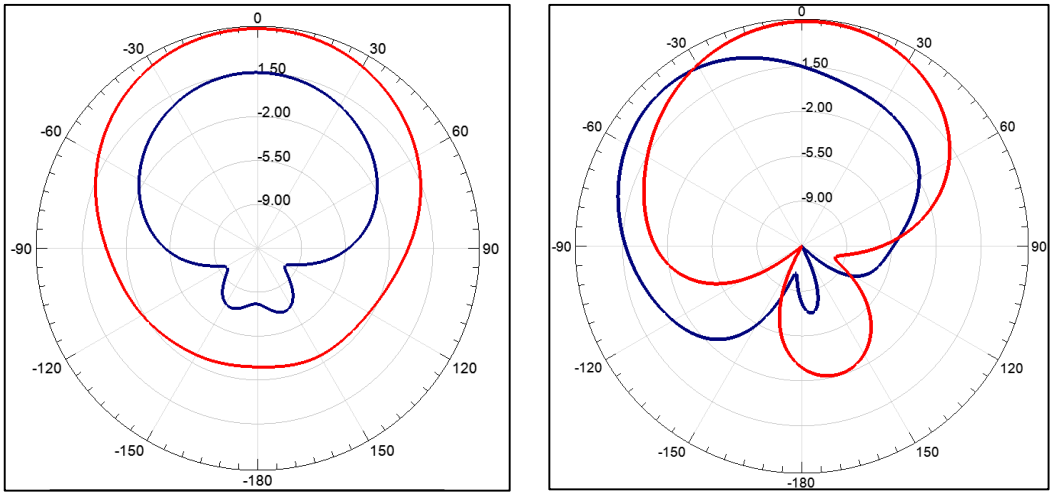

Figure 12: Free space (red) vs human body (blue) comparison in radiation pattern in, H-plane (a) and E-plane (b), for the modified parasitic patch.

3.2 ANTENNAS FOR ULTRA-WIDEBAND APPLICATIONS

After discussions with Dr. Dejan Filipovic, we examined spiral antenna configurations for our application. However, one disadvantage of these antennas is that they are inherently dispersive and can cause severe distortion for the short pulses used in UWB systems. To overcome the dispersive issue, a power spiral antenna topology was developed to have low-dispersion characteristics, and to overcome the axial ratio deterioration of the power spiral at high frequencies, a compound spiral combining an Archimedean spiral at the center and a power spiral taper at the outside is utilized. This geometry improves the frequency performance at the higher frequencies while maintaining good time domain response.

3.2.1 Compound Archimedean-Power spiral antenna

The geometry of the compound spiral antenna is shown in Figure 13. The spiral is terminated with surface mount resistors to reduce the low-frequency energy left in the antenna and reflected by the cavity. The antenna dimensions are shown in Table 1. The VSWR for the antenna is shown in Fig. 14, and the axial ratio and gain are shown in Fig. 15. Note that there is very little difference between the antenna in free-space and on the tissue model. The axial ratio is below 3dB in the desired bandwidth, and the gain shows the typical spiral behavior, with a maximum gain of 12.5 dB (in free-space) and 11.5 dB (on the tissue model). Fig. 16 shows a stable radiation pattern at 3, 7 and 10.5 GHz. The antenna was fabricated and measured. There was a problem with the connector placement in the prototype, and when measured with the 180 degree hybrid, the reflection coefficient showed a great deal of ripple. The antenna was measured as a 2-port device, to reduce the pressure on the connector caused by the hybrid, and the results are shown in Fig. 17. This shows a good agreement with the simulation, but we are working on fabricating another prototype to improve the connection at the antenna terminals.

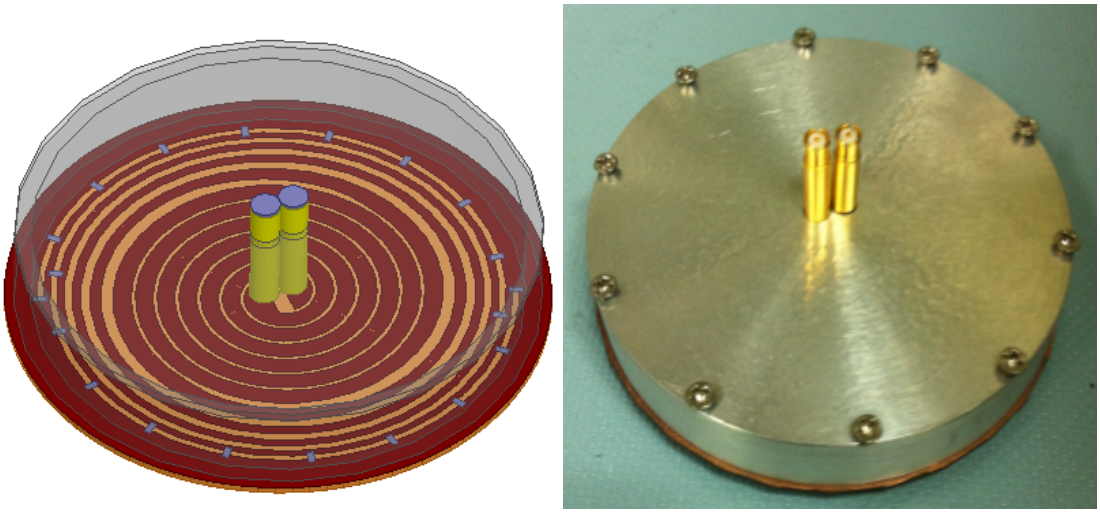

Figure 13. Antenna geometry in HFFS (left) and prototype of the compound slot spiral with a total of twenty 0603 resistors termination and cylindrical cavity. Two 50Ω SMP adapters are connected together by their outer conductor at the center of the spiral acting as the balun feed for the antenna. The antenna is fed by a 180-degree hybrid.

Table 1. Antenna design parameters

Parameters	**Archimedean spiral**	**Power spiral**
Rout	18.5 mm	27.5 mm
Rin	3.15 mm	1 mm
Growth rate (a)	0.8143	9.954
Offset Angle or SMR (δ)	35°	90°
Number of Turns (N)	3	3
Spiral coefficient (n)	Set to 1	3
Dielectric constant	2.2	
Dielectric thickness	0.79 mm	
Dielectric Diameter	64mm	
Number of arms	2	
Cavity height	10 mm	
Cavity Thickness	2 mm	
Coaxial Diameter	3.5 mm	

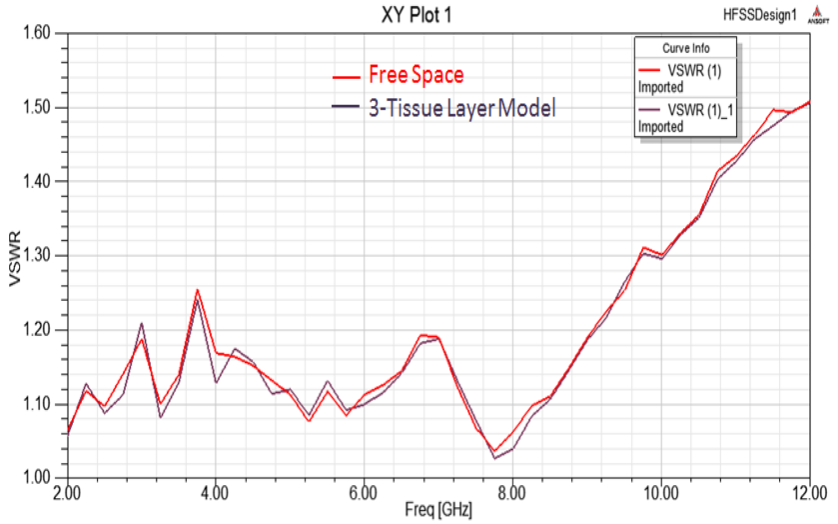

Figure 14. VSWR of cavity-backed compound spiral.

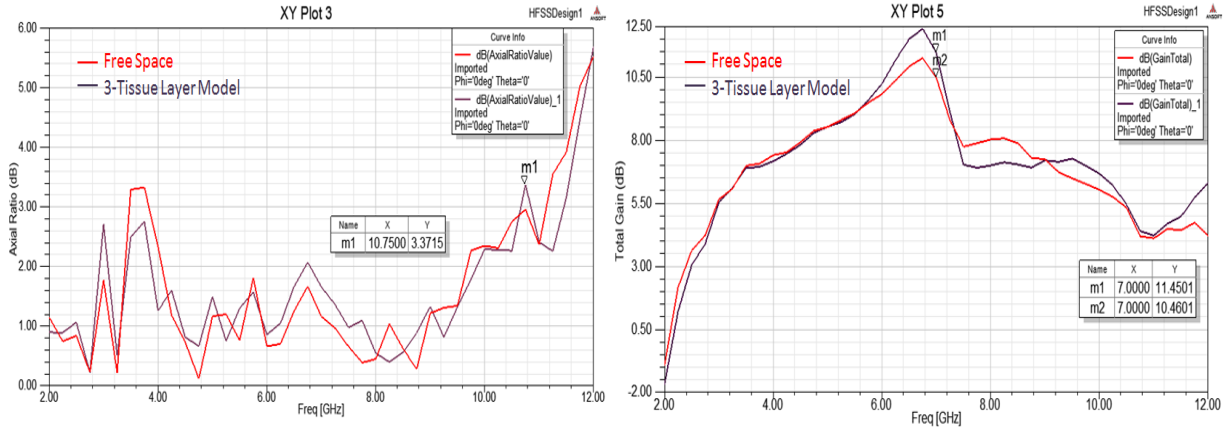

Figure 15. Axial ratio (left) and gain (right) for the compound spiral in free-space (red) and on the 3-layer tissue model (purple).

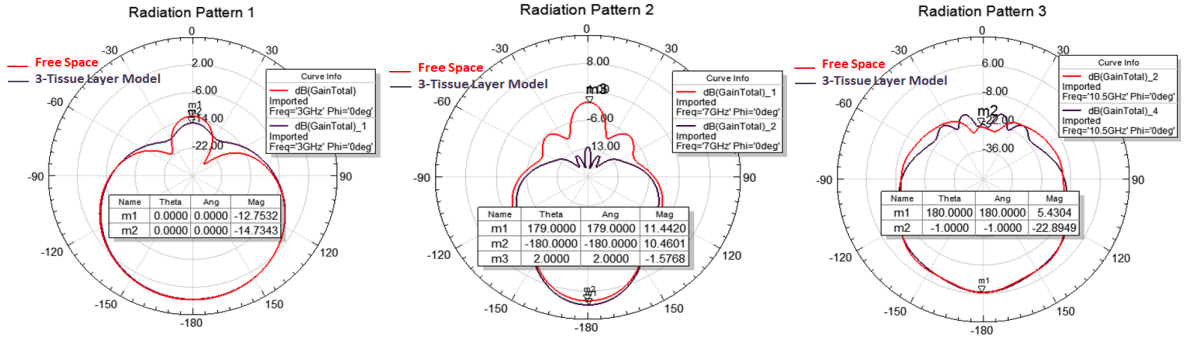

Figure 16. Radiation pattern for the compound spiral at 3 GHz (left), 7 GHz (middle) and 10.5 GHz (right)

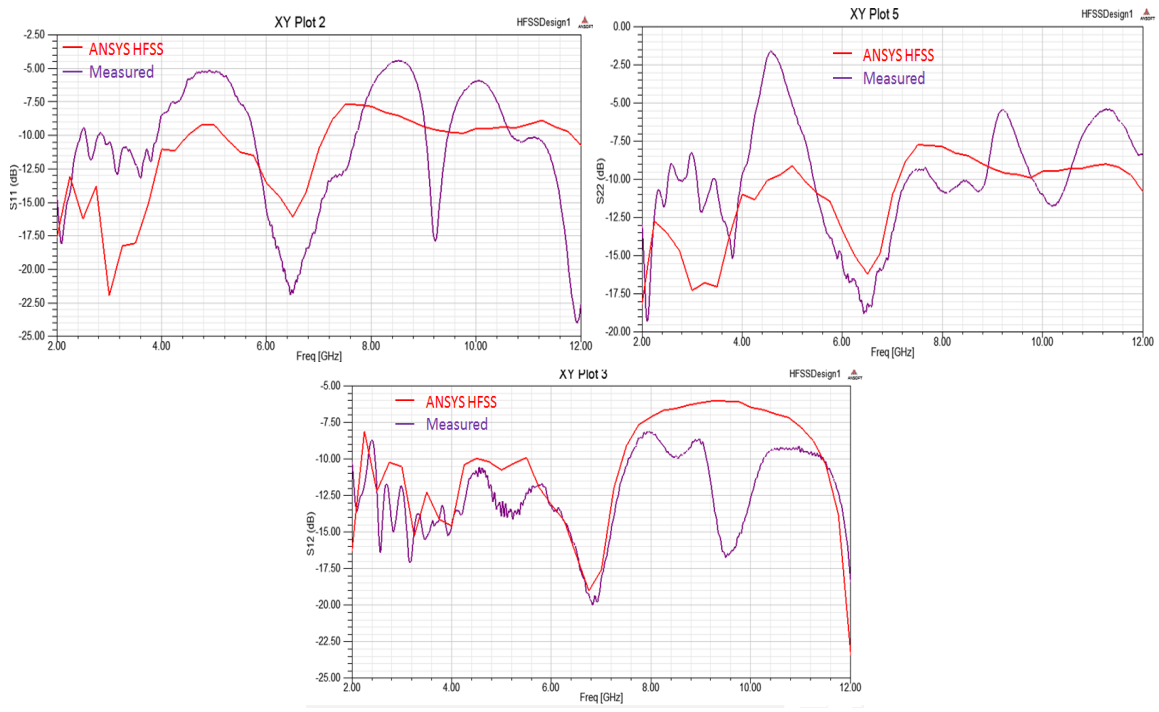

Figure 17. Individual port S-parameters for the compound spiral, measured (purple) and simulated (red). Reflection coefficients are on top, S11 (left) and S22 (right), and S21 is at the bottom

3.3 ANTENNAS FOR V-BAND APPLICATIONS

3.3.1 Linearly Polarized Array

During this year, we worked on the design of a linearly polarized 4x4 microstrip patch array at 60 GHz. We worked on the design of the array element, the feeding network, and the full array. The array was designed to be amenable to steering in one dimension, and we started the design of a Rotman lens to feed the array. Detailed findings are discussed in the following sections.

3.3.1.1 Microstrip-patch

The initial design for the radiating element comes from [1]. The design in [1] has been modified to use an SIW feeding network instead of microstrip lines, thus making this a SIW fed Aperture Coupled Microstrip Patch Antenna (ACMPA) with cavity. The substrate has been replaced with RO4350 (ε_r=3.66) and the dimensions have been adjusted accordingly to accommodate the available substrate thicknesses. Figs. 1 and 2 show the model for the SIW fed ACMPA and Table 1 summarizes the different design parameters.

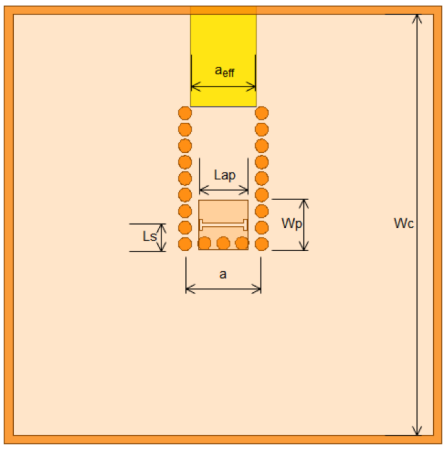

(a)

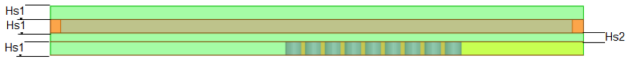

(b)

Fig. 1. (a) Top and (b) side view for the single radiating element for the SIW fed ACMPA with Cavity. The parameters shown are summarized in Table 1

The SIW feed is designed using the design rules presented in [2] and is found in the lowest substrate level, which contained the microstrip line in [1]. Equation (1), which relates the effective width of the SIW, a_{eff}, and the SIW's width measured from the vias' center, *a* using the via radius, *r*, and their separation, *p*. This relationship allows designing and exciting the SIW using the same principles as a solid rectangular waveguide of width a_{eff} [2].

$$a_{eff} = a - \frac{4r^2}{0.95p} \tag{1}$$

The SIW leads to a coupling aperture whose length and width are specified by *Lap* and *Wap* respectively. This is an 'H' shaped aperture where the bar's length is *Lap* and the H's cap height is 3 times the bar's width. The aperture is found a distance Ls from the shorting post wall at the end of the SIW. *Ls* is measured from the center of the aperture to the center of the vias that make up the post wall. The aperture couples the SIW to the layer above, which is made of a thinner substrate. Above this thinner substrate lies an air filled cavity. The cavity may be realized using either a metallic spacer, or a hollowed, metalized, substrate. Its height is equal to *Hs1* to allow the flexibility of using substrate of the same width as the first layer when building the antenna. The cavity is a square cavity with length and width *Wc*. The square patch is found on the underside of the last layer, and its length and width are given by *Wp*.

The reflection coefficient can be seen in Fig. 3. It shows that a -10 dB matching was achieved throughout bandwidth of interest and beyond. The gain at the center frequency of 60.48 GHz is shown in Fig. 4. The antenna achieved a 5.6 dBi gain.

Table 1. SIW Fed ACMPA Parameters

Parameter	Value
Hs1	0.254mm
Hs2	0.168mm
Wp	1.12mm
Lap	1.1mm
Wap	0.08mm
Ls	0.343mm
a	1.5mm
a_{eff}	1.753mm
r	0.15mm
p	0.374mm

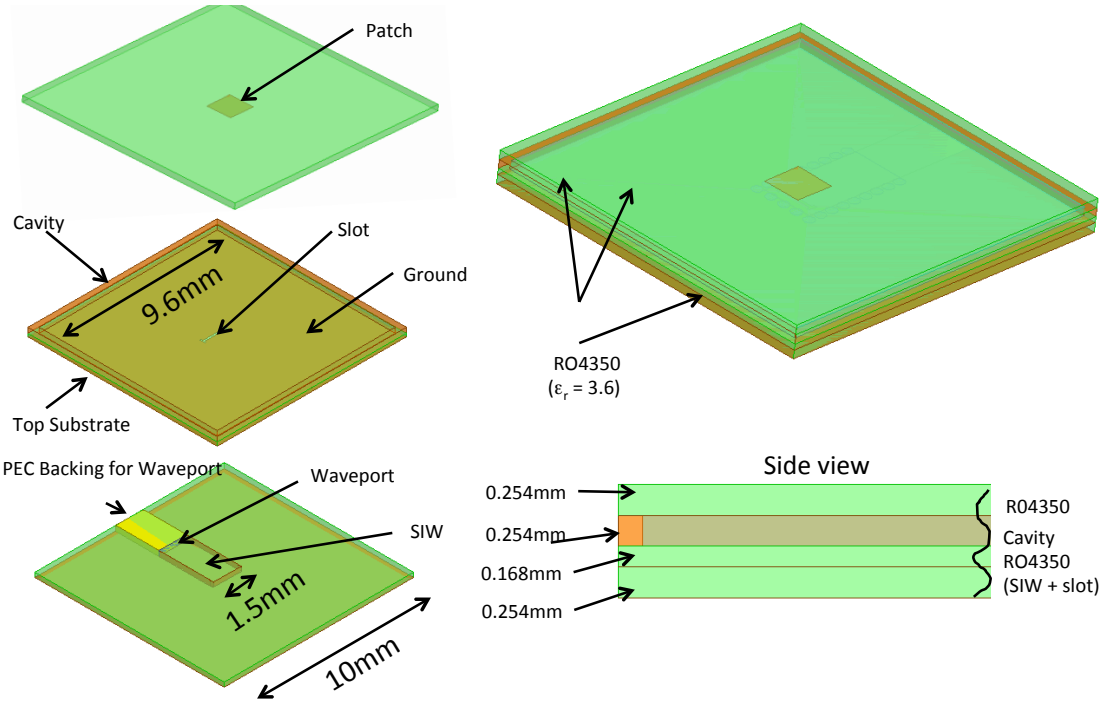

Fig. 2. (a) Top and (b) side view for the single radiating element for the SIW fed ACMPA with Cavity.

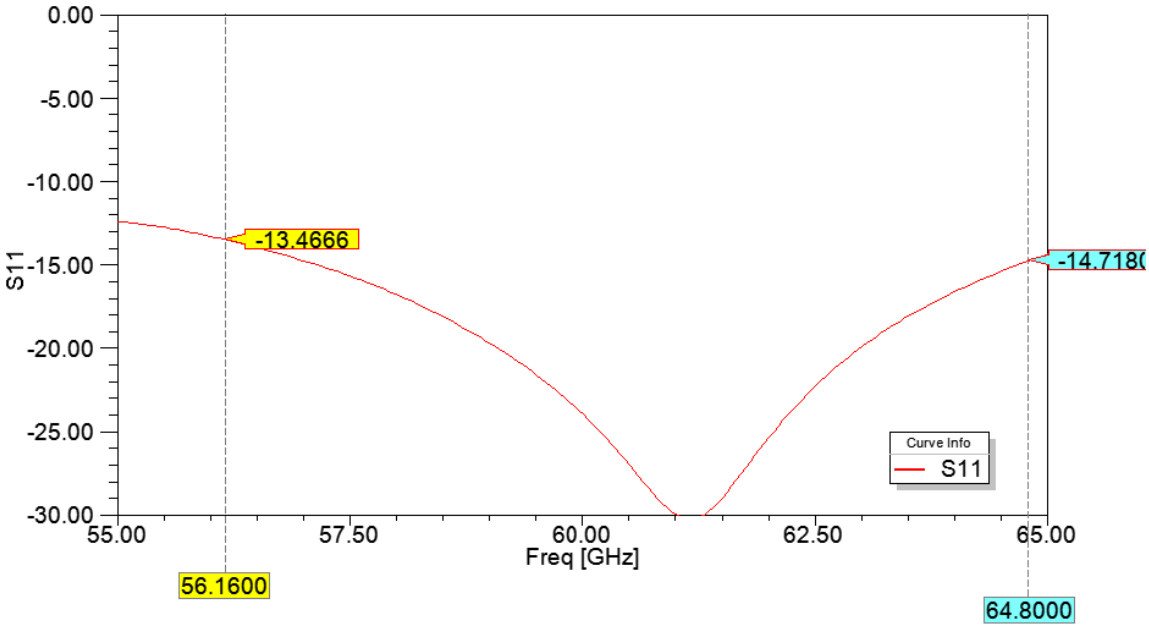

Fig. 3. Reflection coefficient for single element.

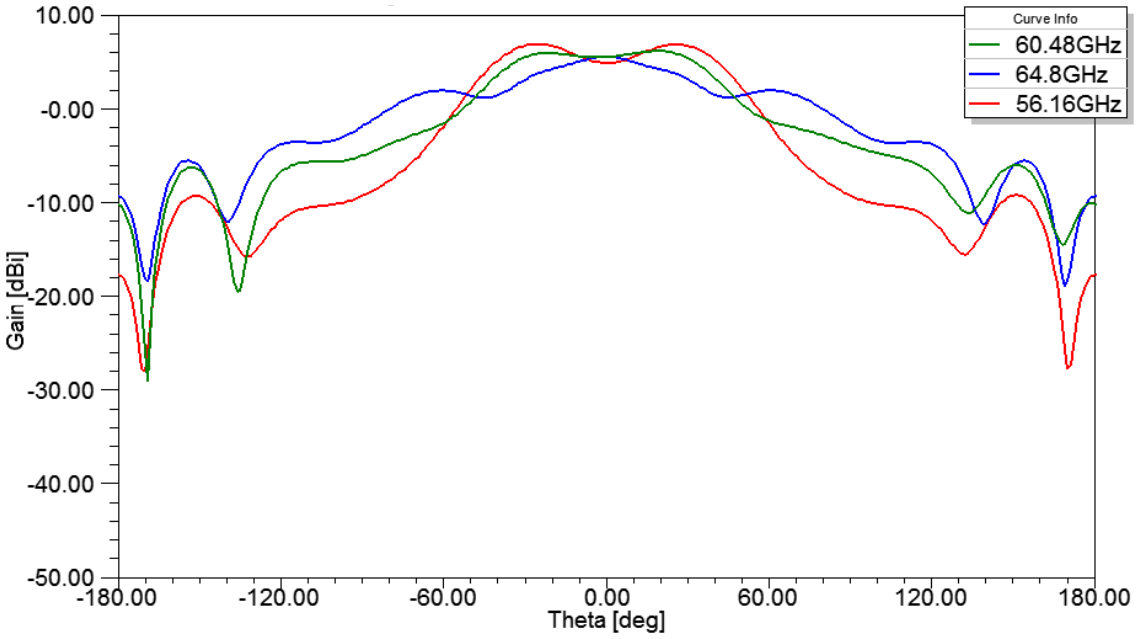

(a)

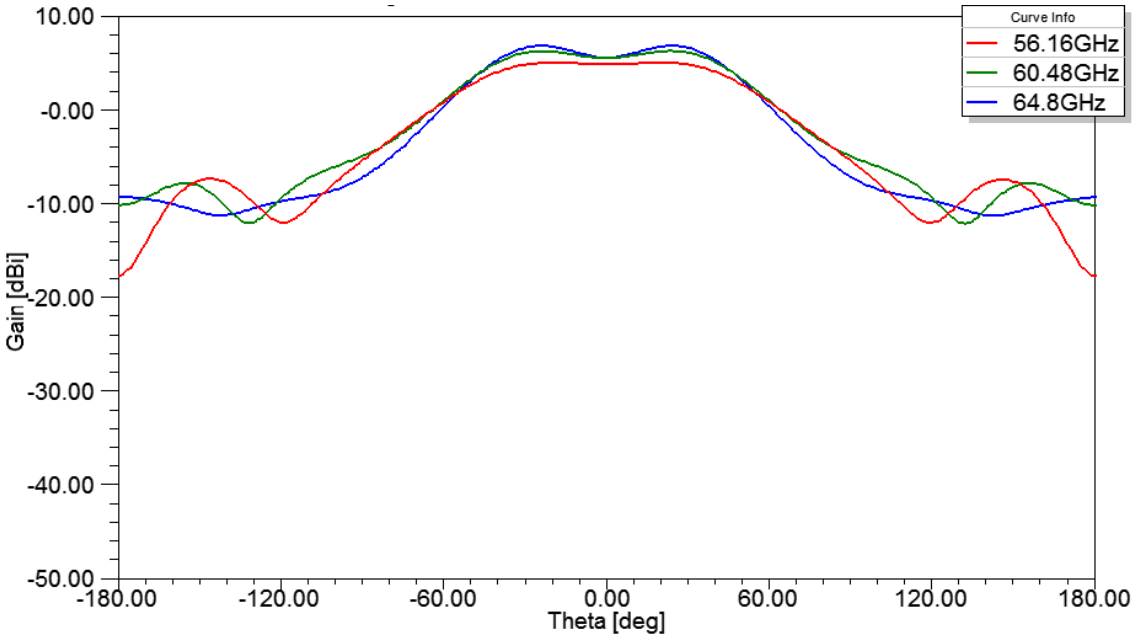

(b)

Fig. 4. E-plane (a) and H-plane (b) patterns for single element.

3.3.1.2 Vertical corporate feed in SIW

Many of the antennas arrays found in the literature use static beams, which must be aimed correctly to obtain significant range. Beam steering would allow more flexibility in this respect. In order to beam-steer, different elements or sections of the array must be excited independently but this is very difficult to do on single layers that are already packed with many SIW channels, like in [3]. Moving vertically allows more flexibility and this work presents a key component in making vertical SIW corporate feeds: the Vertical SIW T-junction (VST)

The VST using coupling slots was designed by first designing a vertical T-junction, similar to those used in [4] and [5] to double the number of elements. The slots to couple between layers in [4] and [5] are longitudinal slots in the lower layer and are matched using a matching post. To the upper layer these are transverse slots. The VST designed here does away with the matching post by terminating the SIW with a transverse slot a set distance away from a shorting post wall. This distance can be modified to accomplish appropriate matching. Matching this three-port network to the SIW within the band of interest allows combining VSTs to make corporate feeds insensitive to the length of the waveguides connecting the elements, which allows accurately spacing the elements being fed. The substrate used for the design is RO4350 (ε_r=3.66) with a thickness of 0.254 mm. Fig. 5 shows the two layers.

The SIW is designed with an effective width of 1.5 mm for a cutoff frequency of 52.2 GHz. The vias used have a radius of 0.15 mm and are spaced by 0.372 mm measured from their center. The two layers are coupled by a coupling aperture, whose length and width are 1.2 mm and 0.1 mm respectively. The

aperture is found at a distance of 0.681 mm from the shorting post wall at the end of the SIW. This distance is measured from the center of the aperture to the center of the vias that make up the post wall.

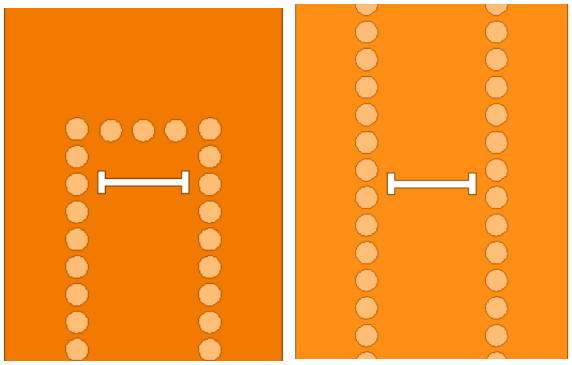

(a) (b)

Fig. 5. (a) Bottom layer, which only contains one port and the aperture. (b) Top layer, which contains 2 ports and the aperture.

We designed different transitions to provide a better match between layers. Therefore, we designed a transition from a 0.254 mm thick substrate to another 0.245 mm substrate, a transition from a 0.254 mm to 0.508 mm, and a transition from 0.508 mm to 0.762 mm. All of them provided good matching and output balance. Table 2 gives the dimensions for the different transitions, and the s-parameters for each case can be seen in Fig. 6. Note that the maximum imbalance is about 0.5 dB, and the maximum loss is about 1.5 dB. Matching is excellent for all cases.

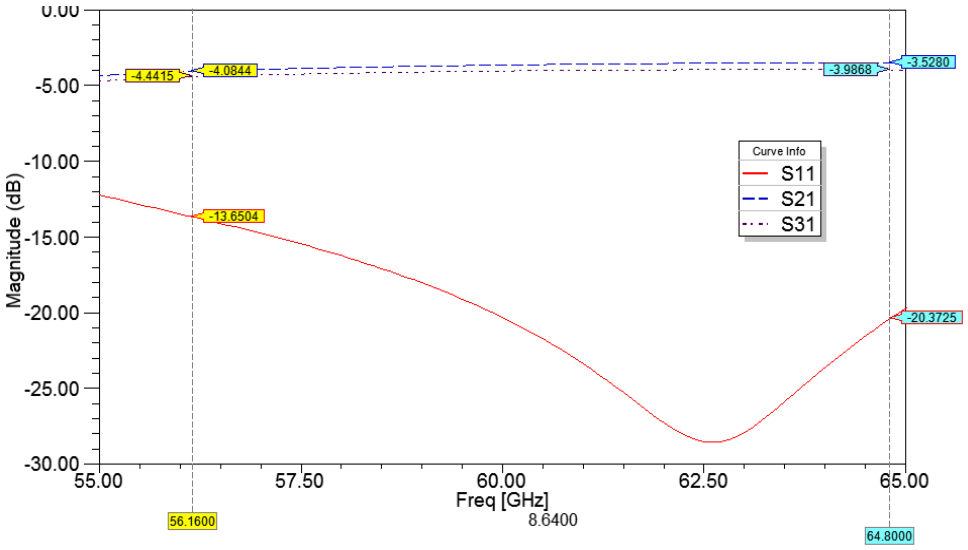

(a) 254µm to 254µm transition.

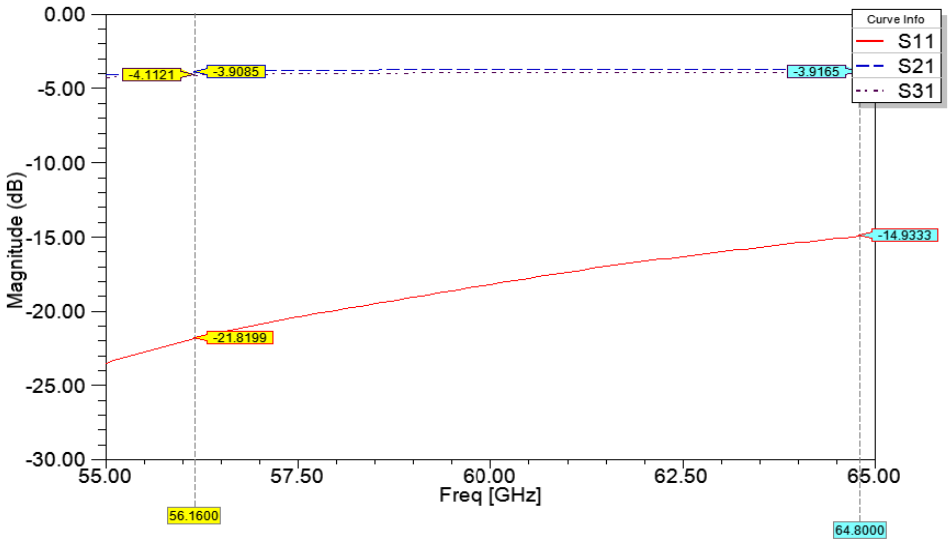

(b) 254µm to 508µm transition

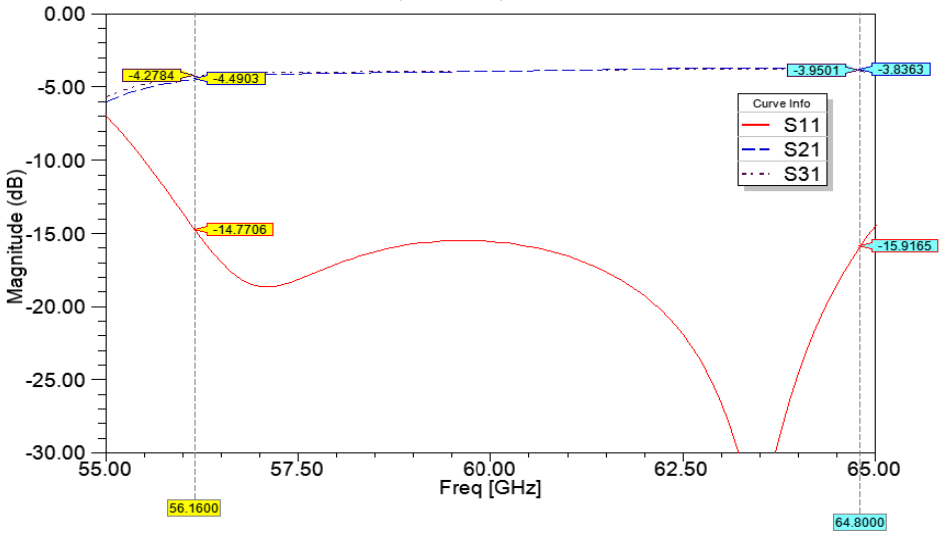

(c) 508µm to 762µm transition.

Fig. 6. S-parameters for different transitions designed

The transmission and reflection coefficients can be seen in Fig. 6. The reflection coefficient shows an excellent match with a value of less than -10 dB from 53.1 GHz to 69.5 GHz, or a 26.9% bandwidth, and a -15 dB bandwidth from 57.9 GHz to 67.0 GHz, or 14.5%. The difference between the transmission coefficients for the two symmetrical ports is less than 0.5 dB throughout the band.

Table 2. Design values for the different transitions designed

Combination	**Lap (mm)**	**Wap (mm)**	**offset (λ_g)**	**a_{top} (mm)**	**a_{bot} (mm)**
254µm to 254µm	1.2	0.10	0.111	1.5	1.5
254µm to 508µm	1.0	0.14	0.050	1.5	1.5
508µm to 762µm	0.9	0.12	0.450	1.5	1.6

3.3.1.3 4x1 subarray

In the design of the array, we found that the thinner substrate transitions would not give us the desired bandwidth. Therefore, we started with the thicker substrate in the bottom (0.762 mm), and ended with the thinner substrate (0.254 mm) to provide the required bandwidth. This is shown in Fig. 7. In addition, we had to change the offset of the coupling slot with respect to the SIW short-circuit to improve the matching. We chose a 0.5 mm offset to complete the matching of the array. The reflection coefficient for different offsets is shown in Fig. 8, and the resulting radiation pattern in Figs. 9 and 10.

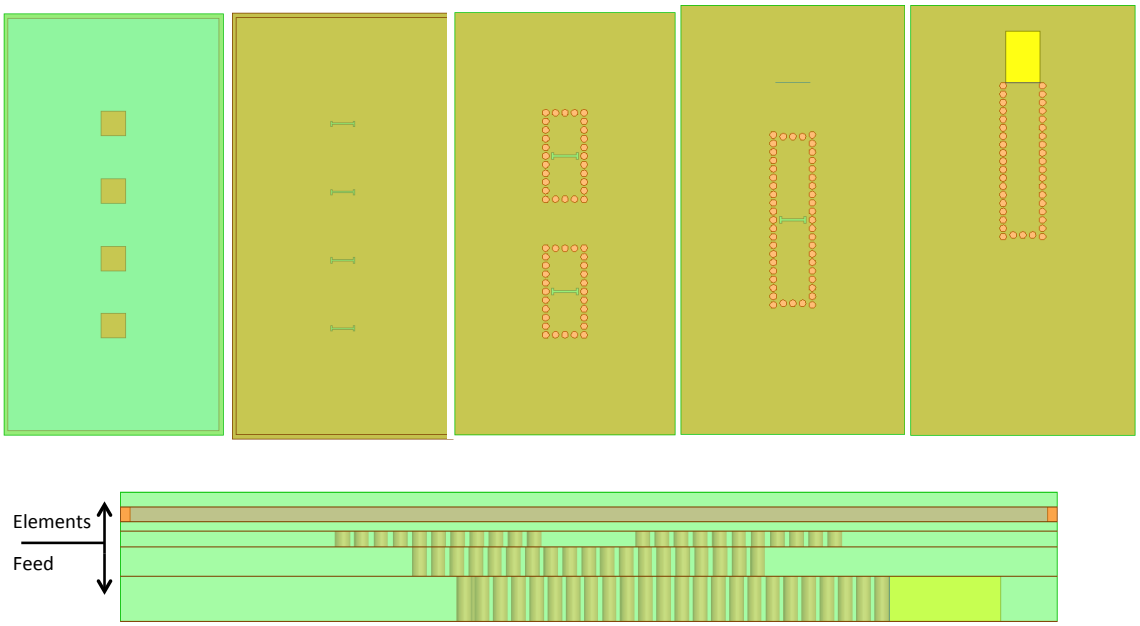

Fig. 7. Layout for the 4x1 sub-array. Layers from patches to SIW feed (top) and substrate cross-section (bottom)

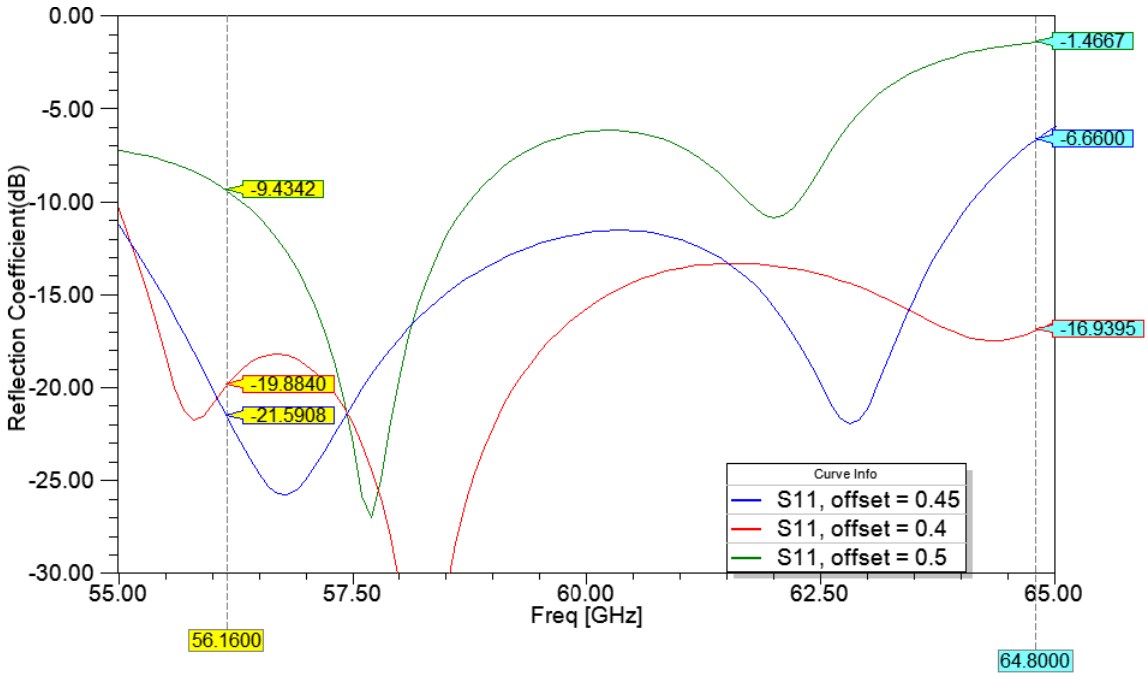

Fig. 8. Reflection coefficient for 4x1 sub-array, for different offsets in the slot location in the transition. The 0.5 mm offset was finally used in the design.

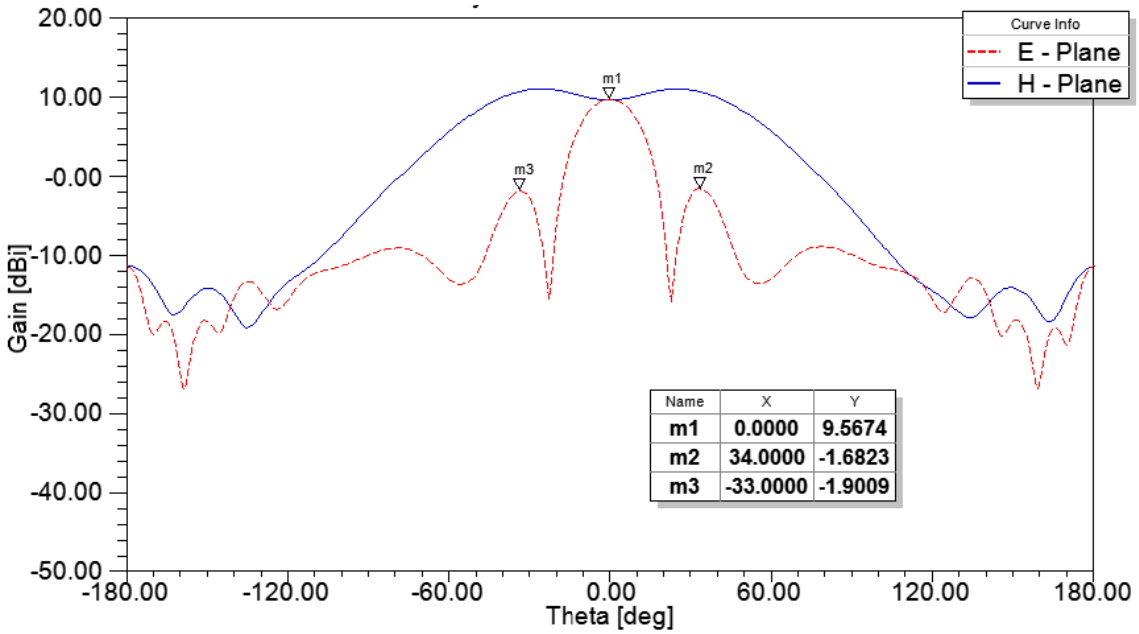

Fig. 9. Gain pattern for the 4x1 array.

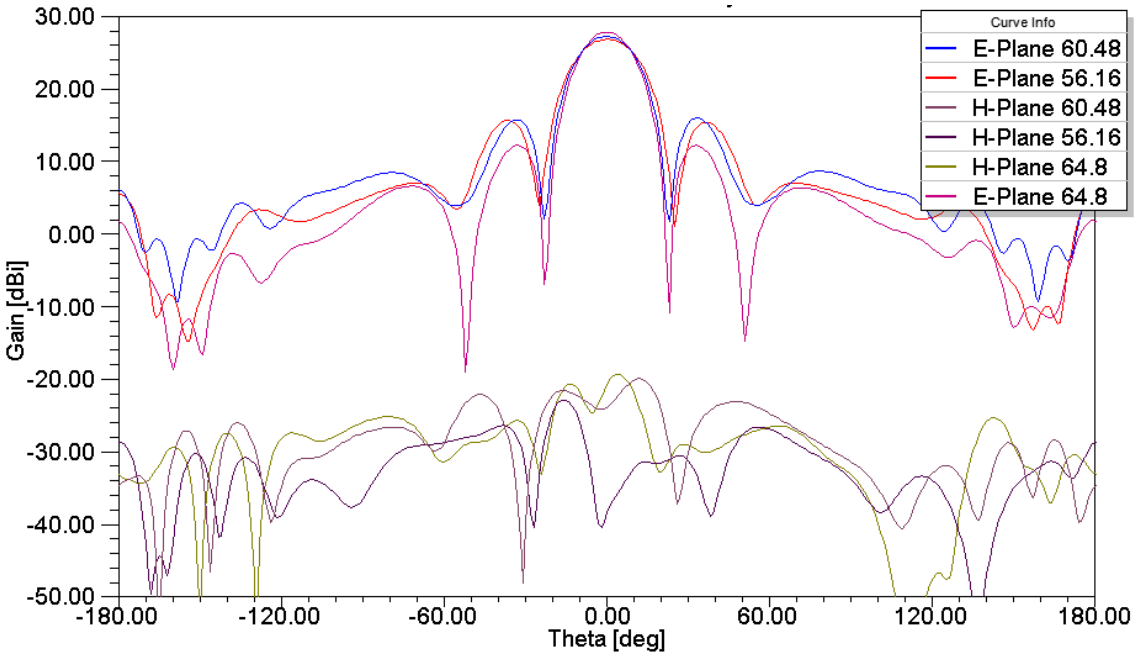

Fig. 10. Gain and cross-polarization in the E-plane as a function of frequency.

3.3.1.4 4x4 array

The complete 4x4 element array was simulated in HFSS, and the layout shown in Fig. 11. The results for the reflection coefficients can be seen in Fig. 12. All four ports are successfully matched to the 14.25% bandwidth of interest. Furthermore the array gain can be seen in Fig. 13. The array achieved a gain of 17 dBi when radiating at broadside. Fig. 14 includes the patterns along the H-plane when the array is excited with a linear phase delay of 60° and 120°. Each lobe can be found at -15° and -30° from the vertical and have a gain of 16.7 dBi and 15.9 dBi respectively. The 120° delay pattern shows a grating lobe located around 60°, which has a gain of 7.5 dBi. Table 3 summarizes the pattern properties as a function of frequency. Our group is working on a Rotman lens implemented in SIW, to feed this array in a off-body BAN application.

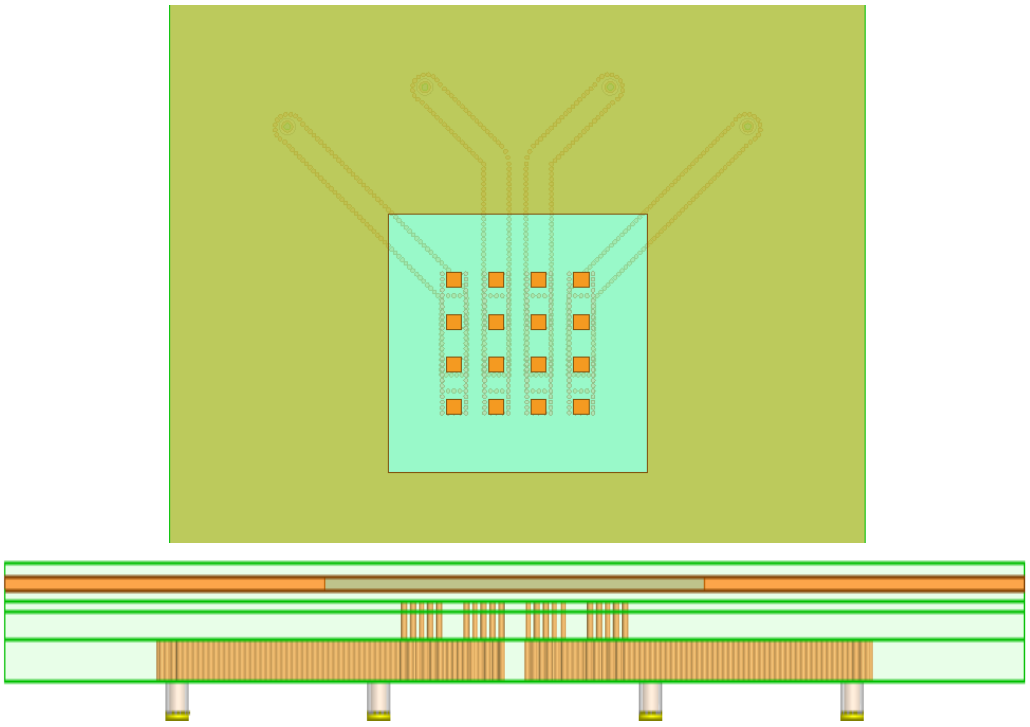

Fig. 11. 4x4 array layout. Top view (top), and cross-section (bottom)

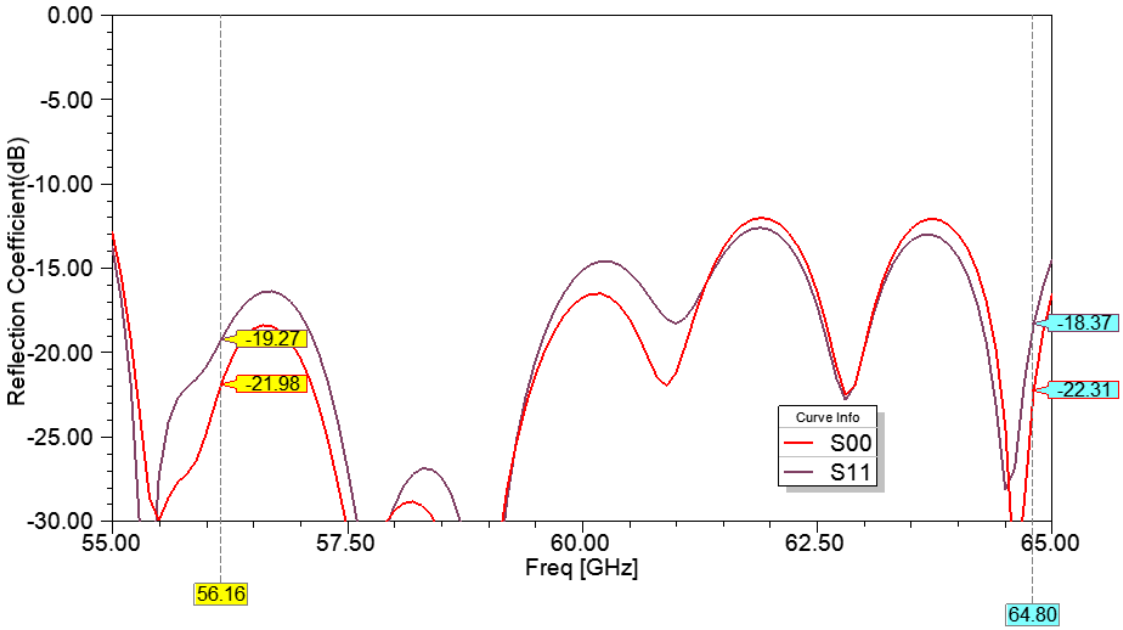

Fig. 12. Reflection coefficient for the 4x4 array. Only two ports are shown due to symmetry.

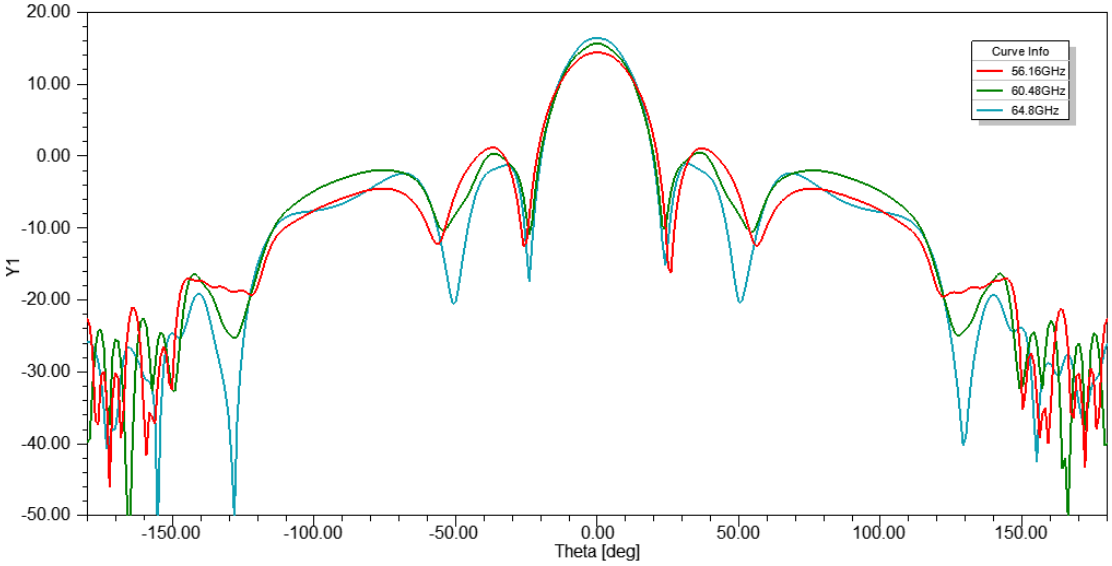

(a) H-plane pattern

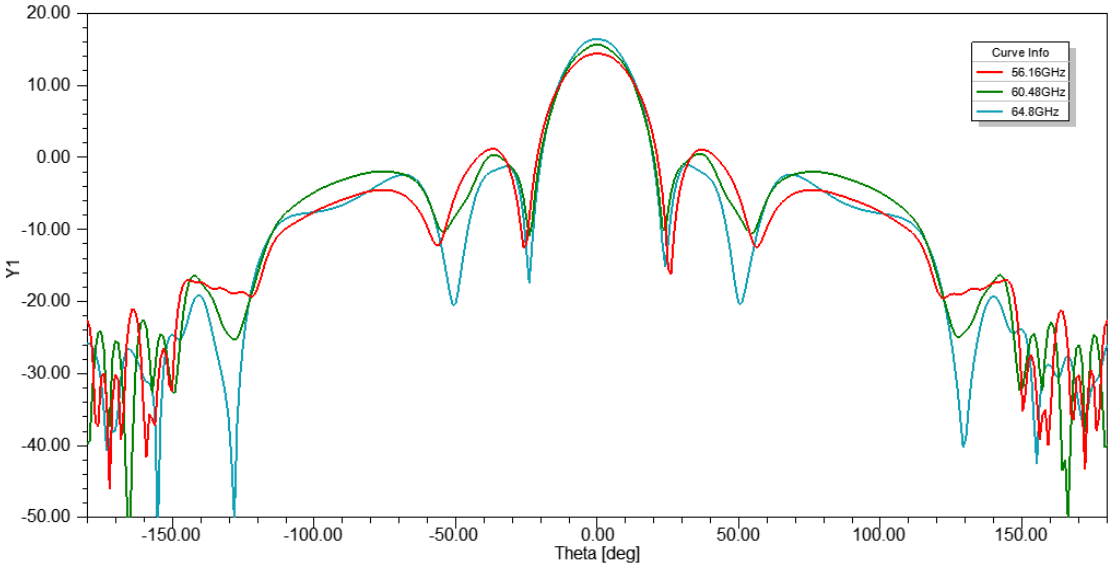

(b) E-plane pattern

Fig. 13. 4x4 array gain pattern as a function of frequency

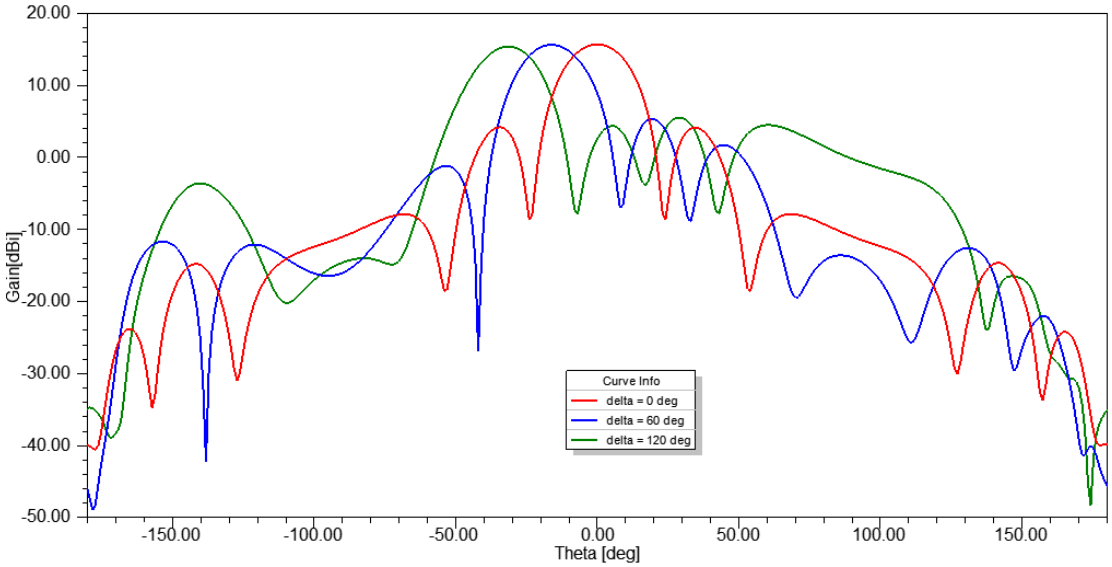

Fig. 14. Gain pattern while scanning on the H-plane at 60 GHz.

Table 3. Summary of Gain Pattern Characteristics

Frequency (GHz)	56.16	60.48	64.8
Gain (dBi)	**14.35**	**15.63**	**16.35**
Directivity (dBi)	18.11	18.84	19.17
Efficiency (%)	42.07	47.75	52.24
E-Plane-3 dB Beamwidth (deg)	22.31	21.91	22.07
H-Plane -3 dB Beamwidth (deg)	**23.06**	**22.37**	**21.02**
E-Plane SLL (dB)	13.20	15.29	17.66
H-Plane SLL (dB)	12.13	11.41	11.5

Delta	**Main Lobe Angle**	**Gain (dBi)**
0°	0°	**15.62**
60°	-15°	**15.55**
120°	-31°	**15.33**

We are ready to send the antenna for fabrication, and should do this in the next month. We planned to fabricate the antenna before the summer period, but the company could not deliver the prototype in time for measurements for the thesis defense of the student.

3.3.1.5 Human body effects

There are not many studies of BANs at 60 GHz, however, [6] is a good example of a study of the effects of skin on a broadside radiating antenna for use in off body communications. Their results are encouraging evidence for the resistance of broadside radiating antennas to the effects of the human

body. In their antenna the ground plane acts as a shield, which helps isolates the microstrip line and patch elements from the skin. Conversely, this also reduces the incident power density (IPD) on the skin, which is limited to $20mW/cm^2$ by the International Commission of Nonionizing Radiation Protection. The antenna shown in [6] complies with this standard at all separations from the phantom.

The design used was a 2^k factorial design with 3 parameters. The parameters are: HFSS solution frequency, antenna type (single element or array), and presence (or absence) of skin. The solution frequency will be varied to show that the results obtained are not dependent on the frequency at which the mesh is made. The antenna type is changed to determine if the skin affects the single element and the array differently. The outputs observed are: the bandwidth, gain, and the front-to-back (FB) ratio. The bandwidth will be determined by observing the reflection coefficient within the frequencies of interest (56.16 GHz to 64.8 GHz). The value for the bandwidth response will be capped at 8.64 GHz, which implies that the antenna has met the minimum requirements for bandwidth. The antenna gain and FB ratio will be measured at the center frequency.

The antenna to be used in this work is a Substrate Integrated Waveguide (SIW) fed, cavity backed, aperture coupled microstrip patch antenna (ACMPA). This antenna is part of a system being designed for BAN off-body communications. The initial design for the radiating element and antenna comes from [1]. The design in [1] has been modified to use an SIW feeding network instead of microstrip lines. The fields in microstrip lines flow in and out of the substrate, and the line electrical properties would be heavily influenced by the skin pressed against it [7]. Substituting microstrip line for SIW, described in [8], is meant to keep the electromagnetic energy isolated from the skin.

A homogeneous skin model was used to model the human body. The homogeneous model was demonstrated in [9] to be sufficient because the strong absorption in the skin impedes interaction with the layer of fat below the dermis. In order to model the skin within HFSS, a material with the appropriate properties was defined. The block of skin is 5 mm thick, which, according to [9], is enough for almost complete power dissipation within the skin. The antenna is placed directly on top of the skin model without leaving any space in between.

The analysis for bandwidth showed that, within the band of interest from 56.16 GHz to 64.8 GHz, the bandwidth remains unaffected by the factors analyzed. Fig. 15 shows the bandwidth for the array with and without skin and how little the reflections are affected by the presence of skin behind the antenna. The radiation pattern for the 1x4 array is shown in Fig. 16, and Fig. 17 shows the field distribution in the skin under the antenna.

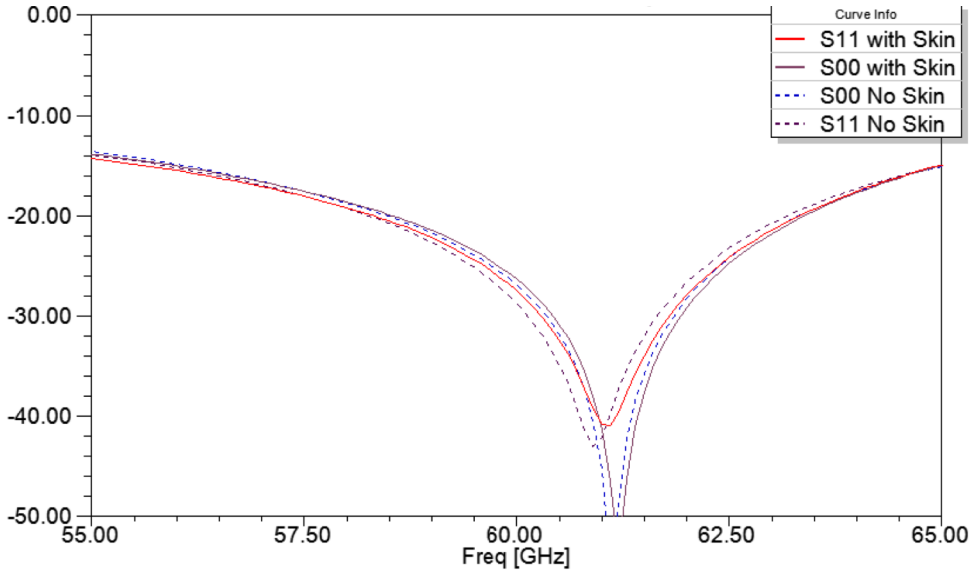

Fig 15. Reflection coefficient for the 4x1 array with and without skin. Only ports 0 and 1 are shown. Ports 2 and 3 have symmetric results.

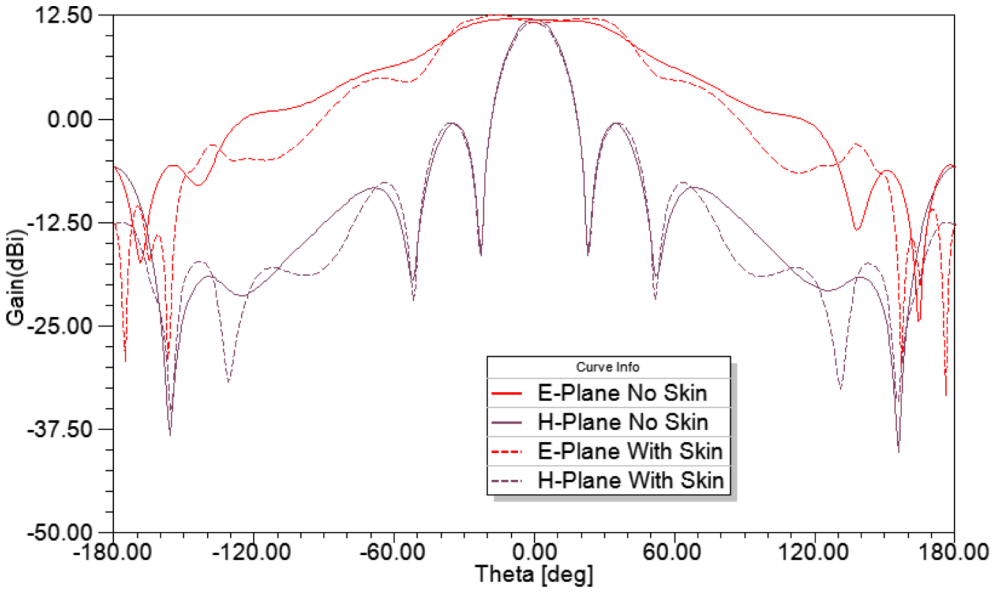

Fig 16. Radiation pattern for the 4x1 array with and without skin

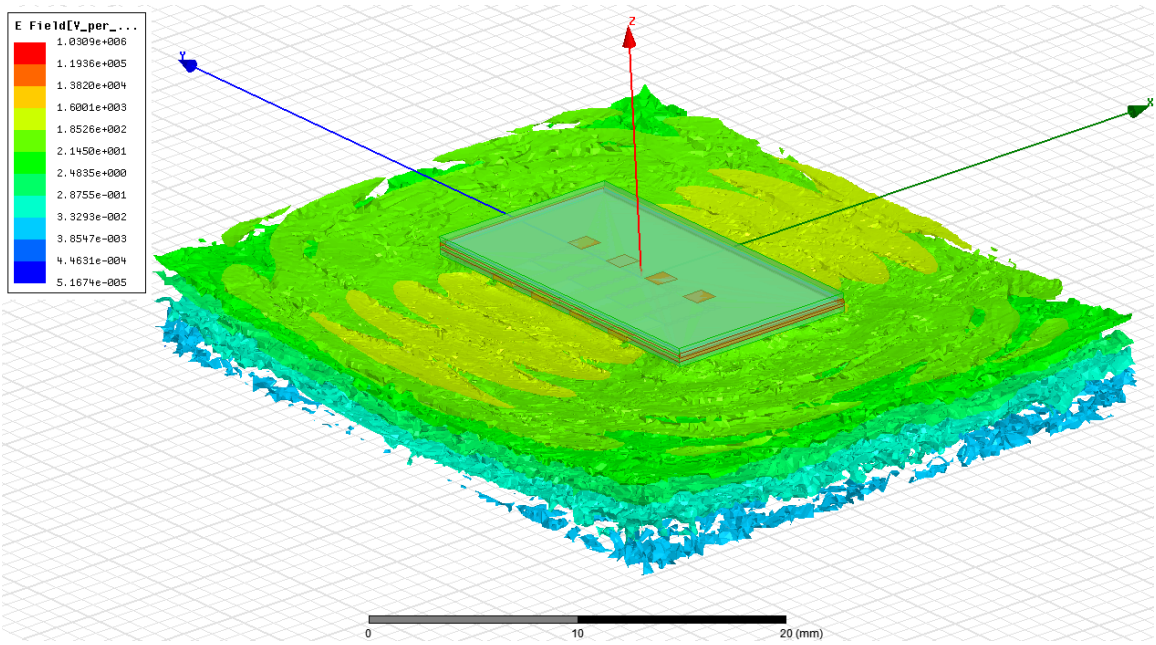

Fig 17. Field distribution in the skin for 4x1 array

3.3.1.6 Rotman lens

We started the design of a Rotman lens to feed the 4x4 array. This is a work in progress, and although the reflection coefficient still needs some work, the phase distribution obtained is nearly linear. Fig. 18 shows the lens design curves and layout. Fig. 19 shows the reflection coefficient for the different input ports, and Fig. 20 shows the phase distribution for the lens.

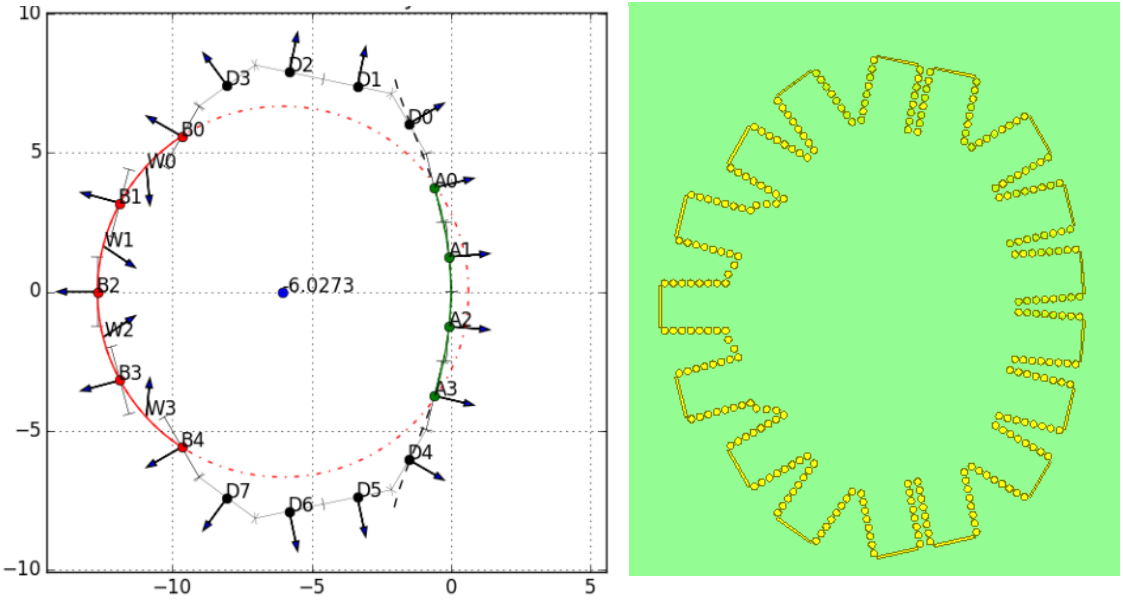

Fig 18. Rotman lens design and layout

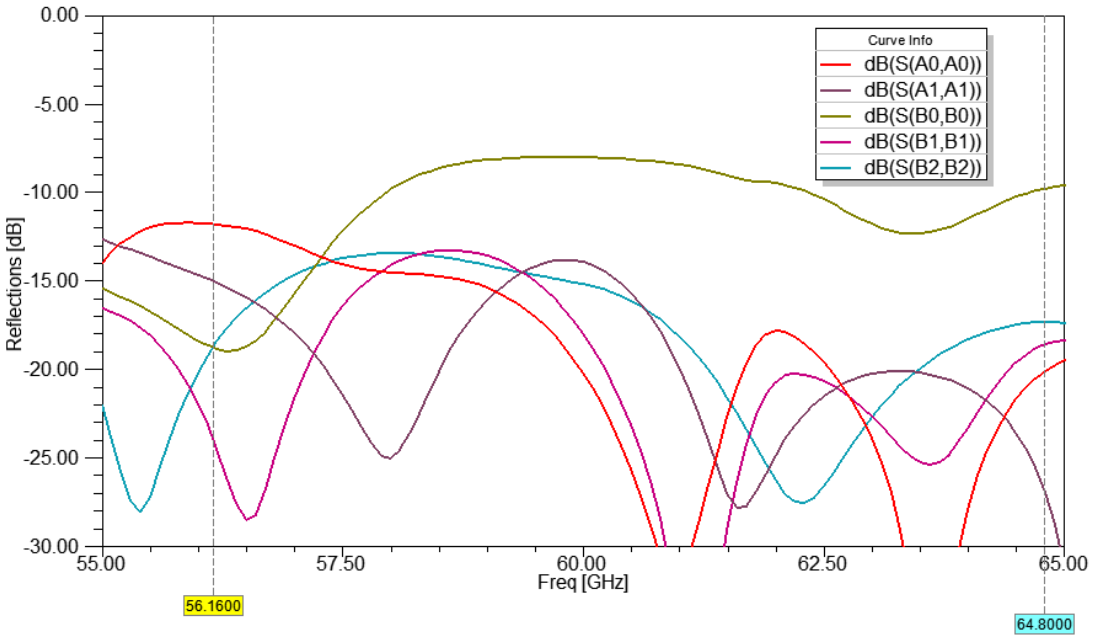

Fig 19. Reflection coefficient for the lens input and output ports. Only 5 ports are shown due to symmetry.

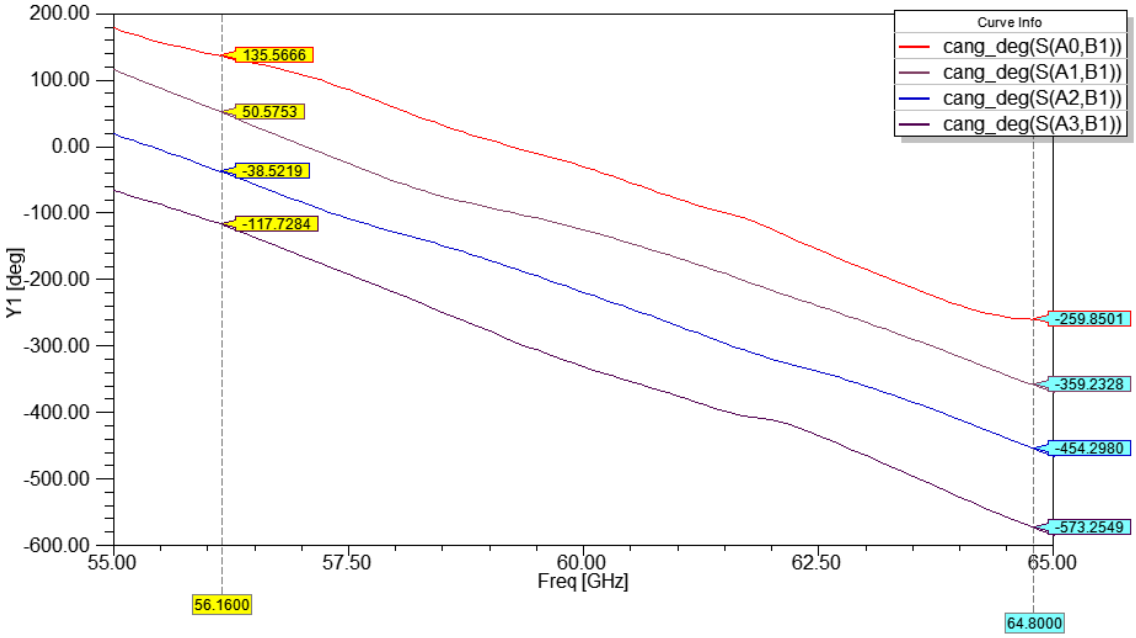

Fig 20. Transmission coefficient phase distribution from port B1

3.3.2 Circularly Polarized Antennas

We designed a circularly-polarized, cavity-backed, multi-layer, aperture-coupled patch, that was used for the design of a 2x2 sequentially-rotated array, to increase the axial ratio bandwidth. We looked into the IEEE 802.11ad and the FCC 13-112 bands for the designs. We also studied the effect in gain and bandwidth of using linear and circular polarized elements in sequentially rotated arrays.

3.3.3 Multi-layer microstrip patch

The initial design for the SIW-fed cavity-backed aperture coupled antenna is based on the work in [10]. The design in [10] was chosen as a starting point due to their wideband impedance bandwidth, and the feed method used to reduce the skin effect on the antenna in BAN applications. The single element impedance bandwidth in [10] was 14.29% from 56.16 GHz to 64.8 GHz. The antenna achieved a broadside gain of 5.58 dBi. The design in [10] was modified to produce circular polarization and to increase the gain by changing the top substrate height. The substrate shared by both patches is Rogers RO 5880 ($\varepsilon_r = 2.2$), instead of air, to reduce the total physical height for maximum gain Fig. 21 shows the antenna model and the design parameters for the circularly polarized patch.

The feeds used in the models shown Fig. 21 were dielectric-filled waveguide, and SIW. The SIW via hole radius, r, is 0.15 mm, the distance between vias, p, is 0.403 mm, and the SIW width, a, is 1.705 mm. The SIW feed design follows [10], which relates the SIW dimensions with the width of a dielectric-filled rectangular waveguide of width a_{eff} [11],

$$a_{eff} = a - \frac{4r^2}{0.95p} \qquad (2)$$

where, a_{eff} is the rectangular waveguide feed width, a, is the SIW width, r, is the radius of the vias, and p, is the distance between vias.

Circular polarization with a single feed point can be achieved using different methods, as discussed in [12]. However, these methods produce narrowband axial ratio (AR) bandwidth. Because of the limited AR bandwidth these methods, the proposed antenna element combines two different methods to improve the axial ratio; truncating one corner of the patch and introducing a diagonal slot on the patch. The dimensions of the truncated corner are initially found through the following equation,

$$d = \frac{\sqrt{w_p^2 + L_p^2}}{2} - L_c \qquad (3)$$

where, d, is the distance between the middle of the patch to the center of the corner cut, W_p and L_p are the patch width and length, respectively, and L_c is the cut distance perpendicular to the cut.

The conventional placing of the slot is centered at the patch center, and rotated $45°$ from the horizontal. By varying the rotation of the slot in the truncated patch, it is possible to increase the AR bandwidth for the element. The proposed antenna has an improved AR bandwidth by rotating the slot only $15°$ from the horizontal. Both the fed and parasitic patches modified by the corner truncation and addition of the slot, to increase the AR bandwidth, as well as the gain for the antenna element.

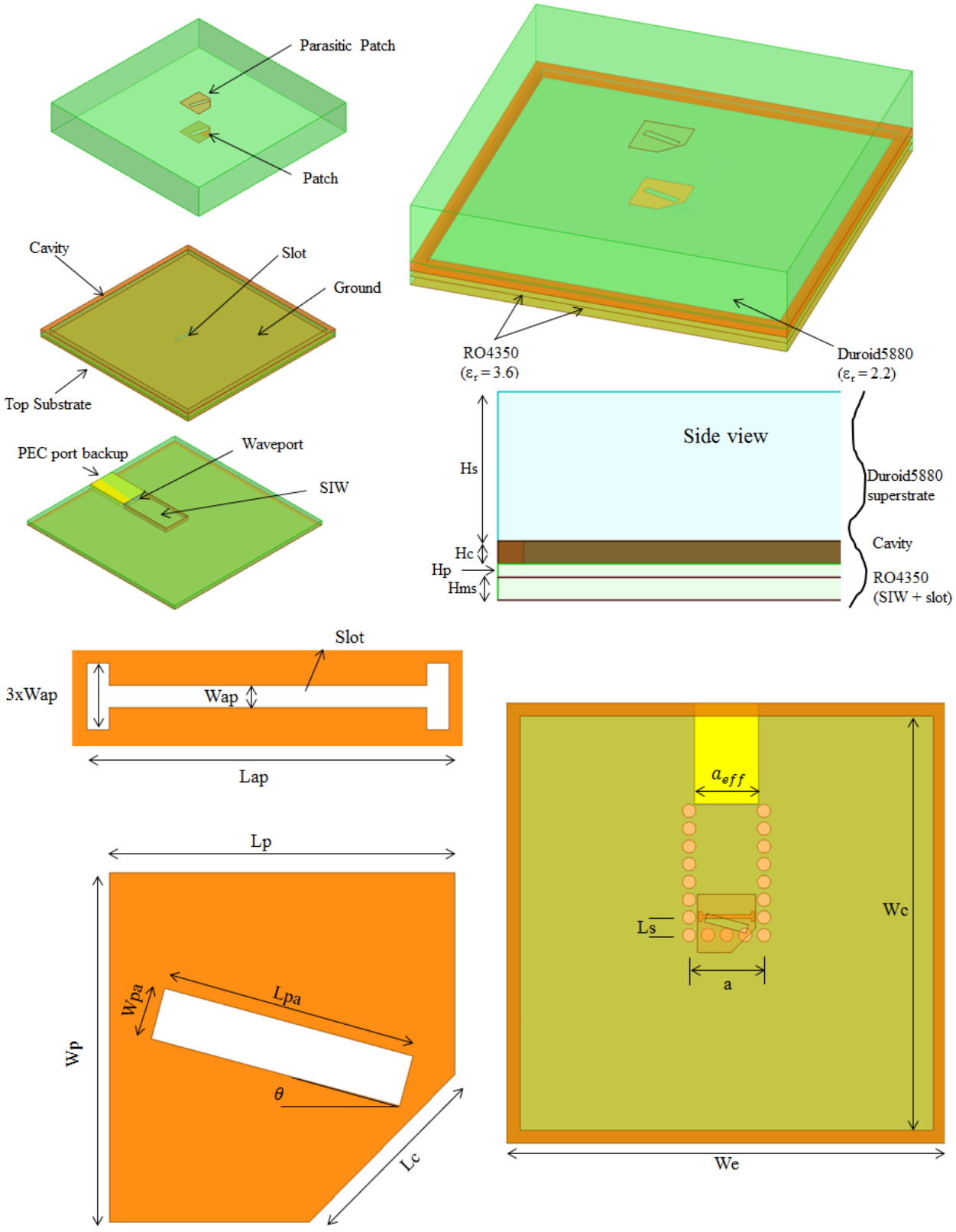

Fig. 21. Antenna geometry and design parameters. The design parameters are summarized in Table 4.

The antenna is fed through aperture coupling. The coupling aperture is a resonant H-slot to help improve the impedance bandwidth. The H-slot aperture was kept smaller than the patch width to maintain its the radiation completely under the patch. The position of the H-slot aperture is selected to improve the impedance matching, as well as the AR bandwidth. The patches are about 2% smaller than the patches in [10], to move the impedance bandwidth to better comply with the IEEE 802.11ad frequency band. The cavity size was not changed. Table 4 shows the parameters and values for the design from Fig. 21.

TABLE 4. SIW Fed ACMPA Radiating Element Parameters.

Parameter	Value	Parameter	Value
H_s	1.7mm	L_{pa}	0.98mm
H_c	0.254mm	θ	15°
H_p	0.168mm	L_c	0.784mm
H_{ms}	0.254mm	a_{eff}	1.47mm
W_{ap}	0.0784mm	a	1.705mm
L_{ap}	1.274mm	L_s	0.419mm
L_p	1.317mm	W_c	9.6mm
W_p	1.317mm	W_e	10mm
W_{pa}	0.196mm		

Fig. 22 shows the reflection coefficient for the antenna fed through SIW (blue curve) and through an equivalent dielectric-filled waveguide (red curve). The antenna was simulated with a SIW feed and with an equivalent dielectric-filled waveguide feed for two reasons. First, the dielectric-filled waveguide model is much simpler to generate and the simulations run significantly faster when the antenna is fed through a dielectric-filled waveguide, providing a quick way to verify the antenna performance. In addition, since the dielectric-filled waveguide has very low losses, simulating both feeding techniques help to quantify the energy loss in the SIW feed. The antenna has an impedance bandwidth that covers almost the entire IEEE 802.11ad frequency band. The single element impedance is 140 Ω at the port, and the reflection coefficient is less than -10 dB from 55.3 GHz to 62.8 GHz. Furthermore, the axial ratio (AR) bandwidth is shown in Fig. 23. and goes from 58.2 GHz to 62.7 GHz (7.8%) which is greater than the 2% found in most cases [12]. Fig. 24. shows the AR at 60 GHz as a function of theta, to determine the feasibility of this element to be used in beam-scanning applications. Note that the AR is less than 3 dB from -19° to 24°. The element has a LHCP gain of 7 dB and a wide beamwidth at 60 GHz (66°), as shown in Fig. 25. Fig. 26. shows the CP gain as a function of frequency. Note that the gain increases from 1.61 dBc at 56.16 GHz to 7.72 dBc at 64 GHz, the gain increases as frequency is increases. The CP gain at the central frequency of 60 GHz is 7.1 dBc. The radiation pattern for the radiating element is shown in Fig. 27. The results for the single radiating element are summarized in Table 5.

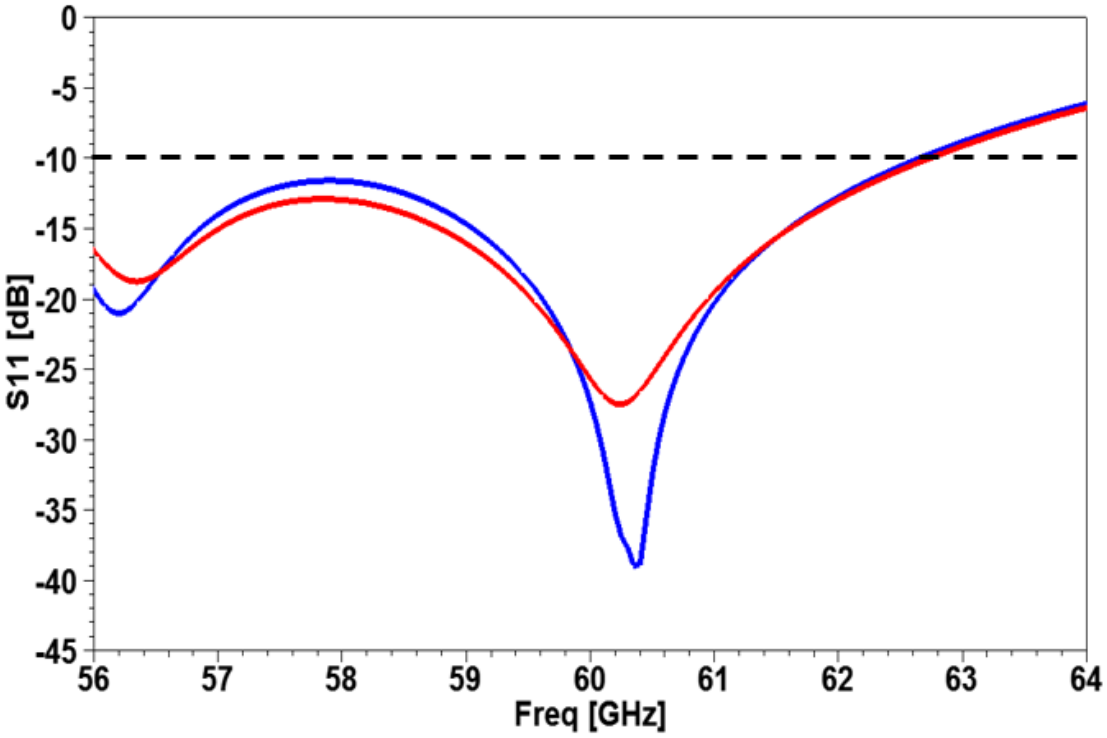

Fig. 22. Reflection coefficient for a single element fed with a dielectric-filled waveguide (red) and with SIW (blue).

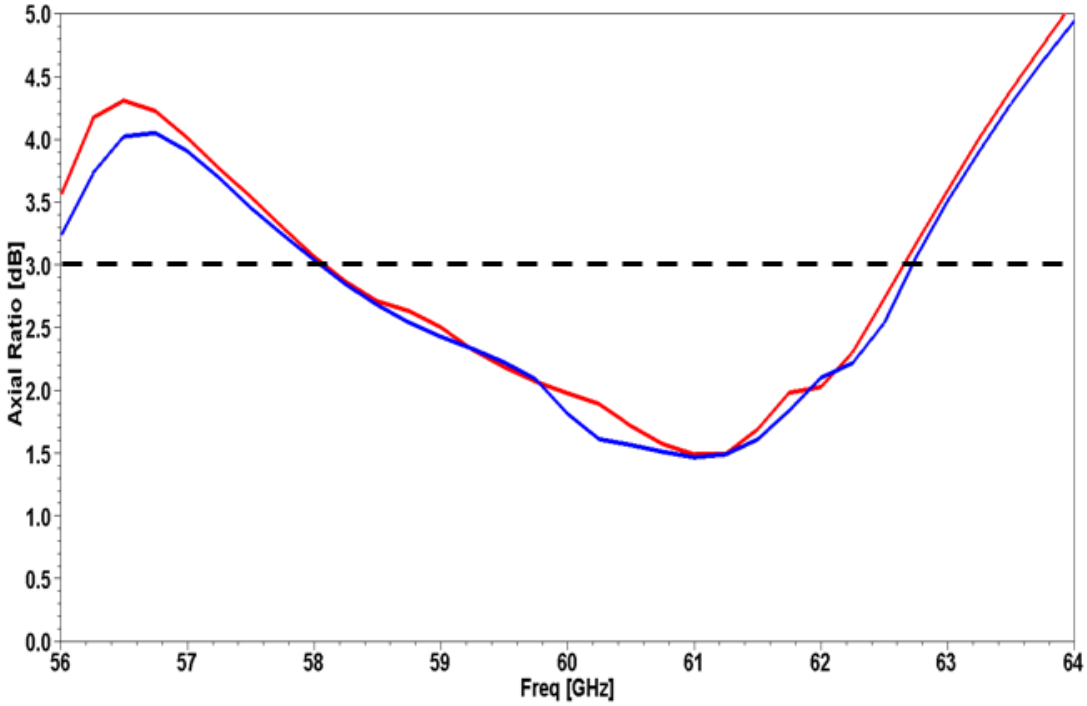

Fig. 23. Axial ratio bandwidth for a single element fed with a dielectric-filled waveguide (red) and with SIW (blue).

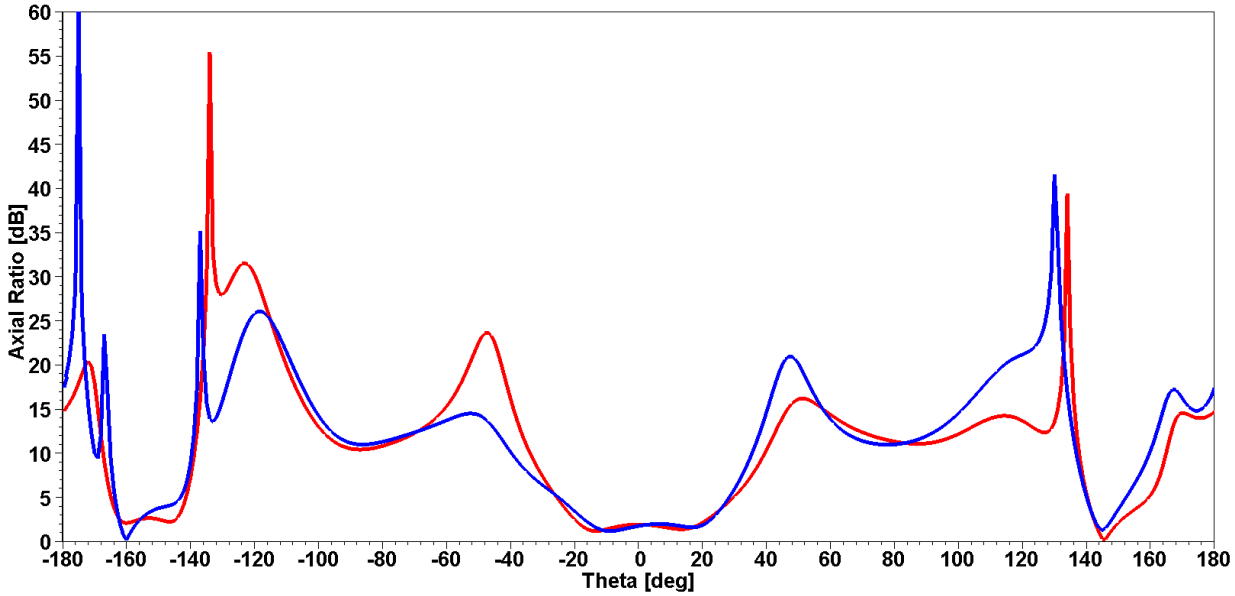

Fig. 24. Axial ratio as a function of theta at 60 GHz for a single element fed with a dielectric-filled waveguide (red) and with SIW (blue).

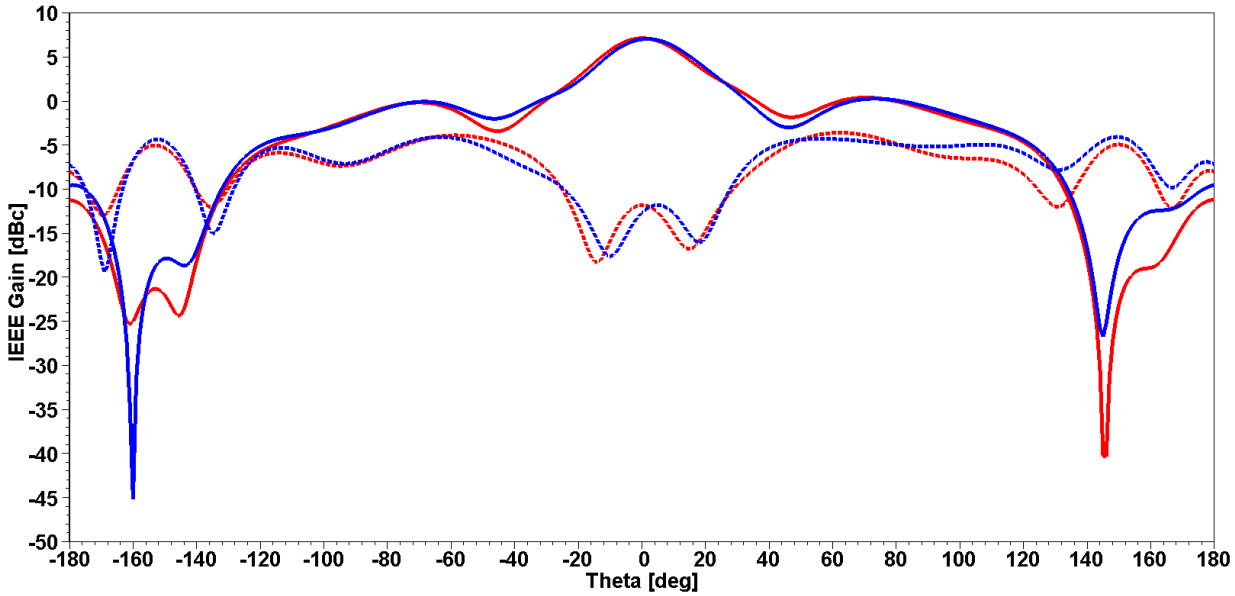

Fig. 25. CP gain pattern for a single element at 60 GHz fed with a dielectric-filled waveguide (red) and with SIW (blue). The dotted line show the cross-polarized gain for the same cases.

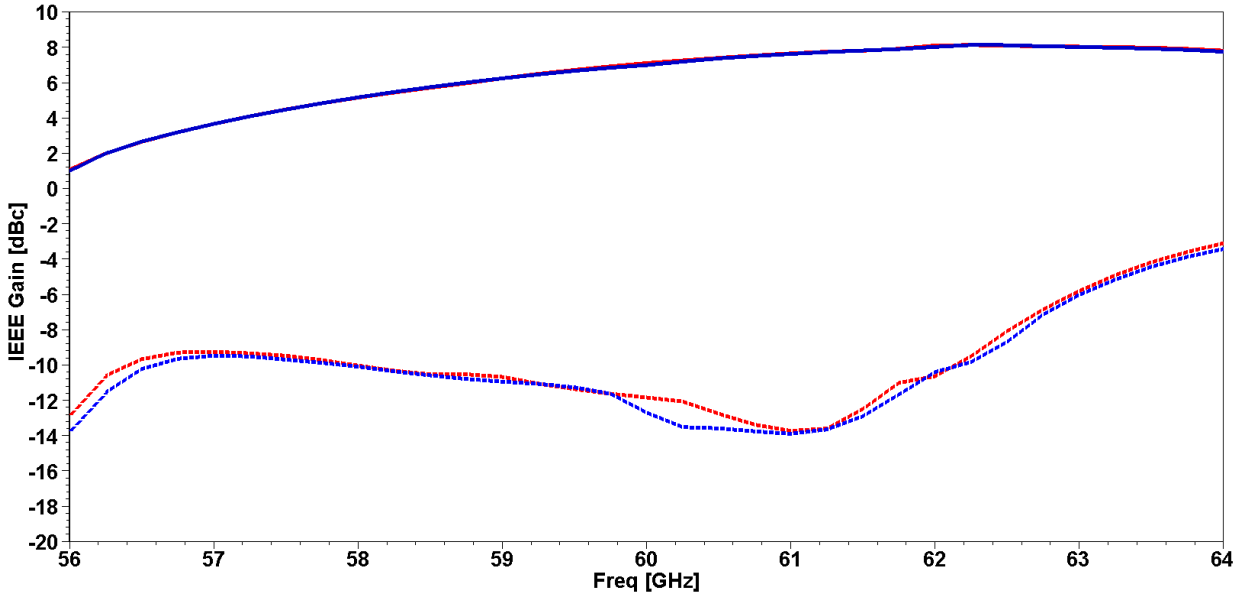

Fig. 26. CP gain for a single element fed with a dielectric-filled waveguide (red) and with SIW (blue). The dotted lines show the cross-polarized gain for the same cases.

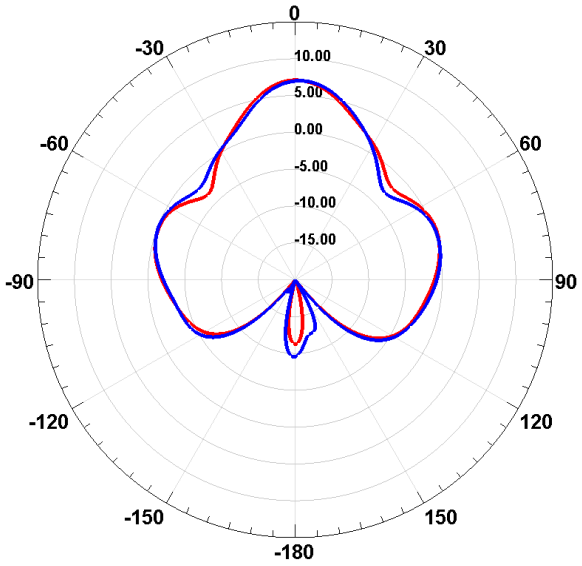

Fig. 27. CP gain pattern for a single element fed with a dielectric-filled waveguide (red) and with SIW (blue) at 60 GHz.

TABLE 5. Single Element Summary Results.

	Dielectric-Filled Waveguide fed	SIW fed
Impedance bandwidth (%)	12.7	12.5
AR Bandwidth (%)	7.4	7.8
Max Gain (dBc)	7.1	7.0
Directivity (dBc)	7.7	7.6
Efficiency (%)	86.5	85.6

A second design was performed to cover the 57-64 GHz unlicensed FCC 13-112 band. Fig. 28 shows the model for the SIW fed ACMPA with a parasitic patch for the FCC unlicensed band and Table 6 summarizes the different design parameters.

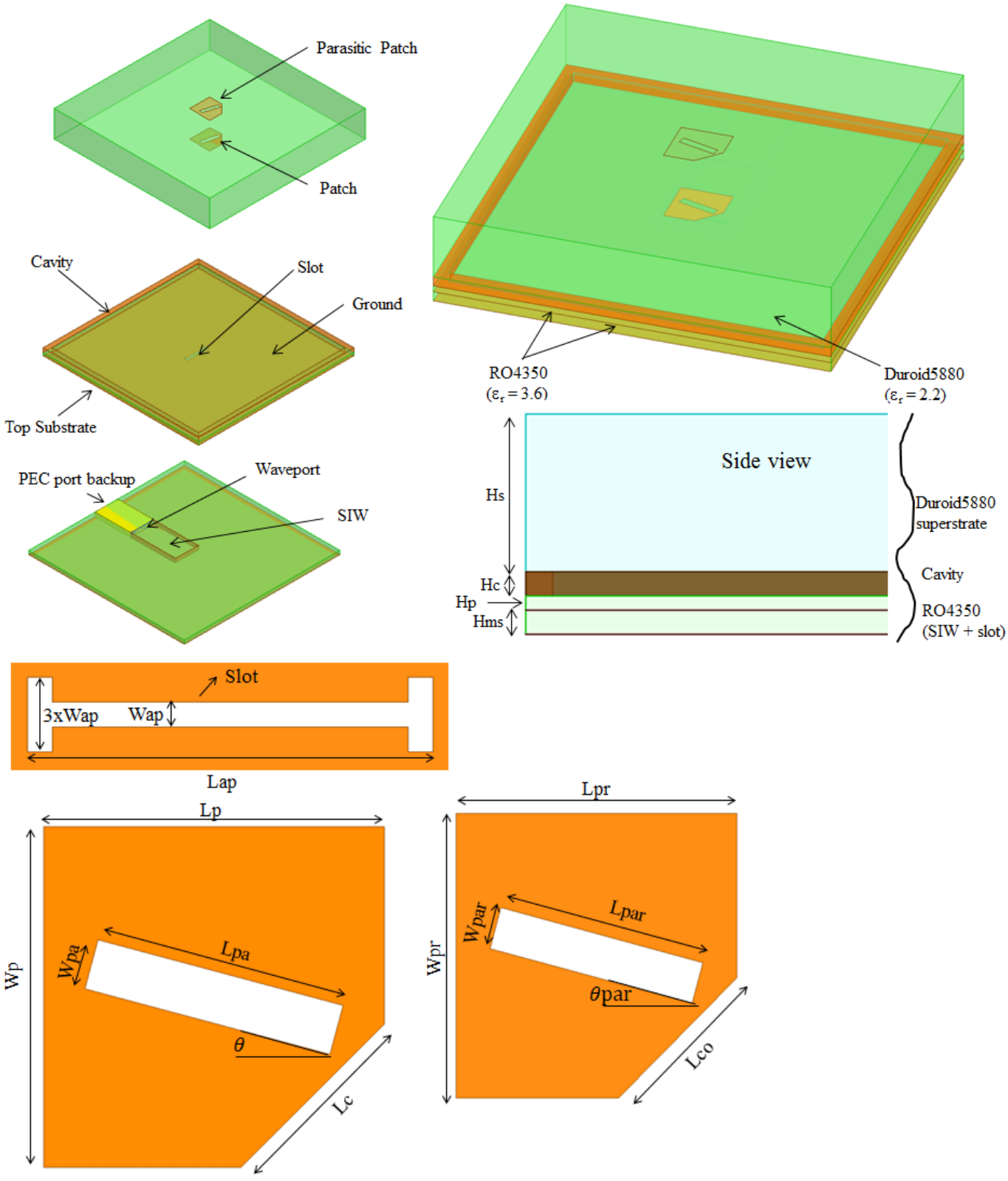

Fig. 28. Antenna design geometry describe by layers. The parameters are summarized in Table 6.

The SIW feed design is the same before, but the SIW substrate height was changed from 0.254 mm to 0.422 mm to increase the feed impedance. At 0.422 mm, the SIW impedance increases without the need of reducing the width a_{eff} of the SIW to match the antenna impedance. The radiating element and the parasitic have different dimensions to improve the reflection coefficient, as well as the axial ratio bandwidth. The substrate cavity was increased to provide more area for the complete SIW feed and the transition to 1.85 mm coaxial line.

The single element kept the same restriction of using an H-slot aperture smaller than the width of the radiating element. The dimensions of the H-slot aperture were changed to improve the matching between the antenna and the SIW feed.

TABLE 6. SIW Fed ACMPA Radiation Element Different Parameters.

Parameter	Value	Parameter	Value
$\boldsymbol{H_s}$	1.702mm	$\boldsymbol{L_{pa}}$	0.98mm
$\boldsymbol{H_c}$	0.254mm	$\boldsymbol{\theta}$	15°
$\boldsymbol{H_p}$	0.168mm	$\boldsymbol{L_c}$	0.784mm
$\boldsymbol{H_{ms}}$	0.422mm	$\boldsymbol{W_{pr}}$	1.34mm
$\boldsymbol{W_{ap}}$	0.08mm	$\boldsymbol{L_{pr}}$	1.34mm
$\boldsymbol{L_{ap}}$	1.25mm	$\boldsymbol{L_{par}}$	0.997mm
$\boldsymbol{L_p}$	1.317mm	$\boldsymbol{W_{par}}$	0.199mm
$\boldsymbol{W_p}$	1.317mm	$\boldsymbol{L_{co}}$	0.68mm
$\boldsymbol{W_{pa}}$	0.196mm	$\boldsymbol{\theta_{par}}$	15°

The reflection coefficient is shown in Fig. 29. Note that -10 dB matching was achieved for the band of interest. The axial ratio bandwidth is shown in Fig. 30. Note that the AR bandwidth covers from 58.1 GHz to 63.7 GHz. Fig. 31. shows the AR as a function of theta at 60 GHz, to verify the feasibility of using this element for beam-scanning applications. The AR is below 3 dB from -7° to 8°. The CP gain at 60 GHz has 6.5 dB sidelobes at -26° and 27°, as shown in Fig. 32. Fig. 33 shows the CP gain as a function of frequency. Note that the gain increases from 5.39 dB at 57 GHz to 8.09 dB at 64 GHz. The CP gain at central frequency of 60 GHz is of 8.5 dBc. The gain pattern for the radiating element is shown in Fig. 34. The results for the single radiating elements are summarized in Table 7.

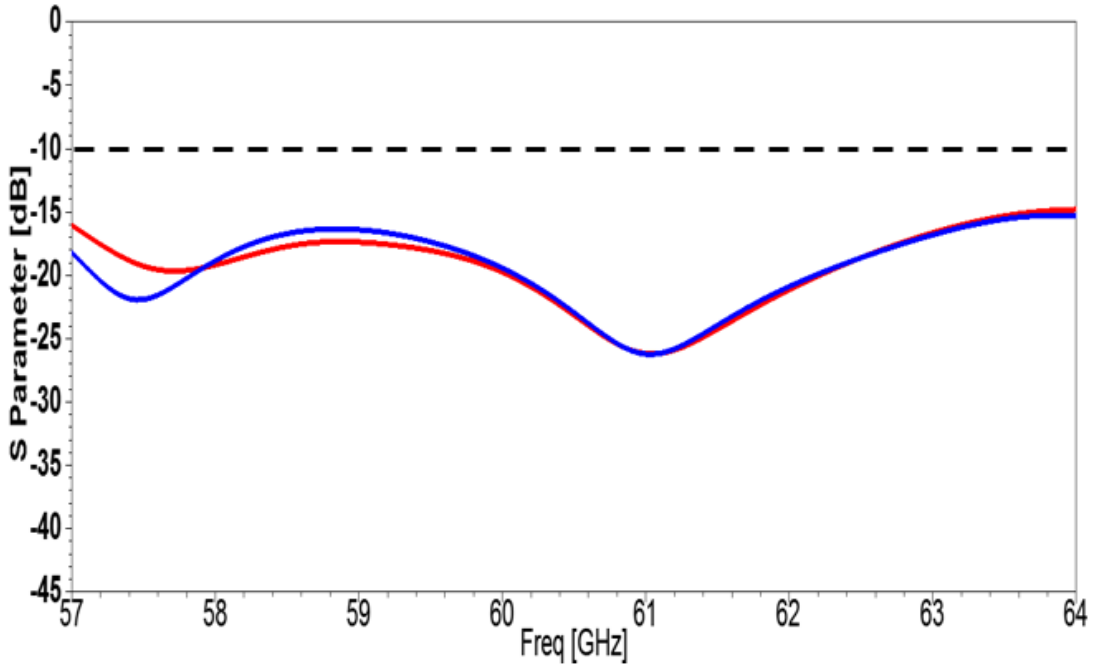

Fig. 29. Reflection coefficient for a single element fed with a dielectric-filled waveguide (red) and with SIW (blue).

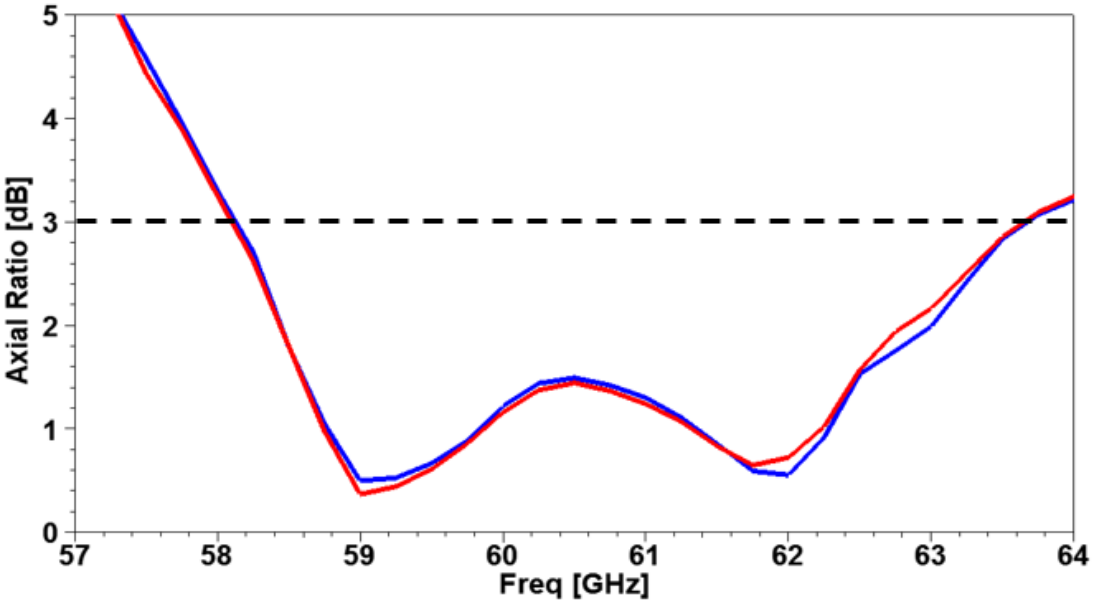

Fig. 30. Axial ratio bandwidth for a single element fed with a dielectric-filled waveguide (red) and with SIW (blue).

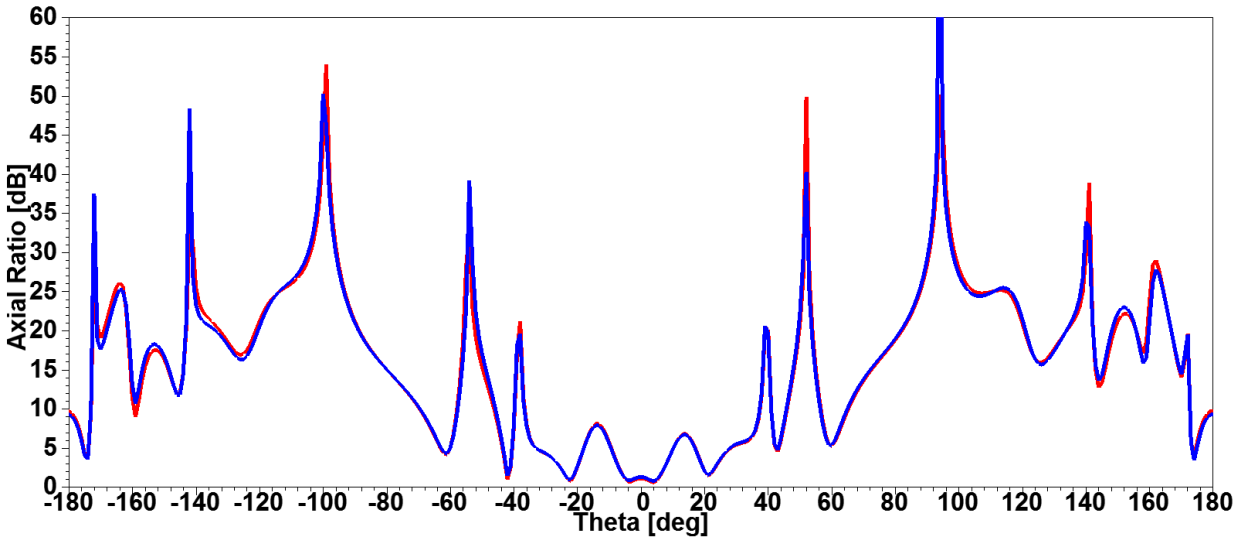

Fig. 31. Axial ratio as a function of theta at 60 GHz for a single element fed with a dielectric-filled waveguide (red) and with SIW (blue).

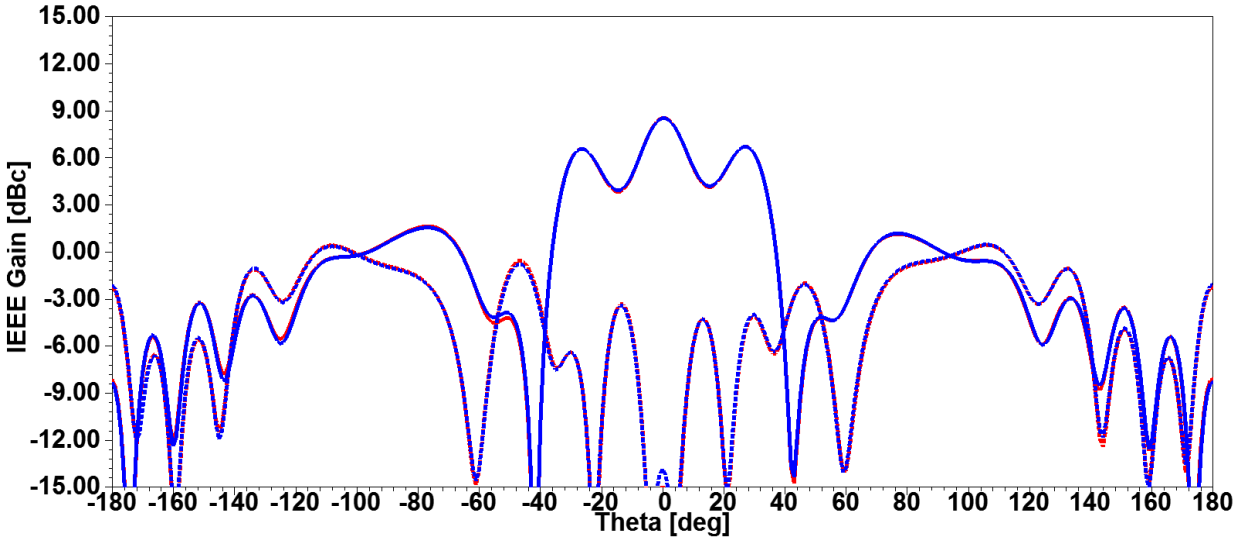

Fig. 32. CP gain pattern for a single element at 60 GHz fed with a dielectric-filled waveguide (red) and with SIW (blue). The dotted lines show the cross-polarized gain for the same cases.

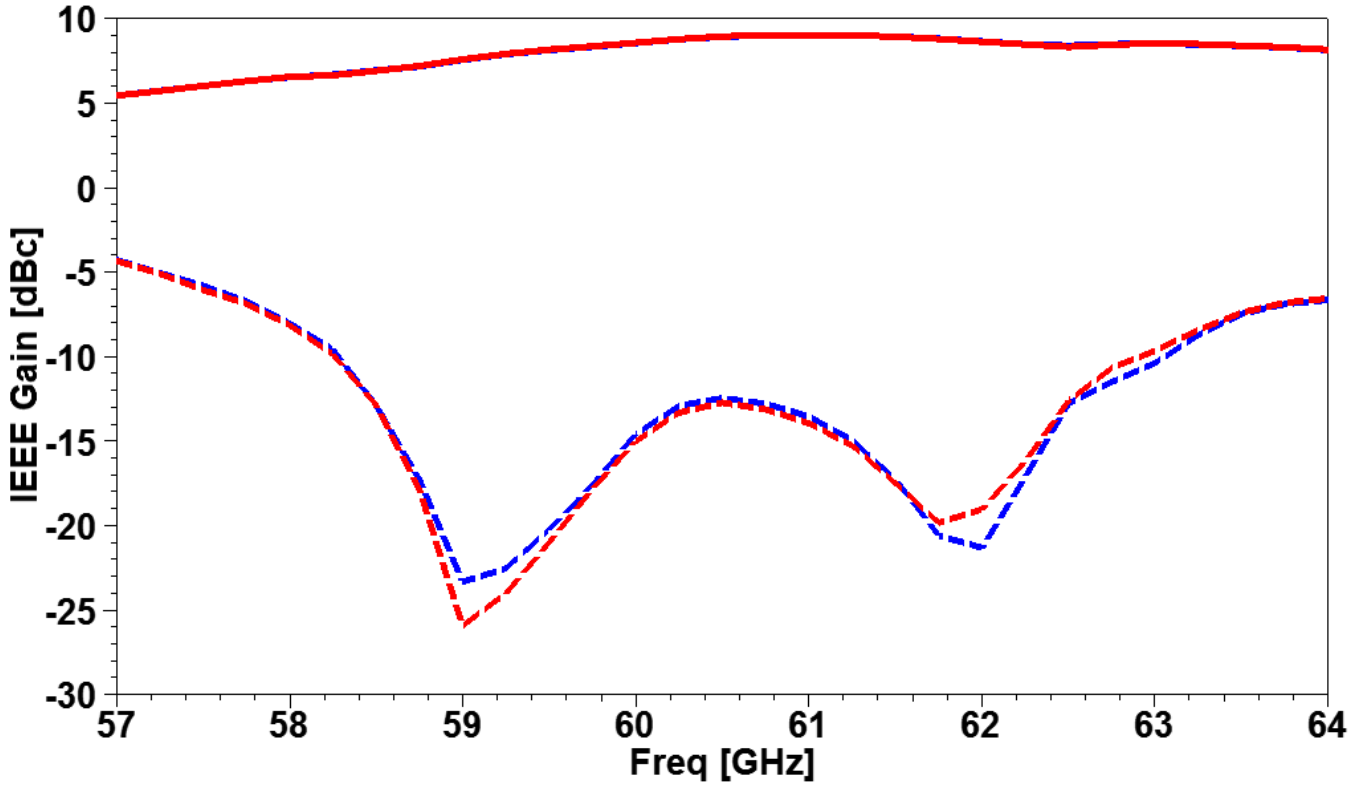

Fig. 33. CP gain for a single element fed with a dielectric-filled waveguide (red) and with SIW (blue). The dotted lines show the cross-polarized gain for the same cases.

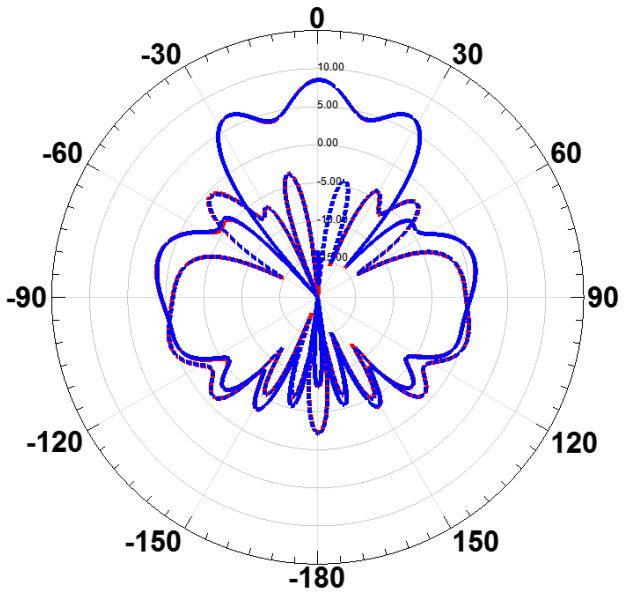

Fig. 34. CP gain pattern for a single element fed with a dielectric-filled waveguide (red) and with SIW (blue) at 60 GHz.

TABLE 7. Single Element Summary Results.

	Dielectric-Filled Waveguide fed	SIW fed
Impedance bandwidth (%)	11.6	11.6
AR Bandwidth (%)	9.2	9.2
Max Gain (dBc)	8.5	8.5
Directivity (dBc)	9.2	9.2
Efficiency (%)	86.2	85.8

3.3.4 2x2 array

We performed a study of the effects in gain and axial ratio bandwidth of using linear and circularly polarized elements in sequentially rotated arrays. Four 2x2 sequentially rotated arrays antenna models were created using LP and CP elements. On both cases, the base design is a square microstrip patch. The patches were designed to operate at a 60 GHz central frequency an air substrate 0.254 mm thick, and using lumped ports for feeding. CP elements consist of square patches with truncated corners and a single feed point; the LP elements also have a single feed point. Both phase distributions of $0°, 90°, 180°, 270°$, and $0°, 90°, 0°, 90°$ were considered for each patch type. Fig. 35. shows the four array configurations. The dots in the patches represent the feed position in each element.

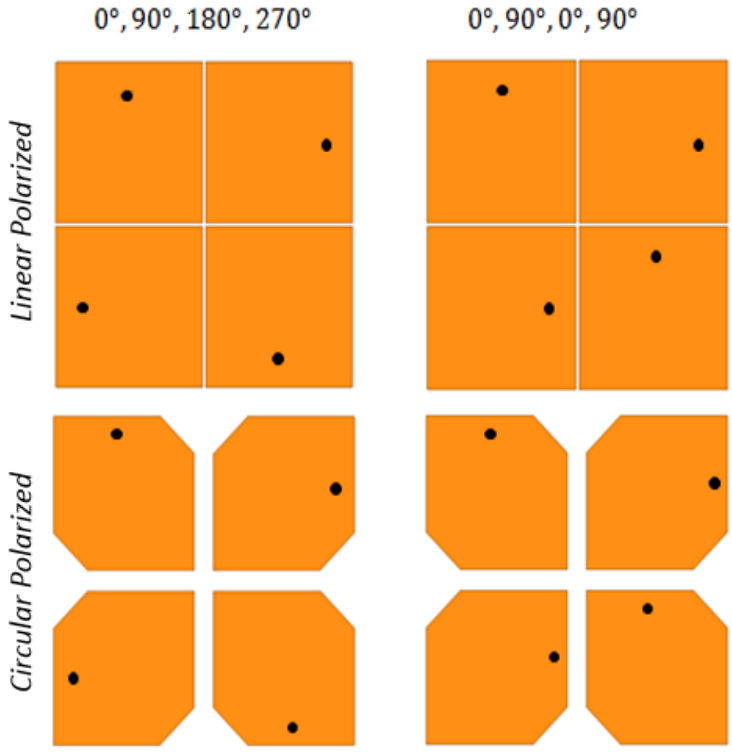

Fig. 35. Array design for sequentially rotated methods.

The single element patches for CP and LP have a reflection coefficient behavior shown in Fig. 36. The red curve is the LP element reflection coefficient, and the blue curve is the reflection coefficient for the CP element. The LP element has an impedance bandwidth of 6.5%, from 58.1 GHz to 62 GHz, and CP element has an impedance bandwidth of 12.8%, from 57.2 GHz to 65 GHz. The axial ratio for the CP element is shown in Fig. 37.

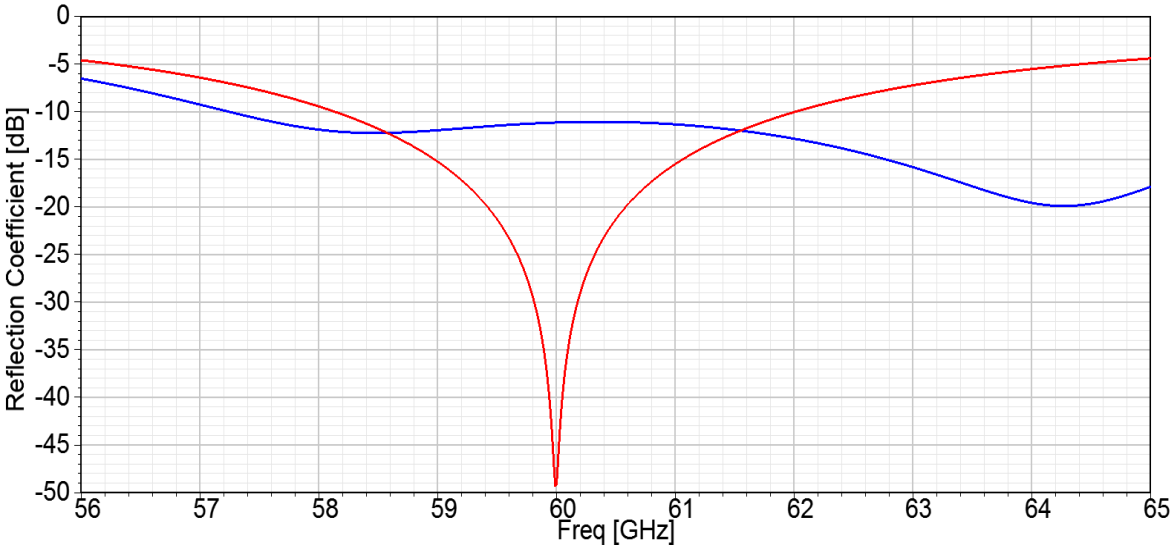

Fig. 36. Reflection coefficient for LP element (red) and CP element (blue).

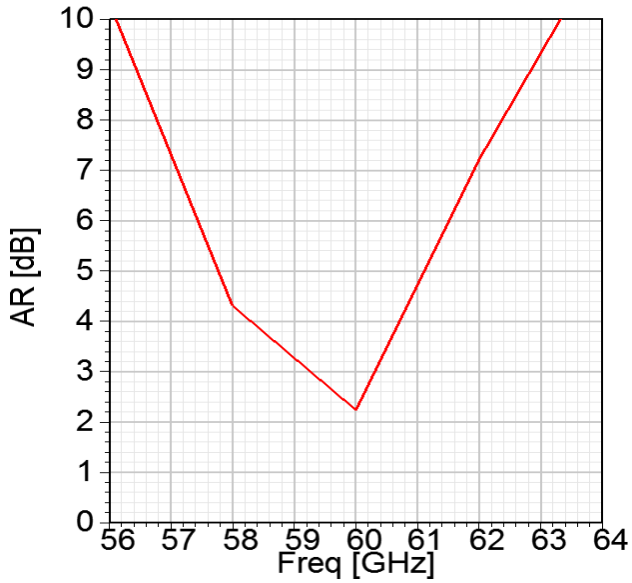

Fig. 37. Axial ratio for the CP element.

The 2x2 sequentially rotated arrays for CP and LP main differences came from the single element polarization. Fig. 38 shows CP gain of the array configurations when the distance between elements is varied. The phase distributions used does not have a significant effect in the array performance. The CP array configurations show a gain of 6 dBc above the LP array configurations. The electric field vectors

for both configurations is shown in Fig. 39 as the phase progresses. Note that there is no energy in two of the patches when the phase is $45°$ and $132°$. On the other hand, all patches have energy in the CP as the phase progresses, which explains the 6 dB difference in gain between the LP elements and CP elements arrays.

In the four sequentially rotated configurations the axial ratio bandwidth covers the entire band of interest from 55 to 64 GHz. The axial ratio bandwidth is shown in Fig. 40 where all the configurations have an AR lower than 1 dB. Comparing all the results from the simulations of the four configurations, is concluded that using a CP single element for the sequentially rotated to array improves the antenna gain as well the axial ratio bandwidth.

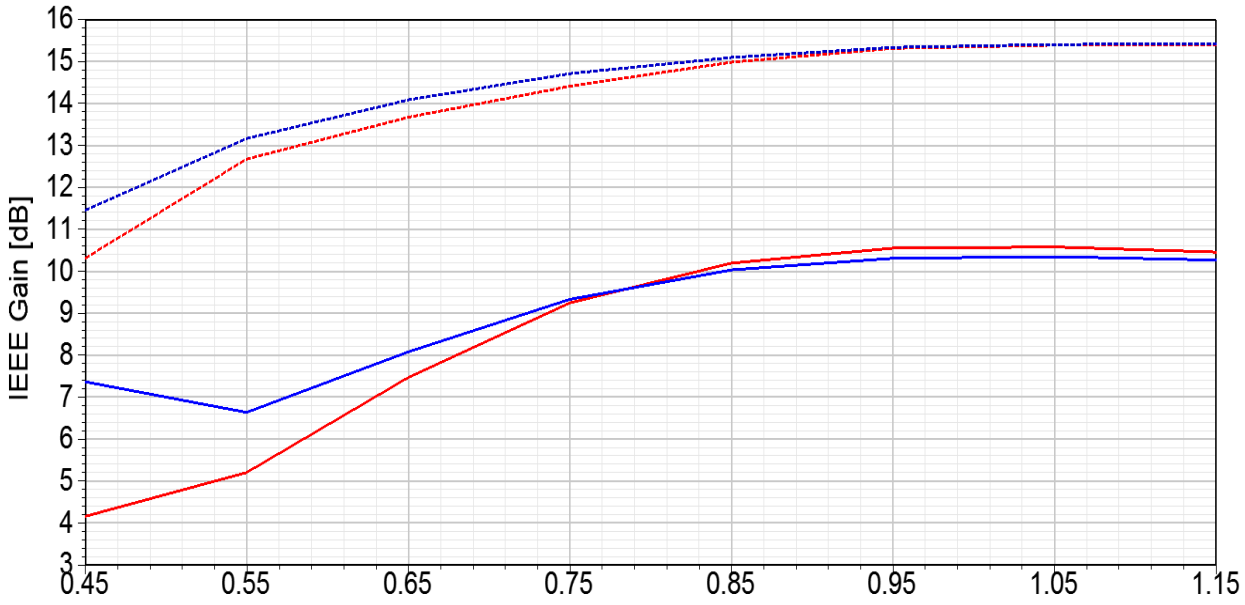

Fig. 38. CP gain LP and CP arrays sequentially rotated as function of distance between elements. The CP array $0°, 90°, 180°, 270°$ (blue dotted), CP array $0°, 90°, 0°, 90°$ (red dotted), LP array $0°, 90°, 180°, 270°$ (blue), LP array $0°, 90°, 0°, 90°$ (red).

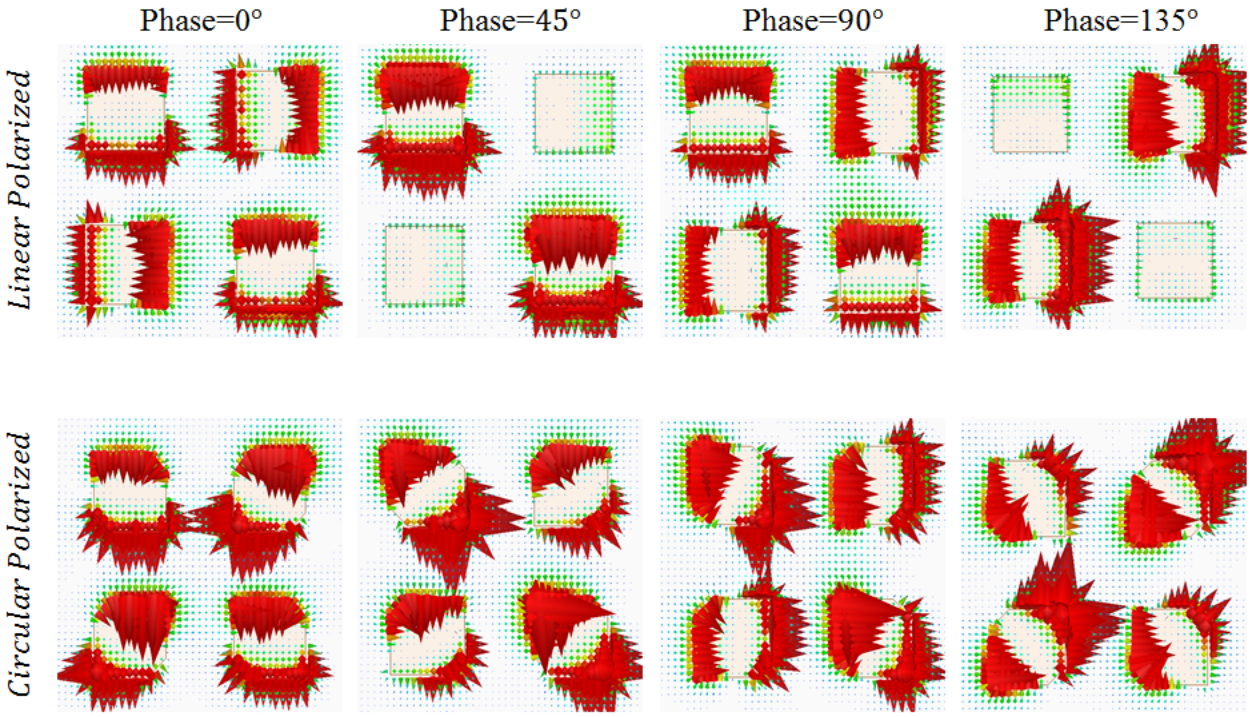

Fig. 39. Electric fields vectors for the LP and CP arrays over the patches for different phases.

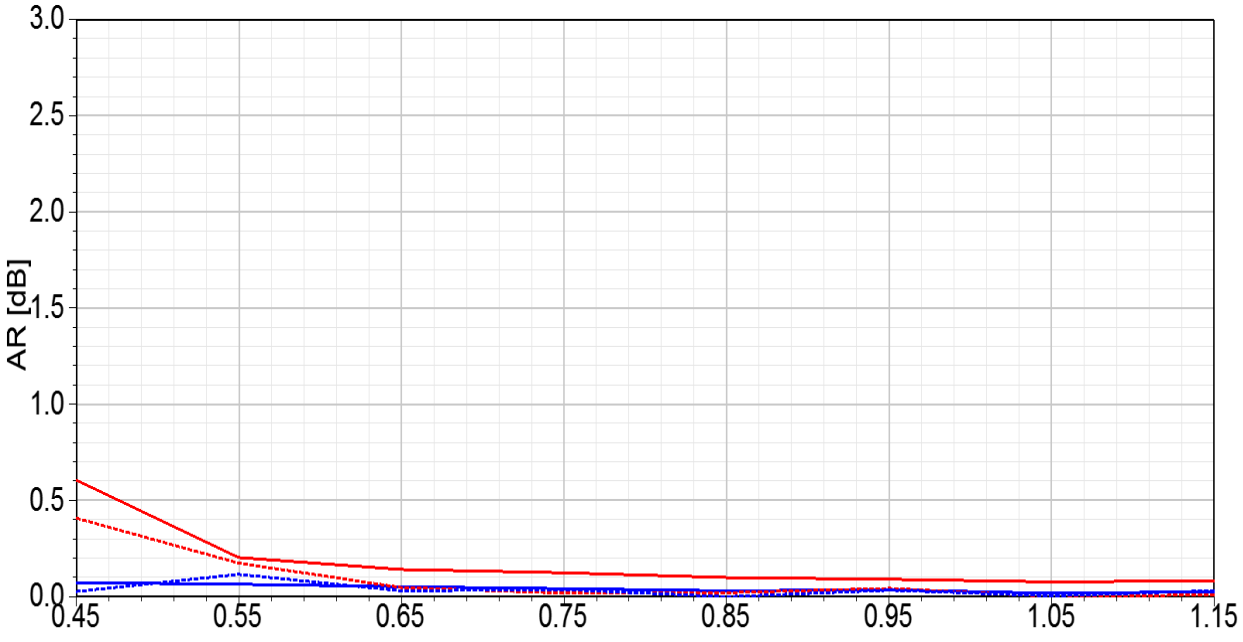

Fig. 40. Axial Ratio vs separations between elements in the arrays.

Taking these results into account, we designed two arrays, one for the IEEE 802.11ad band and the other for the FCC 13-112 band. Given that element is left hand circularly polarized (LHCP), the patches were rotated by 90 degrees from each other, moving in a counter-clockwise fashion in the array, as shown in Fig. 41. Furthermore, the elements were fed with a 90-degree phase progression.

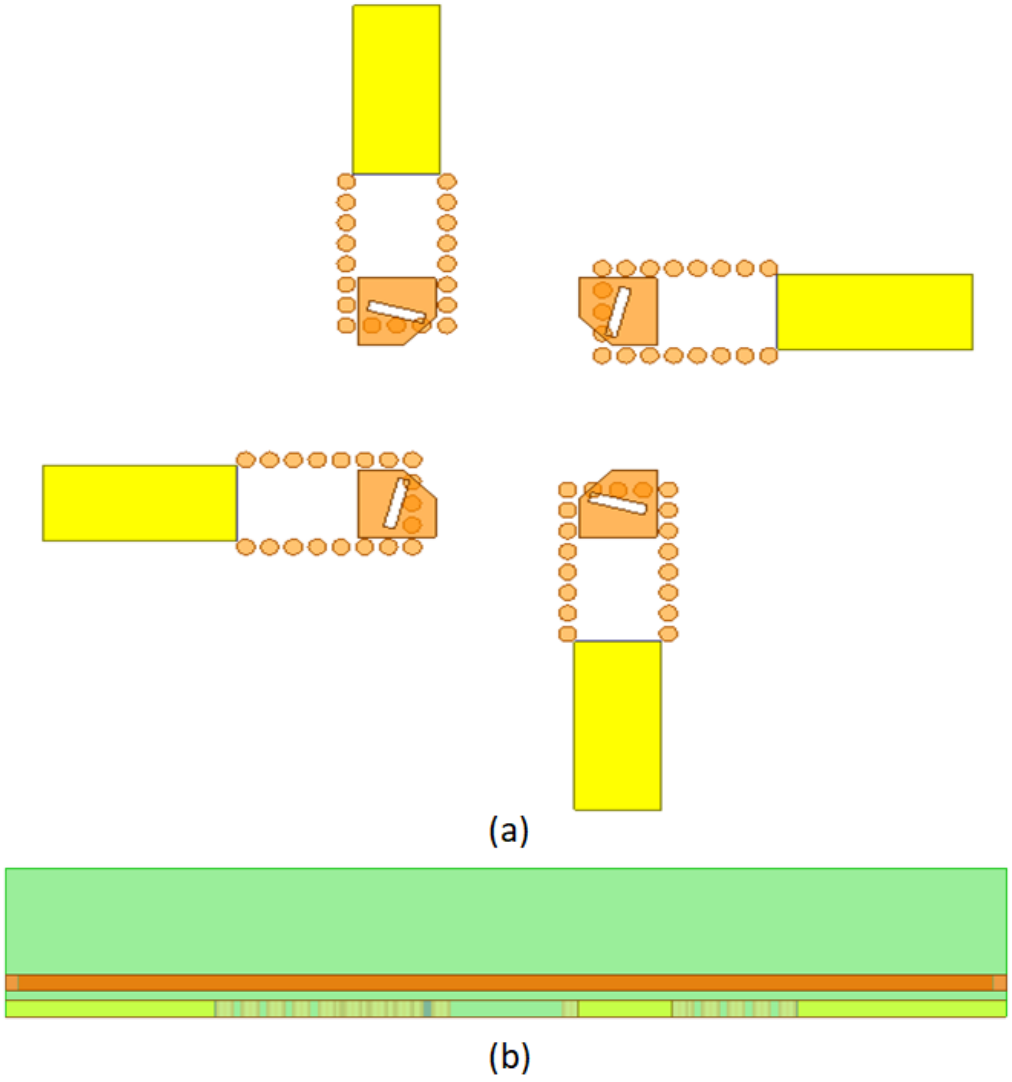

Fig. 41. (a) Top and (b) side view of the 2x2 array using elements described on Fig. 21.

The element spacing in the array was varied to find the best results in terms of axial ratio, CP gain and bandwidth for the project. Fig. 42. shows the CP gain as the element separation is varied from 0.4λ to 1.10λ. When the separation is lower, the gain is lower, but the beam-steering capabilities are greater. On the other hand, the gain increases when the separation is greater. Since the array is not required to greatly steer the beam, the 0.75λ separation was selected. The reflection coefficient and Z parameters for this configuration are shown in Fig. 43, and Fig. 44. The 2x2 array reflection coefficient is less than -10 dB from 56 GHz to 62.7 GHz (11.3%). The impedance bandwidth of the single element was 12.5%, and for the 2x2 array was reduced to 11.3%. The results for the axial ratio are shown in Fig. 45, and Fig.

46. The axial ratio bandwidth is greatly improved, because of the sequential rotation method. The axial ratio is lower than 3 dB for the radiation pattern, going from -16° to 16° in theta.

The CP gain at 0.75λ separation between elements is shown in Fig. 347, and Fig. 4.8. The circular gain has been increased about 6 dBc from the single element with a CP gain of 13.6 dBc. The radiation pattern is shown in Fig. 49. Finally, the radiation efficiency of the 2x2 array without considering the long dielectric-filled waveguide or SIW feeds is shown in Fig. 50. Table 8 summarizes the results.

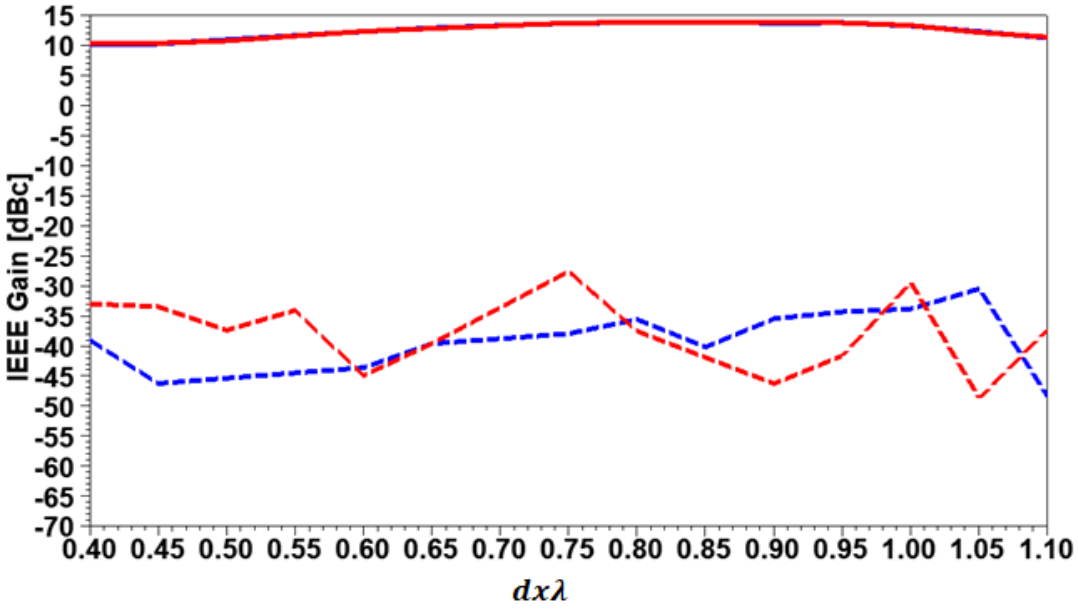

Fig. 42. CP gain variation with element separation for the elements fed with a dielectric-filled waveguide (red) and with SIW (blue) at 60 GHz. The dotted lines show the cross-polarized gain for the same cases.

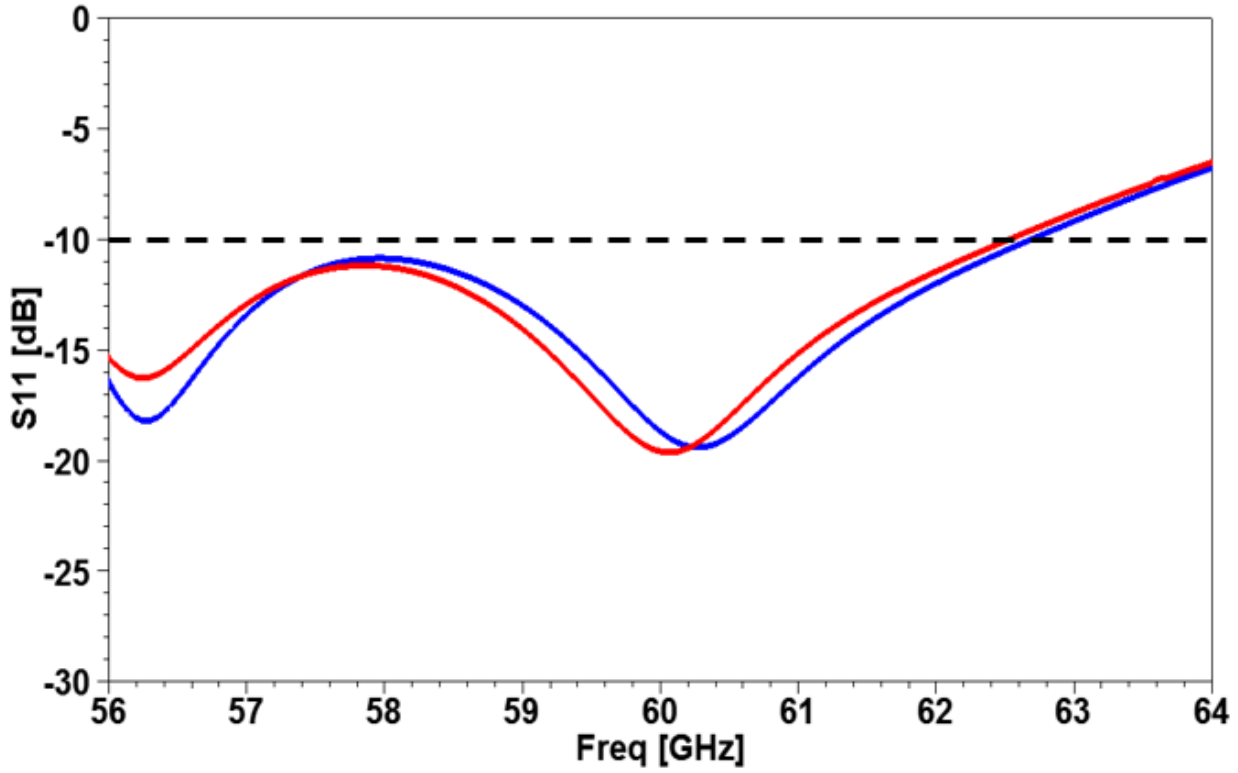

Fig. 43. Reflection coefficient for the 2x2 array for the elements fed with a dielectric-filled waveguide (red) and with SIW (blue).

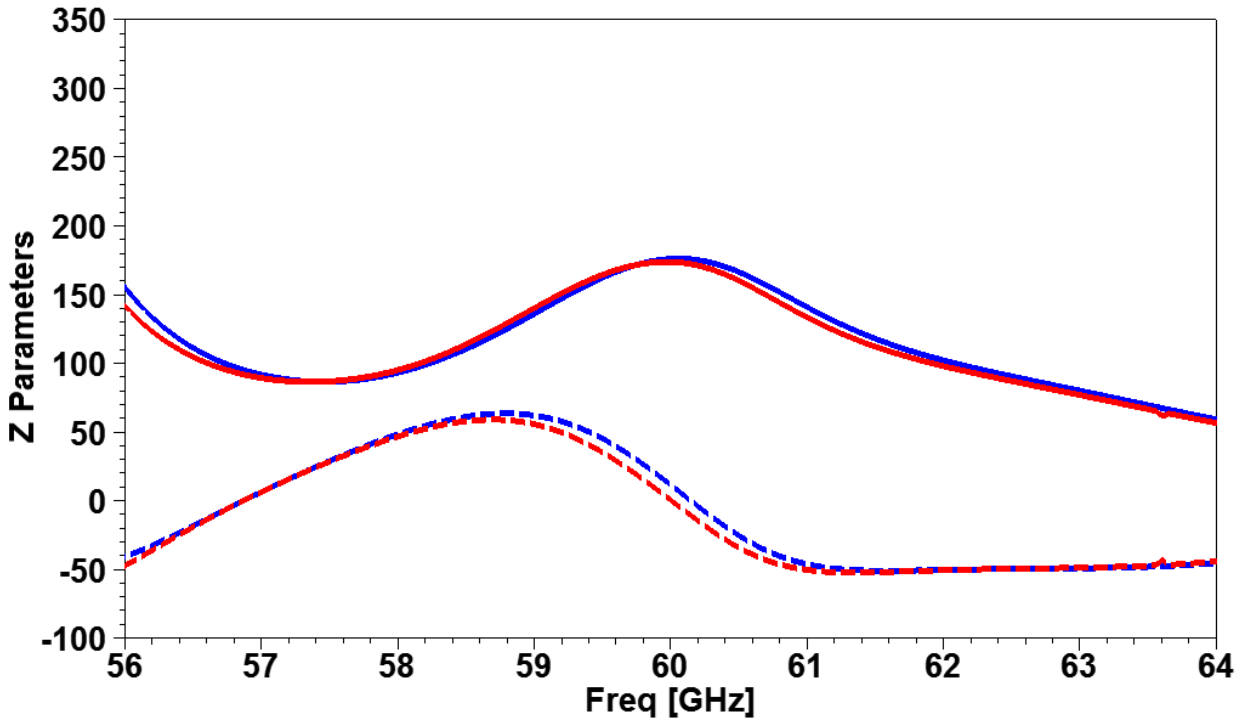

Fig. 44. Z11 parameters for the 2x2 array for the elements fed with a dielectric-filled waveguide (red) and with SIW (blue). The solid lines represent the resistance, and the dotted lines show reactance.

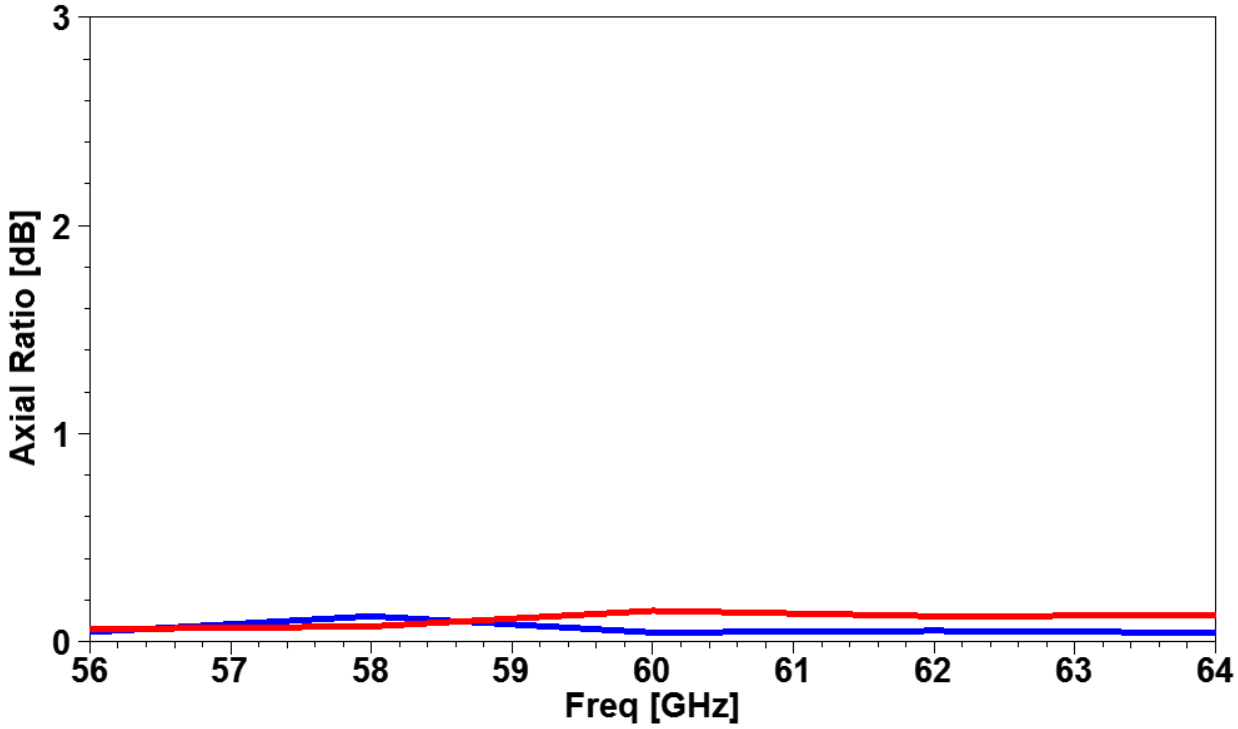

Fig. 45. Axial ratio as function of frequency for the 2x2 array for the elements fed with a dielectric-filled waveguide (red) and with SIW (blue).

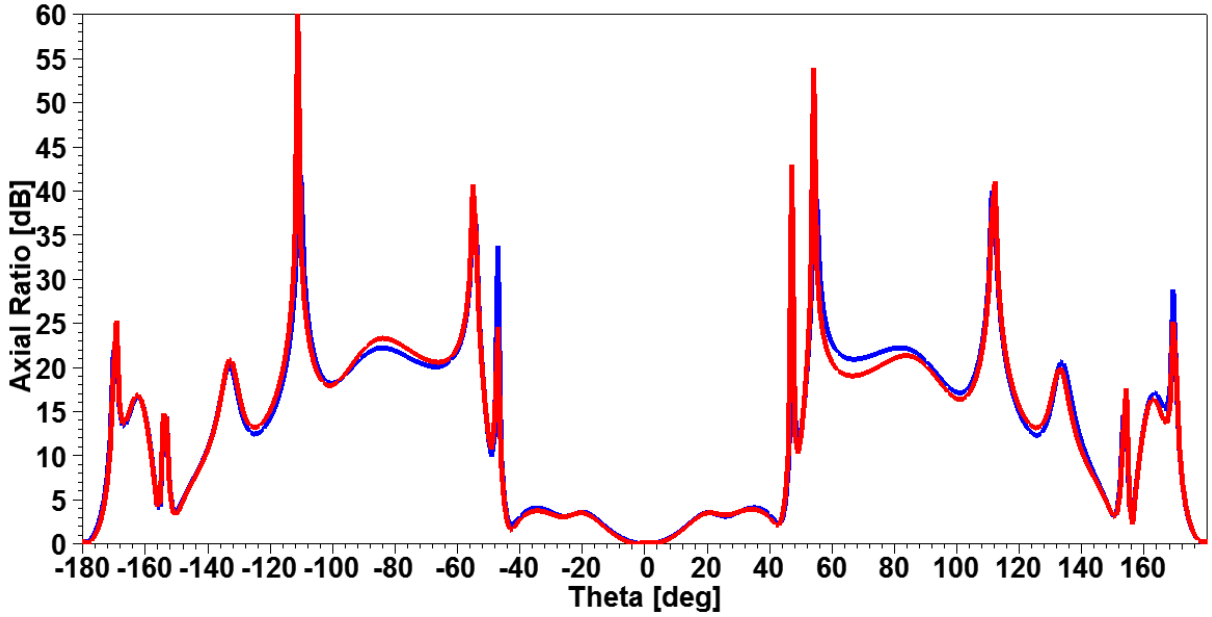

Fig. 46. Axial ratio for the 2x2 array as a function of theta for the elements fed with a dielectric-filled waveguide (red) and with SIW (blue) at 60 GHz.

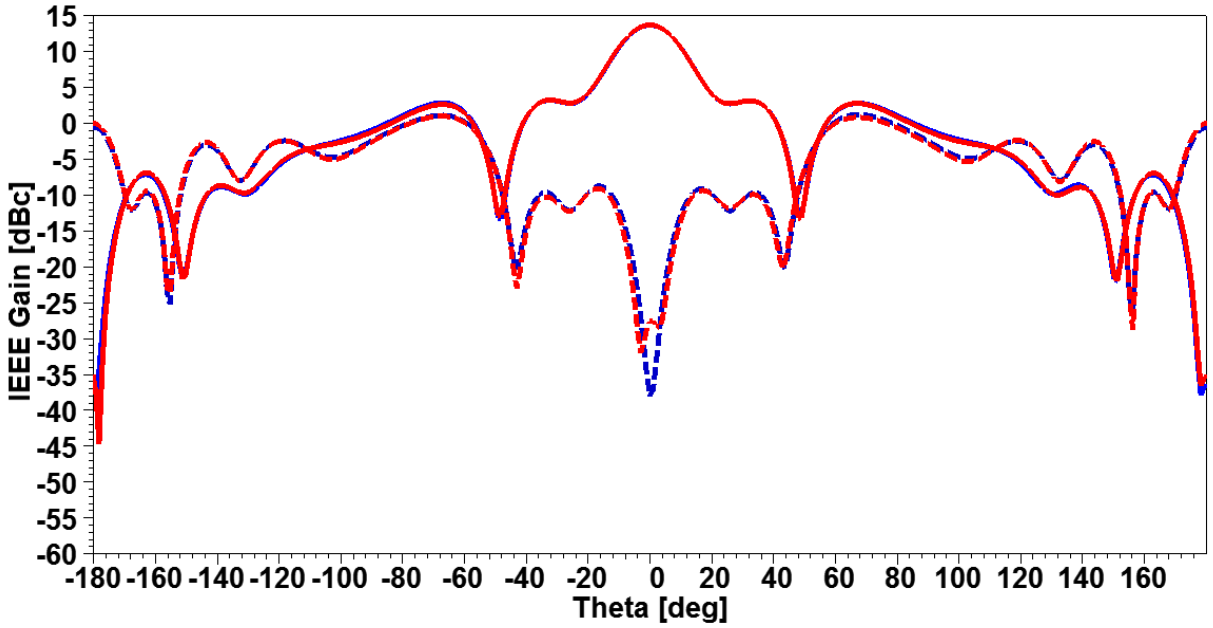

Fig. 47. CP gain pattern for the 2x2 array for the elements fed with a dielectric-filled waveguide (red) and with SIW (blue) at 60 GHz. The dotted lines show the cross-polarized gain for the same cases.

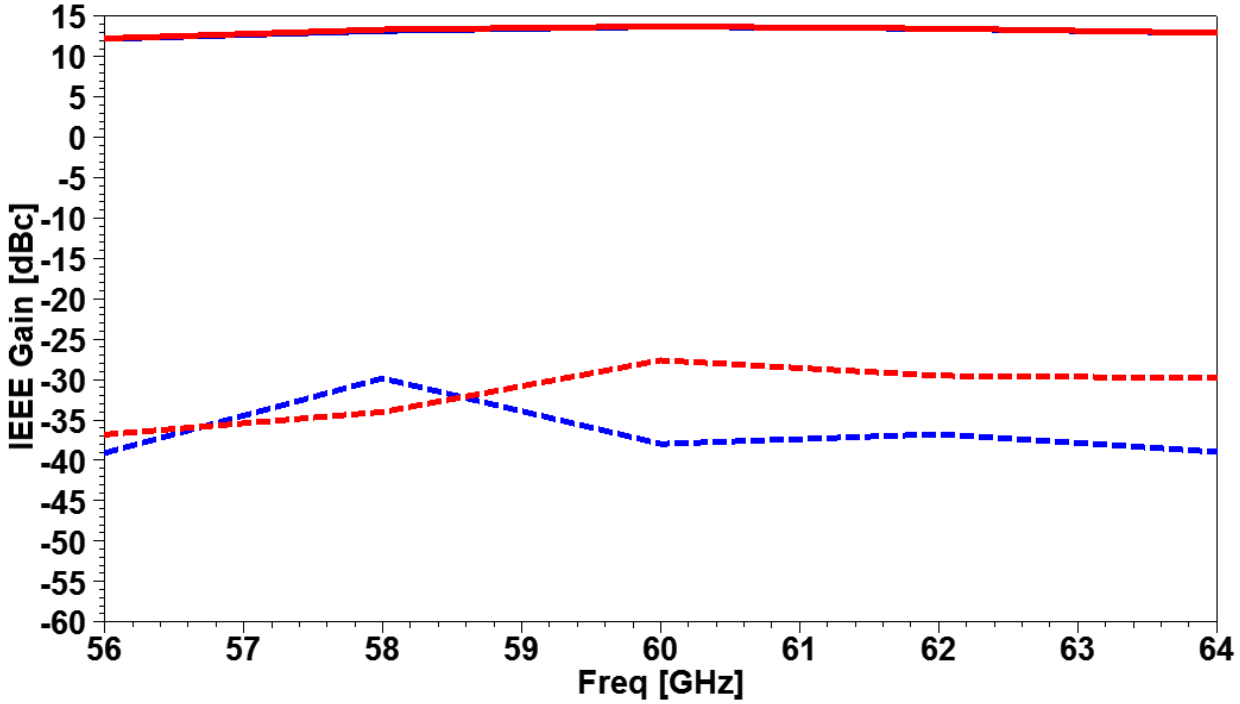

Fig. 48. CP gain as a function of frequency for the 2x2 array antenna for the elements fed with a dielectric-filled waveguide (red) and with SIW (blue). The dotted lines show the cross-polarized gain for the same cases.

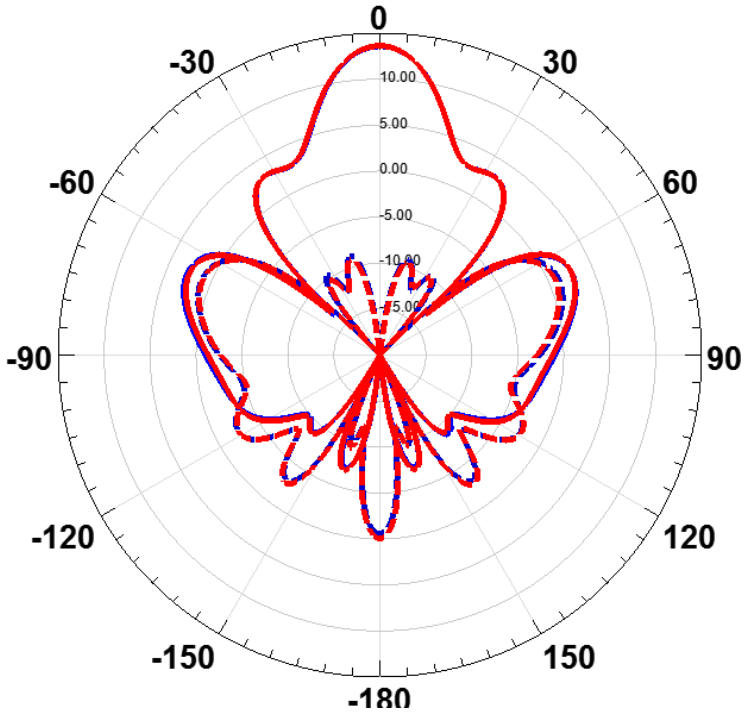

Fig. 49. CP gain pattern for the 2x2 array for the elements fed with a dielectric-filled waveguide (red) and with SIW (blue) at 60 GHz. The dotted lines show the cross-polarized gain for the same cases.

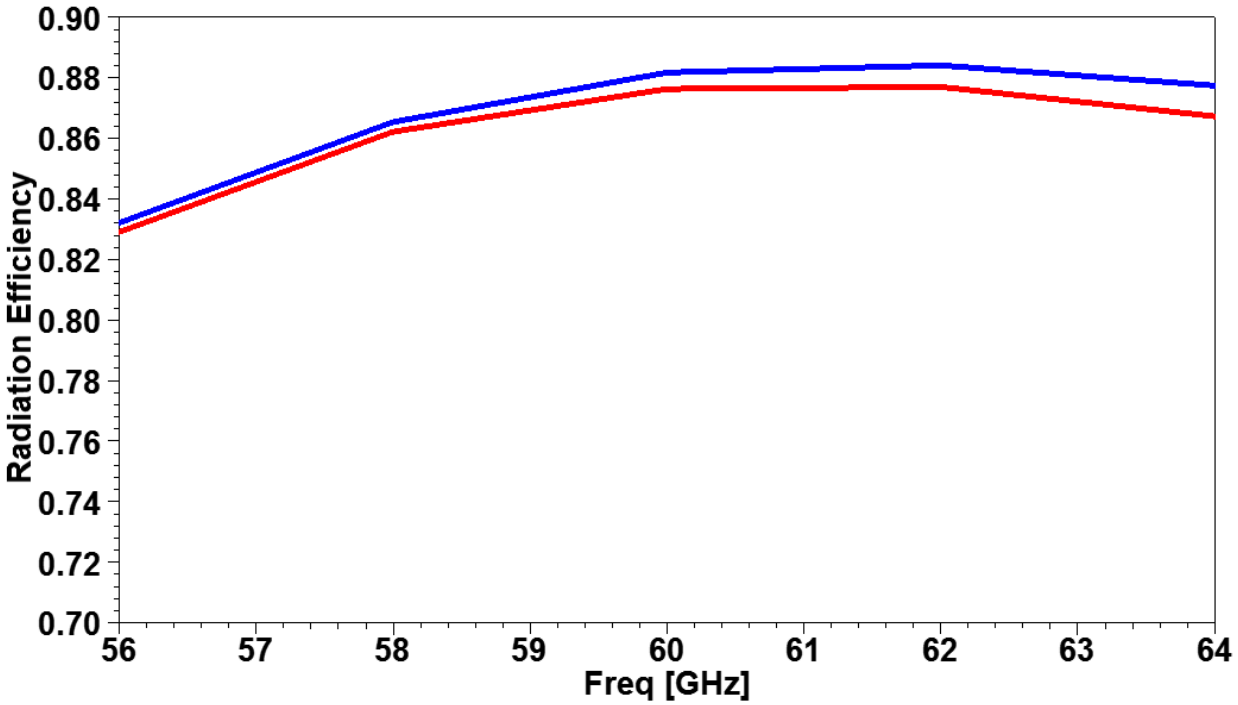

Fig. 50. Radiation efficiency as a function of frequency for the 2x2 array for the elements fed with a dielectric-filled waveguide (red) and with SIW (blue).

TABLE 8. 2x2 Array Summary Results.

	Dielectric-Filled Waveguide Fed	SIW Fed
S11 (%)	11.0	11.3
AR Bandwidth (%)	13.3	13.3
Z Parameters	173	176+11j
Max Gain (dBc)	13.6	13.6
Cross Polarization (dBc)	-27.6	-38
Radiation Efficiency (%)	87.6	88.1

The design procedure was repeated for the FCC 13-112 unlicensed band. The element spacing in the array was varied to find the best results in terms of axial ratio, CP gain and bandwidth for the project. Fig. 51. shows the CP as the element separation is varied from 0.4λ to 1.10λ. Since the array is not required to greatly steer the beam, the 0.75λ separation was selected. The reflection coefficient and Z parameters for this configuration are shown in Fig. 52, and Fig. 53. The impedance bandwidth keep the same bandwidth of the single element. The axial ratio bandwidth greatly improved, because of the sequentially rotation method. The results for the axial ratio are shown in Fig. 54, and Fig. 55. Note that the AR is less than 3 dB from $-29°$ to $29°$.

The CP gain at 0.75λ separation between elements is shown in Fig. 56, and Fig. 57. The CP gain at the central frequency of 60 is of 12.7 dBc. The CP radiation pattern is shown in Fig. 58. Finally, the radiation efficiency of the 2x2 element array without considering long dielectric-filled waveguide or SIW feeds is shown in Fig. 59. Table 9. summarizes the results.

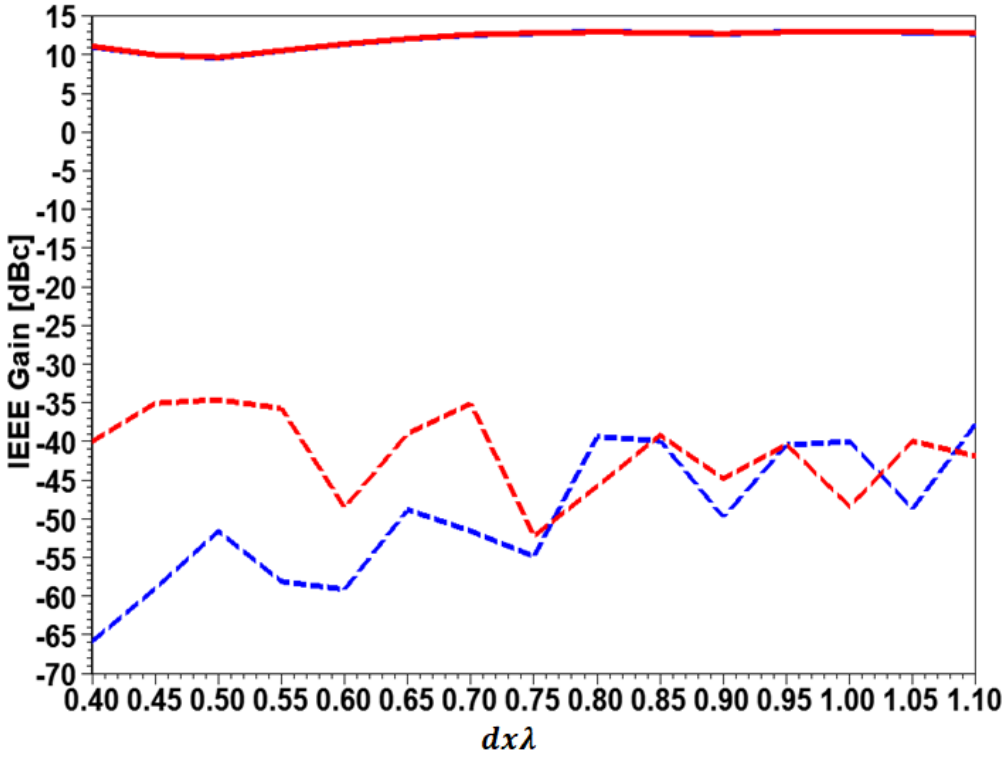

Fig. 51. CP gain variation with element separation for the elements fed with a dielectric-filled waveguide (red) and with SIW (blue) at 60 GHz. The dotted lines show the cross-polarized gain for the same cases.

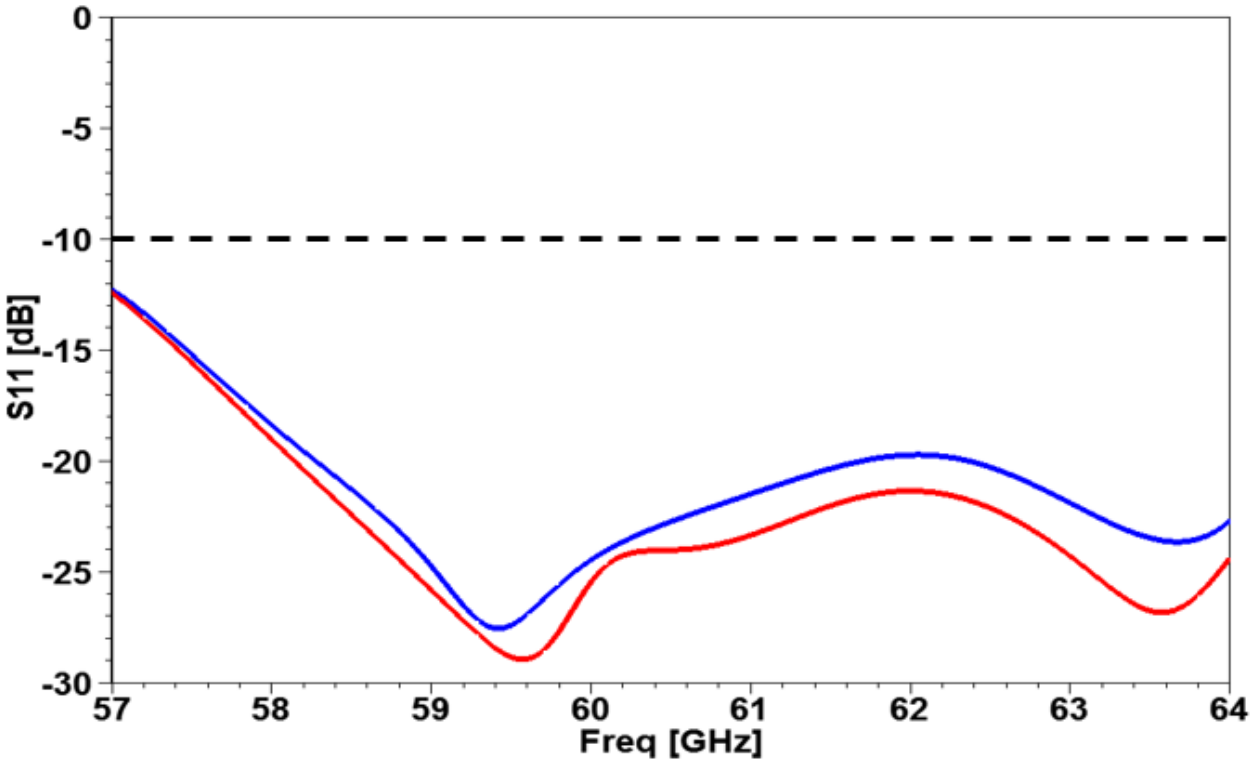

Fig. 52. Reflection coefficient for the 2x2 array for the elements fed with a dielectric-filled waveguide (red) and with SIW (blue).

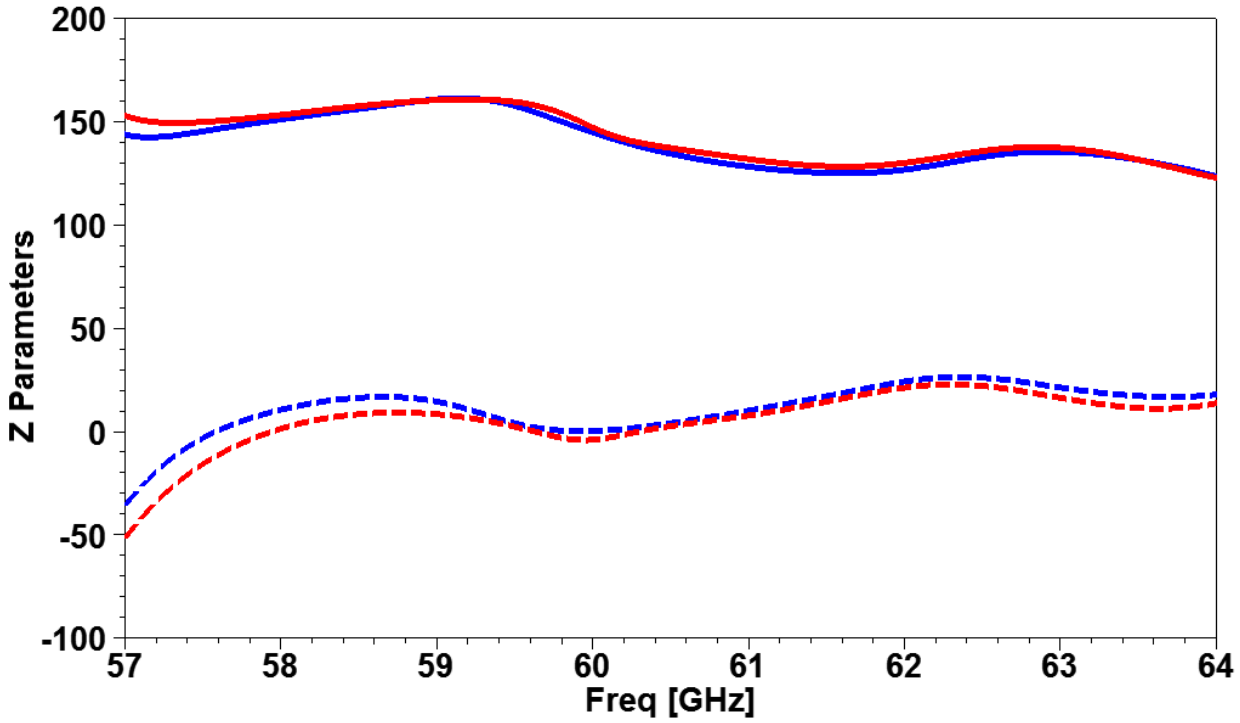

Fig. 53. Z11 parameters for the 2x2 array for the elements fed with a dielectric-filled waveguide (red) and with SIW (blue). The solid lines represent the resistance, and the dotted lines show reactance.

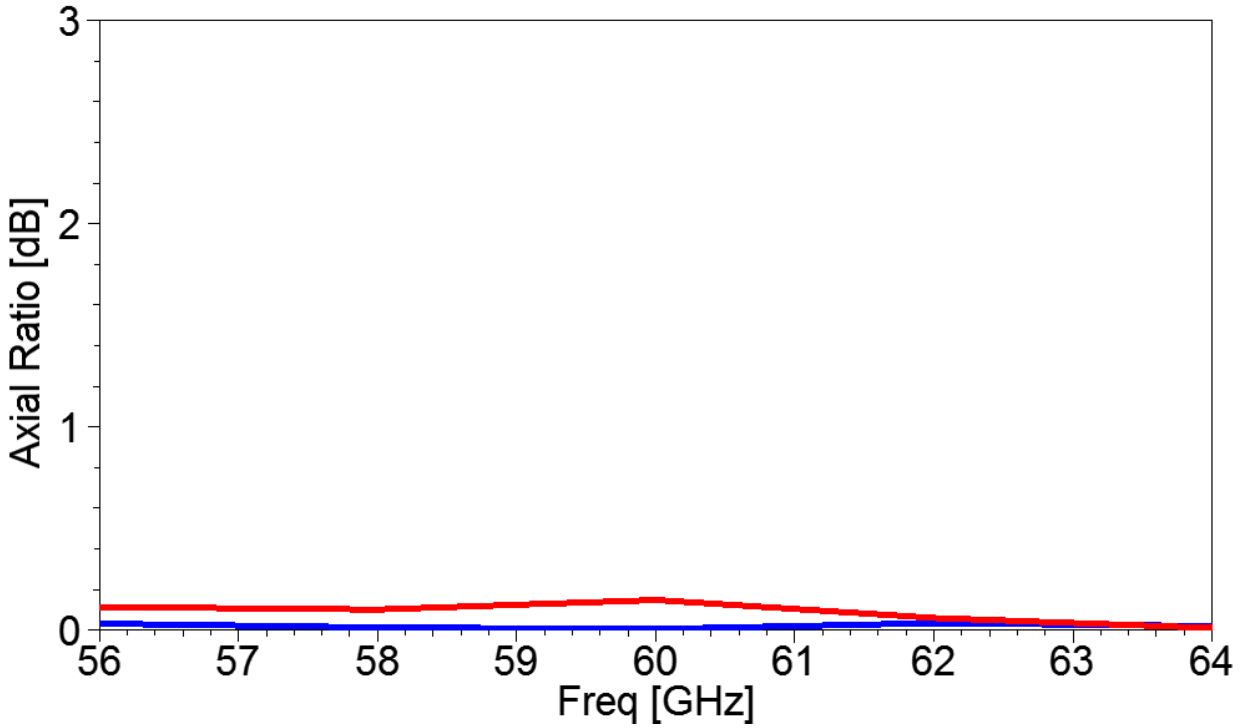

Fig. 54. Axial ratio as a function of frequency for the 2x2 array for the elements fed with a dielectric-filled waveguide (red) and with SIW (blue).

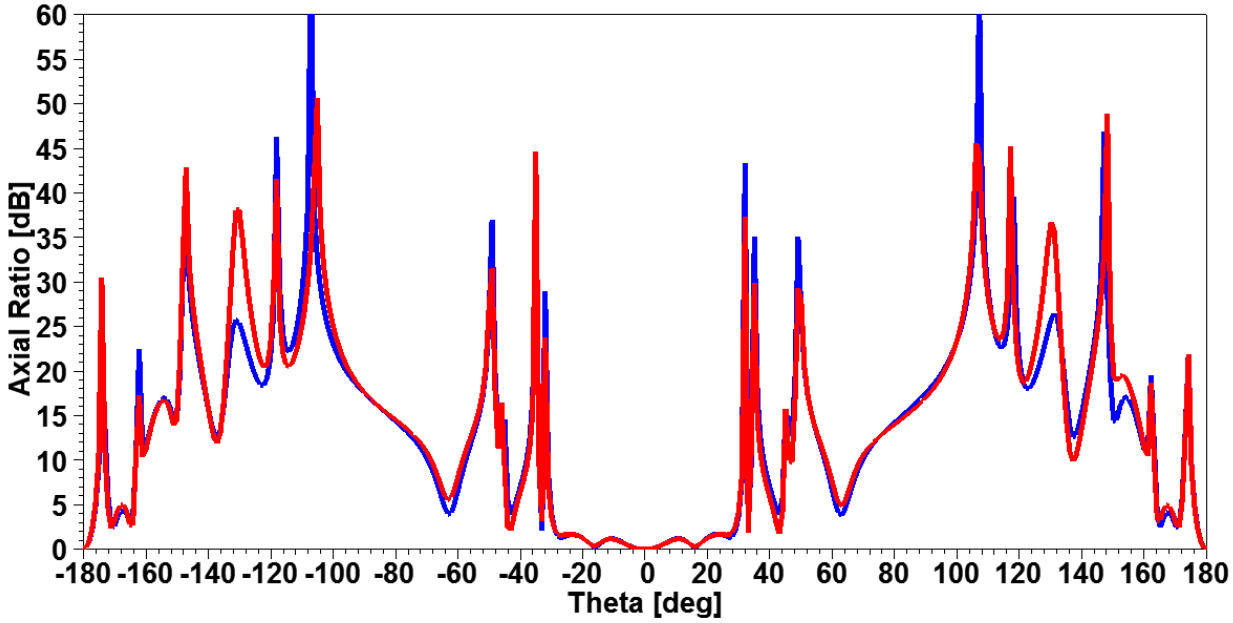

Fig. 55. Axial ratio for the 2x2 array as a function of theta for the elements fed with a dielectric-filled waveguide (red) and with SIW (blue) at 60 GHz.

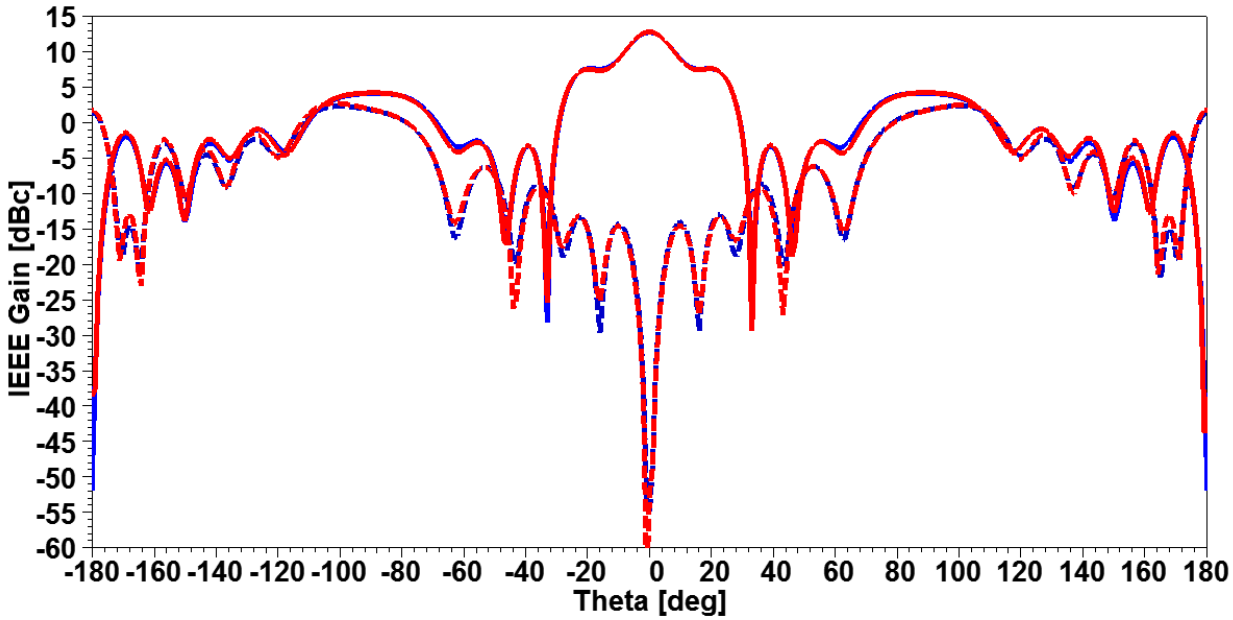

Fig. 56. CP gain pattern for the 2x2 array for the elements fed with a dielectric-filled waveguide (red) and with SIW (blue) at 60 GHz. The dotted lines show the cross-polarized gain for the same cases.

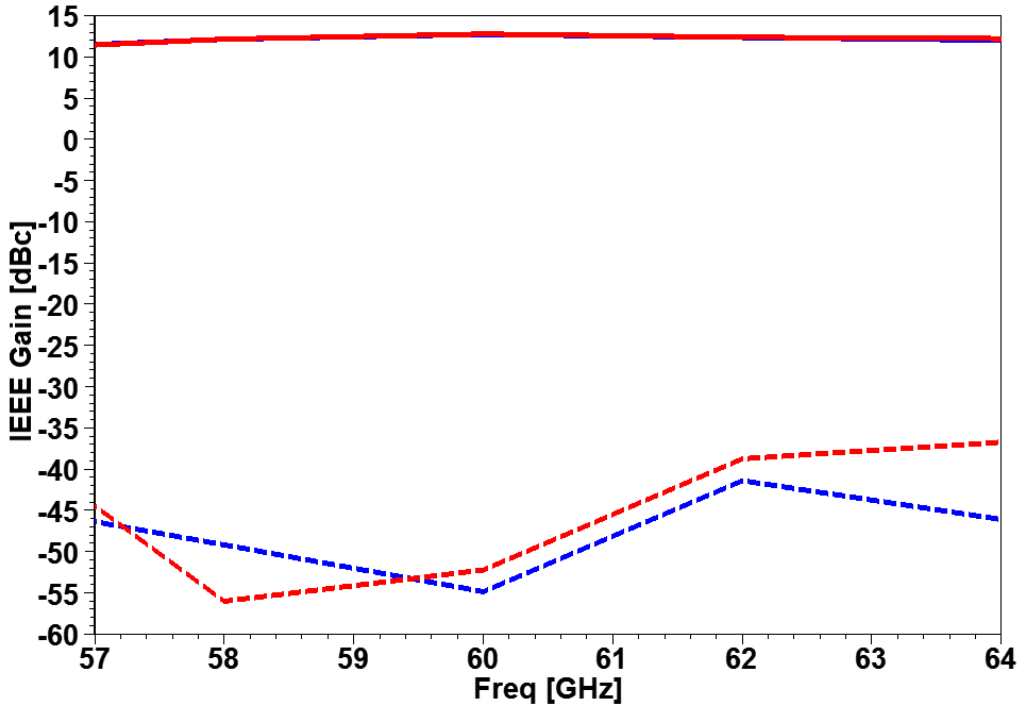

Fig. 57. CP gain as a function of frequency for the 2x2 array antenna for the elements fed with a dielectric-filled waveguide (red) and with SIW (blue). The dotted lines show the cross-polarized gain for the same cases.

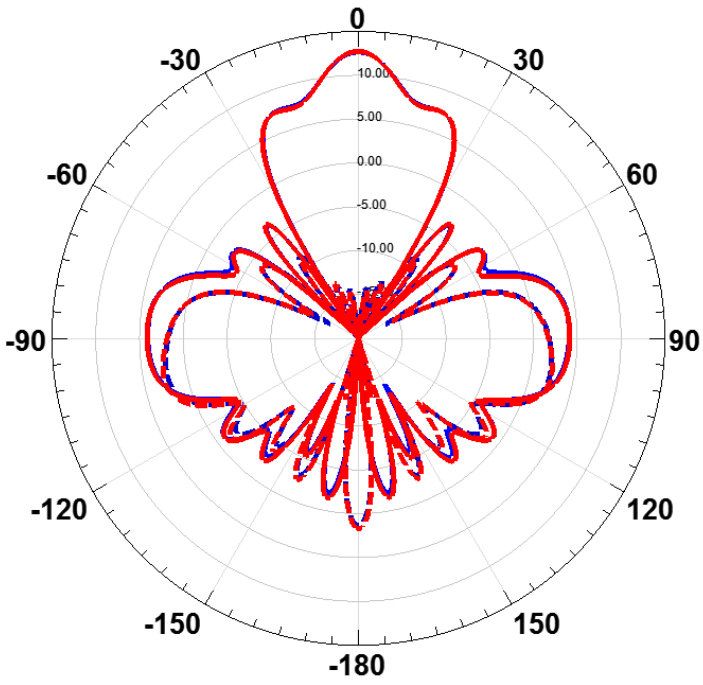

Fig. 58. CP gain pattern for the 2x2 array for the elements fed with a dielectric-filled waveguide (red) and with SIW (blue) at 60 GHz. The dotted lines show the cross-polarized gain for the same cases.

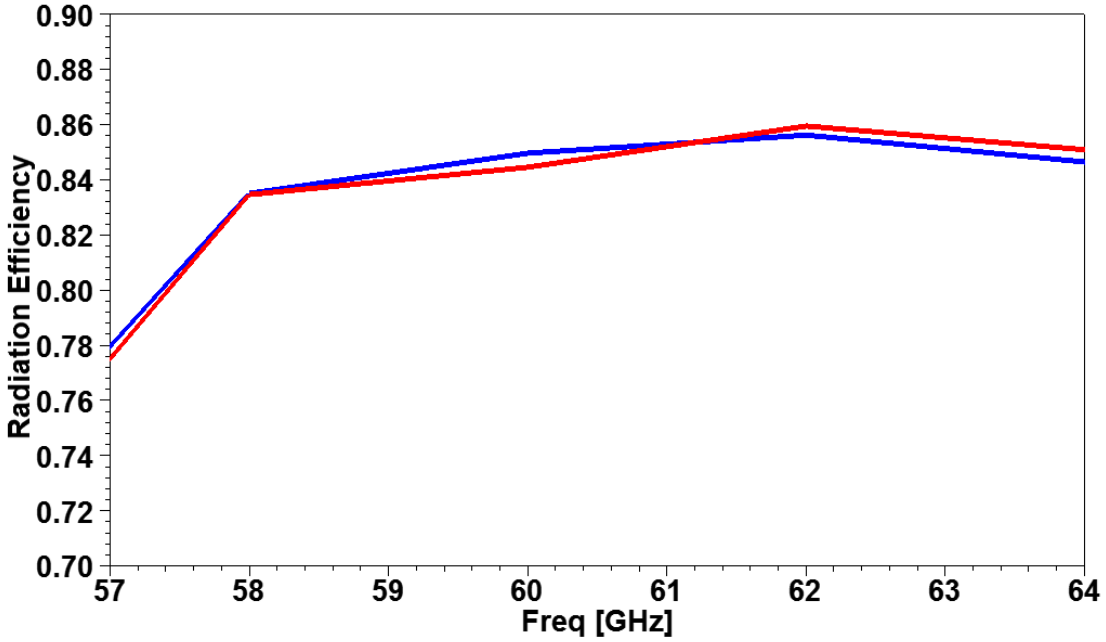

Fig. 59. Radiation efficiency as a function of frequency for the 2x2 array for the elements fed with a dielectric-filled waveguide (red) and with SIW (blue).

TABLE 9. 2x2 Array Summary Results.

	Dielectric-Filled Waveguide Fed	SIW Fed
S11 (%)	11.6	11.6
AR Bandwidth (%)	11.6	11.6
Z Parameters	147-4j	145
Max Gain (dBc)	12.7	12.7
Radiation Efficiency (%)	84.4	84.9

4 CONCLUSIONS

We completed several designs for antennas for body-centric wireless communications, in particular for off-body communications applications. Designs for applications at 2.4 GHz, UWB, and V-band frequencies were developed, taking in to consideration the effects of the human body in the design. Linear polarized elements at 2.4 GHz and 60 GHz were developed, as well as dual-linear elements for 24 GHz, and circularly polarized elements for UWB and V-band. Linear and circularly polarized arrays were designed at V-band, and a study of the effect in axial ratio bandwidth and gain, of using linear and circular polarized elements in sequentially rotated arrays. A logical next step would be the integration of the antennas with appropriate sensors for actual applications.

5 REFERENCES

[1] Antti E. I. Lamminen, Jussi Säily, and Antti R. Vimpari, "60-GHz Patch Antennas and Arrays on LTCC with Embedded-Cavity Substrates", *IEEE Transactions On Antennas and Propagation, Vol. 56, NO.9,* September 2008

[2] Bozzi, M.; Georgiadis, A.; Wu, K., "Review of substrate-integrated waveguide circuits and antennas," in *Microwaves, Antennas & Propagation, IET* , vol.5, no.8, pp.909-920, June 6 2011

[3] Yujian Li; Kwai-Man Luk, "Low-Cost High-Gain and Broadband Substrate- Integrated-Waveguide-Fed Patch Antenna Array for 60-GHz Band," in *Antennas and Propagation, IEEE Transactions on* , vol.62, no.11, pp.5531-5538, Nov. 2014

[4] Yue Li; Zhi Ning Chen; Xianming Qing; Zhijun Zhang; Junfeng Xu; Zhenghe Feng, "Axial Ratio Bandwidth Enhancement of 60-GHz Substrate Integrated Waveguide-Fed Circularly Polarized LTCC Antenna Array," in *Antennas and Propagation, IEEE Transactions on* , vol.60, no.10, pp.4619-4626, Oct. 2012

[5] Junfeng Xu; Zhi Ning Chen; Xianming Qing; Wei Hong, "Bandwidth Enhancement for a 60 GHz Substrate Integrated Waveguide Fed Cavity Array Antenna on LTCC," in *Antennas and Propagation, IEEE Transactions on* , vol.59, no.3, pp.826-832, March 2011

[6] Chahat, N.; Zhadobov, M.; Le Coq, L.; Alekseev, S.I.; Sauleau, R., "Characterization of the Interactions Between a 60-GHz Antenna and the Human Body in an Off-Body Scenario," in *Antennas and Propagation, IEEE Transactions on* , vol.60, no.12, pp.5958-5965, Dec. 2012.

[7] D. M. Pozar, "*Microwave Engineering*," 4th Edition, Wiley, 2012.

[8] Deslandes, D.; Ke Wu, "Accurate modeling, wave mechanisms, and design considerations of a substrate integrated waveguide," in *Microwave Theory and Techniques, IEEE Transactions on* , vol.54, no.6, pp.2516-2526, June 2006.

[9] M. Ahadobov, N. Chalhat, R. Sauleau, C. Le Quement and Y. Le Drean, "Millimeter-Wave Interactions with the Human Body: State of Knowledge and Recent Advances," *International Journal of Microwave And Wireless Technologies,* **3,** 2, April 2011, pp. 237-247.

[10] C. A. M. Hernandez and R. A. R. Solís, "Design of V-band SIW fed cavity backed aperture coupled microstrip patch array element for applications in body area networks," *2016 IEEE International Symposium on Antennas and Propagation (APSURSI)*, Fajardo, 2016, pp. 1235-1236.

[11] M. Bozzi, A. Georgiadis and K. Wu, "Review of substrate-integrated waveguide circuits and antennas," in *IET Microwaves, Antennas & Propagation*, vol. 5, no. 8, pp. 909-920, June 6 2011.

[12] Steven Shichang Gao; Qi Luo; Fuguo Zhu, "Introduction to Circularly Polarized Antennas," in *Circularly Polarized Antennas* , 1, Wiley-IEEE Press, 2014, pp.328